New Jersey Institute of Technology
Digital Commons @ NJIT

Dissertations | Electronic Theses and Dissertations

Fall 1-31-2011

Seismic characterization of recycled aggregate concrete

Amin Jamali
New Jersey Institute of Technology

Follow this and additional works at: https://digitalcommons.njit.edu/dissertations

Part of the Civil Engineering Commons

Recommended Citation

Jamali, Amin, "Seismic characterization of recycled aggregate concrete" (2011). *Dissertations*. 238.
https://digitalcommons.njit.edu/dissertations/238

This Dissertation is brought to you for free and open access by the Electronic Theses and Dissertations at Digital Commons @ NJIT. It has been accepted for inclusion in Dissertations by an authorized administrator of Digital Commons @ NJIT. For more information, please contact digitalcommons@njit.edu.

Copyright Warning & Restrictions

The copyright law of the United States (Title 17, United States Code) governs the making of photocopies or other reproductions of copyrighted material.

Under certain conditions specified in the law, libraries and archives are authorized to furnish a photocopy or other reproduction. One of these specified conditions is that the photocopy or reproduction is not to be "used for any purpose other than private study, scholarship, or research." If a, user makes a request for, or later uses, a photocopy or reproduction for purposes in excess of "fair use" that user may be liable for copyright infringement,

This institution reserves the right to refuse to accept a copying order if, in its judgment, fulfillment of the order would involve violation of copyright law.

Please Note: The author retains the copyright while the New Jersey Institute of Technology reserves the right to distribute this thesis or dissertation

Printing note: If you do not wish to print this page, then select "Pages from: first page # to: last page #" on the print dialog screen

NJIT
New Jersey's Science &
Technology University

The Van Houten library has removed some of the personal information and all signatures from the approval page and biographical sketches of theses and dissertations in order to protect the identity of NJIT graduates and faculty.

ABSTRACT

SEISMIC CHARACTERIZATION OF RECYCLED AGGREGATE CONCRETE

by
Amin Jamali

There are significant environmental benefits of recycling waste concrete and reusing it as aggregate for structural concrete, but the use of Recycled Aggregate Concrete (RAC) is yet limited to non-structural applications such as road sub-base. Widespread application of RAC in areas such as seismic design requires an improved knowledge of RAC behavior under multiaxial state of stresses.

The main objective of this research is the characterization of seismic properties of RAC by developing a stress-strain model which can reasonably describe the behavior under both unconfined and confined conditions. An extensive experimental program, including testing of several plain RAC cylinders as well as reinforced RAC columns, was conducted. There are numerous variables influencing the behavior of confined RAC, creating unlimited experimental possibilities, so the tests parameters were chosen to be limited to square columns with normal strength RAC and rectilinear tie configurations.

Stress-strain curves were obtained for several 4 inches by 8 inches RAC cylinders with compressive strength from 2.5 ksi to 7.5 ksi. Based on the experimental results, a new model for stress-strain behavior of plain RAC was developed. Up to an axial strain of 0.0025, a nonlinear equation is considered for the ascending branch, which is primarily a function of compressive strength and elastic modulus, while the descending branch is a straight line and is a function of compressive strength. A sustaining branch was proposed where the plain RAC is capable of sustaining 10% of the compressive strength.

44 reinforced RAC columns, 10 inches by 10 inches in section and 32 inches in height with nine different combination of tie patterns and spacings were tested under quasi-static (1.6×10^{-5} per in.) and dynamic (1.6×10^{-2} per in.) axial straining rates. The columns with a volumetric ratio of ties of 1.5% more were capable of sustaining the load than the columns with lower volumetric ratios. Under the fast straining rate, the columns showed about 27% increase in strength. The columns with sufficient and well-distributed lateral confinement did not also show any stiffness degradation under cyclic loading.

Special attention was paid to recording the axial strains at which vertical cracks were developing, as well as the strains at which the cover was no longer effective. These strains were indicative of the gradual transition of axial stresses from cover to the core. Based on these strains and contributions of concrete and longitudinal steel in for each column, a new one-of-a-kind stress-strain model for confined RAC was proposed. The model is comprised of an ascending-transition-descending structure would be suitable to define the behavior. The ascending branch proposed for plain RAC is applicable for confined RAC as well. The transition zone starts at a strain of 0.0020 and ends at a strain where the cover is completely ineffective. The descending branch is a straight line and primarily a function of the lateral reinforcement. The variables required to define the curve were described in terms of the compressive strength of plain RAC, the yield strength of steel tie and the volumetric ratio of the confinement steel.

The proposed models for plain and confined RAC were examined under the flexural loading condition using two identical RAC beams. The nonlinear load-deformation of the beam predicted using the proposed RAC models agreed with the experimental results to within 10%.

SEISMIC CHARACTERIZATION OF RECYCLED AGGREGATE CONCRETE

by
Amin Jamali

A Dissertation
Submitted to the Faculty of
New Jersey Institute of Technology
in Partial Fulfillment of the Requirements for the Degree of
Doctor of Philosophy in Civil Engineering

Department of Civil and Environmental Engineering

January 2011

Copyright © 2011 by Amin Jamali

ALL RIGHTS RESERVED

.

APPROVAL PAGE

SEISMIC CHARACTERIZATION OF RECYCLED AGGREGATE CONCRETE

Amin Jamali

Dr. Mohamad Ala Saadeghvaziri, Dissertation Co-Advisor Date
Professor of Civil Engineering, New Jersey Institute of Technology

Dr. Mohamed Mahgoub, Dissertation Co-Advisor Date
Assistant Professor of Civil Engineering, New Jersey Institute of Technology

Dr. Dorairaja Raghu, Committee Member Date
Professor of Civil Engineering, New Jersey Institute of Technology

Dr. John R. Schuring, Committee Member Date
Professor of Civil Engineering, New Jersey Institute of Technology

Dr. Nazhat Aboobaker, Committee Member Date
Project Manager, New Jersey Department of Transportation

BIOGRAPHICAL SKETCH

Author: Amin Jamali

Degree: Doctor of Philosophy

Date: January 2011

Undergraduate and Graduate Education:

- Doctor of Philosophy in Civil Engineering,
  New Jersey Institute of Technology, Newark, NJ, 2011

- Master of Science in Civil Engineering,
  K. N. Toosi University of Technology, Tehran, Iran, 2000

- Bachelor of Science in Civil Engineering,
  Razi University, Kermanshah, Iran, 1998

Major: Civil Engineering

Presentations and Publications:

Amin Jamali and Mohamad Ala Saadeghvaziri, "Shear Transfer Mechanism in Slab-on-Girder Bridges," Fifth International Conference on Bridge Maintenance, Safety and Management (IABMAS10), Philadelphia, PA, July 2010.

Amin Jamali and Mohamad Ala Saadeghvaziri, "Controlled Composite Action to Eliminate Deck Cracking," The AISC Structures Congress/ North American Steel Construction Conference (NASCC), Orlando, Florida, May 2010.

Mohamad Ala Saadeghvaziri and Amin Jamali, "An Innovative Concept to Eliminate Deck Cracking," Transportation Research Board 88th Annual Meeting, Washington DC, January 2009.

Mohamad Ala Saadeghvaziri and Amin Jamali, "Application of FRPs in development of high performance continuity connections," Fourth International Conference on FRP Composites in Civil Engineering (CICE2008), Zurich, Switzerland, July 2008.

To: Bābā and Māmān

ACKNOWLEDGMENT

First and foremost I present my sincerest gratitude to Dr. Mohamad Ala Saadeghvaziri, my research advisor, who greatly supported me throughout my PhD studies with his patience and knowledge. One simply could not wish for a better or friendlier advisement. I also offer my sincere thankfulness to my research co-advisor, Dr. Mohamed Mahgoub, who made this work possible by his invaluable comments and continuous support.

I am very grateful to the members of my doctoral dissertation committee, Dr. John R. Schuring, Dr. Dorairaja Raghu and Dr. Nazhat Aboobaker who generously gave their precious time and expertise to read and better my work.

It is an opportunity to show my appreciation to the Concrete Industry Management program at NJIT for their financial support to this study. I am also very thankful to: William Araujo from NJIT, Frank Johansson from Mechanical Components Inc., Ricardo Arocha, Rob Roberts, Gilbert Morales, Michael McKendrick, Terry Mooney and Bill Hall from Weldon Materials Inc., Giacomo Abrusci from Bronx CFS steel Inc., Jamie M. Gentoso and David White from Sika Inc. and Mike Mota from CRSI.

I thank all the CEE staff specially Mr. Allyn Luke for his generous laboratory support, Dallas Link, Marion Balavender and Bob Morris.

I owe all my accomplishments to my truly exceptional family. There has not been a single moment in my life without their unconditional support and desire for my success. Words are not able to express my gratitude to them. All the credit of accomplishing this study belongs to them.

TABLE OF CONTENTS

Chapter	Page
1 INTRODUCTION…….....……..……	1
1.1 Motivation….....……..…….....	1
1.1.1 Saving Natural Resources…….....	1
1.1.2 Landfills and Generation of Construction and Demolition Debris ……...	2
1.2 Current Applications of RAC …….…….....	4
1.3 Significance of Research and Objective ……..	4
1.4 Scope……	5
1.5 Contents……	6
2 LITERATURE REVIEW…….. ……	7
2.1 Properties of Plain RAC…….……..	7
2.1.1 Compressive Strength……	7
2.1.2 Modulus of Elasticity…….	10
2.1.3 Tensile and Flexural Strength……...…….	11
2.1.4 Bond Strength……	11
2.1.5 Creep and Shrinkage……..	12
2.1.6 Freeze-Thaw Resistance……	12
2.1.7 Permeability, Carbonation and Chloride Ion Penetration……..	14
2.1.8 Density and Workability of RAC……...……...	15
2.1.9 Summary of RAC Properties……..……..	16
2.2 Behavior of RAC Beams……..	17

TABLE OF CONTENTS
(Continued)

Chapter **Page**

2.3 Behavior of Confined Concrete ……..… 20

2.3.1 Behavior of Unconfined Concrete under Monotonic Load……... 20

2.3.2 Behavior of Unconfined Concrete under Cyclic Load…….. 21

2.3.3 Behavior of Confined Concrete……. 22

2.3.3.1 Active Confinement……... 23

2.3.3.2 Passive Confinement……..... 23

2.3.4 Mechanism of Confinement……... 23

2.3.5 Parameters Influencing Rectangular Confinement…… 25

2.3.5.1 Volumetric Ratio of Transverse Reinforcement…… 26

2.3.5.2 Characteristics of Transverse Reinforcement…… 26

2.3.5.3 Tie Spacing…… 27

2.3.5.4 Longitudinal Reinforcement……... 27

2.3.5.5 Size of Ties……. 27

2.3.5.6 Other Factors……... 28

2.3.6 Concrete Models……..…. 28

2.4 Summary…….. 32

3 EXPERIMENTAL WORK…….…… 33

3.1 General……...……...……... 33

3.2 Materials……..…… 33

3.2.1 Original Concrete and Recycled Coarse Aggregates (RCA)……. 33

TABLE OF CONTENTS
(Continued)

Chapter	Page
3.2.2 Column RAC mix……..	34
3.2.3 Plain RAC Strength……	38
3.2.4 RAC Cylinders for Developing Stress-Strain model…….	40
3.2.5 Longitudinal and Lateral Steel……...…	41
3.3 Fabrication of Columns……	44
3.3.1 Forms…….	44
3.3.2 Casting and Curing……	44
3.3.3 Reinforcing Cages……..	45
3.3.4 Column Designation……..	47
3.3.5 Glass Fiber Reinforced Polymer confinement……...	49
3.4 Instrumentation……	50
3.4.1 External Instrumentation……	50
3.4.2 Internal Instrumentation…….	51
3.5 Test Setup…….	53
3.5.1 Capping……..	53
3.5.2 Positioning…….	53
3.5.3 Loading Unit and Data acquisition System……...	54
3.6 Loading Procedure……...	54
4 ANALYSIS AND DISCUSSION OF TEST DATA……..	56
4.1 Test Observations ……	56

TABLE OF CONTENTS
(Continued)

Chapter **Page**

4.1.2 Plain RAC Cylinders...……..……. 56

4.1.2 Reinforced RAC Columns.…… 56

4.2 Contribution of Cover and Core Concrete……... 63

4.2.1 Spalling Mechanism…….. 63

4.2.1 Transition of Stresses……. 63

4.2.2 Concrete Contributions……. 67

4.3 Effects of Reinforcement Variables on Behavior of RAC Columns ……..... 69

4.3.1 Effect of Volumetric Ratio …… 69

4.3.2 Effect of Tie Spacing ……...……. 70

4.3.3 Effect of Tie Configuration …….. 72

4.4 Effect of Loading Rate on Strength and Ductility of RAC Columns……. 73

4.4.1 Effect of Loading Rate on Strength…….…….. 73

4.4.2 Effect of Loading Rate on Ductility…….. 75

4.5 Effect of Cyclic Loading…….. 79

5 ANALYTICAL PREDICTION OF RAC STRESS-STRAIN BEHAVIOR…….. 83

5.1 General……. 83

5.2 Development of Stress-Strain Formulation for Plain RAC…….. 83

5.2.1 Experimental Stress-Strain Curves…… 83

5.2.2 Proposed Stress-Strain Model for Plain RAC…… 87

5.3 Model for Confined RAC……. 90

TABLE OF CONTENTS
(Continued)

Chapter **Page**

5.3.2 Stress-Strain Curve of Confined RAC……..……..... 98

5.3.3 Experimental and Predicted Values of Ks Factor……. 100

5.3.4 Transition and Descending Branches.……... 102

5.3.5 Sample Analysis…… 106

6 EXAMINATION OF RAC MODELS IN FLEXURE……... 109

6.1 Numerical Analysis……..... 109

6.1.1 Material and Geometrical Properties……. 109

6.1.2 Calculation of Deflections……. 113

6.2 Experimental Results ……... 115

7 CONCLUSIONS.....……..……... 121

7.1 General……... ..……...… 121

7.2 Conclusions from the Experimental Study...…….…….….. 121

7.3 Conclusions from the Analytical Study……... 122

7.3.1 Proposed Model for Plain RAC……. 122

7.3.2 Proposed Model for Confined RAC…….. 124

7.4 Recommendation for Future Research……. 125

APPENDIX A FAILURE MODE OF RAC COLUMNS…...……... 126

APPENDIX B DETERMINATION OF CONCRETE CONTRIBUTION…… 136

APPENDIX C EXPERIMENTAL STRESS-STRAIN CURVES…….. 142

REFERENCES ……... 152

LIST OF TABLES

Table		Page
1.1	Building-related C&D Debris Generation in 1996……..…....	3
1.2	Building-related C&D Debris Generation in 2003…….	3
2.1	Compressive Strengths of Recycled Concrete……	8
2.2	Compressive Strengths of Original and Recycled Concrete……...	9
2.3	Frost Resistance of RAC……...……..	14
2.4	Specific Gravity of Natural and Recycled Aggregates……...	16
2.5	Summary of RAC Properties……..	17
2.6	Proposed Models for Confined Normal Concrete……..	32
3.1	Results of RCA Sieve Analysis …….	35
3.2	Compressive Strength of the Original Concrete…….	35
3.3	RAC Mix Proportions…….	36
3.4	Physical Properties of Recycled Aggregates……..	37
3.5	Compressive Strengths of Cylinder Samples on the Day of Column Testing vs. the Strengths on the Day of Obtaining Stress-Strain Curves……..	39
3.6	Mix Proportions for Target Strengths of 2500 psi to 7000 psi……...	41
3.7	Mechanical Properties of Longitudinal Steel……..	43
3.8	Mechanical Properties of Tie Steel…….	43
3.9	Details of the Specimens…….	48
4.1	Strains Corresponding to Cracking Condition of RAC Columns……...	65
4.2	Calculated and Experimental Axial Strengths and Contributions……..	68

LIST OF TABLES
(Continued)

Table **Page**

4.3 Calculated and Experimental Dynamic Axial Strengths…… 76

4.4 Variation of Static-to-Dynamic Axial Strength Ratios with Respect to ρ_s ……... 77

5.1 Experimental Values of Strength Enhancement due to Confinement, K_s ……. 101

6.1 Predicted Curvature and Deflection Values ……... 120

LIST OF FIGURES

Figure		Page
1.1	The US annual production of sand and gravel……	2
1.2	Composition of demolition debris …….	3
1.3	(left) States recycling concrete as aggregate, (right) States recycling concrete as aggregate base…….	4
2.1	Modulus of elasticity as a function of cement/water ratio……..	11
2.2	Effect of fly ash on creep of RAC……..	13
2.3	Effect of water/binder ratio and fly ash on RAC shrinkage……	13
2.4	Half-cell potentials of rebars in RAC and normal concrete……...	15
2.5	Chloride Ion penetration in normal concrete and RAC……..	15
2.6	Load-deformation of RAC versus NAC beams……..	19
2.7	Cracking of RAC and NAC beams…….	19
2.8	Typical monotonic stress-strain behavior of normal concrete……	21
2.9	Typical cyclic stress-strain behavior of normal concrete……	22
2.10	Effect of hydrostatic pressure on concrete strength……	24
2.11	Stress-strain curves from triaxial compression tests……...	25
2.12	Effect of confinement on strength and ductility…….	25
2.13	Confinement by circular spirals……..	26
2.14	Confinement by rectangular ties…….	26
2.15	Concrete stress-strain model proposed by Sheikh and Uzumeri, 1982…….....	31
2.16	Concrete stress-strain model proposed by Mander et al., 1988……..	31

LIST OF FIGURES
(Continued)

Figure **Page**

3.1 Weldon Materials crushing facilities, New Jersey…….. 34

3.2 Stress-strain curves of the original concrete…….. 35

3.3 "TSAM" and normal mixing approach……... 37

3.4 Improvement of ITZ by employing "TSMA"……. 37

3.5 Compressive strength of the finalized RAC mix…… 38

3.6 Mixing arrangements…….. 38

3.7 Testing machine used for measuring strength of concrete cylinders…….. 40

3.8 Typical stress-strain curves for plain RAC cylinders……. 40

3.9 (left) Longitudinal rebars samples, (right) Tie steel samples…….. 42

3.10 Tensile behavior of longitudinal rebars (left) and tie steel (right)…….. 43

3.11 Plywood forms…… 44

3.12 Tie configurations……... 46

3.13 Tie spacing and end extra reinforcement…… 47

3.14 Example cages…… 47

3.15 Additional end confinement using GFRP laminates……... 50

3.16 Measuring axial deformation of cylinder by a pair of extensometers…… 51

3.17 CEA-06-240UZ-120 electrical strain gauge (trimmed to 4×9 mm)……... 52

3.18 Examination of bond quality of a strain gauge installed on 3/16" steel wire……. 53

3.19 Location of tie strain gauges……... 53

3.20 Application of hydro-stone® gypsum cement……. 54

LIST OF FIGURES
(Continued)

Figure **Page**

3.21 1000-kip MTS815 servo-hydraulic loading unit and other hardware…… 55

4.1 RAC stress strain curves vs. models for normal concrete…….. 57

4.2 Typical failure of RAC and normal concrete cylinders…….. 57

4.3 Axial deformation of column B1-2……. 58

4.4 Failure of Column A1-1 under static loading……. 60

4.5 Failure of Column B2-2 under static loading……. 61

4.6 Failure of Column C3-2 under static loading……. 62

4.7 Tie strain versus longitudinal strains…….. 66

4.8 Concrete contribution and stress transition zone…… 66

4.9 Determination of concrete contributions for Columns A1-1 and A1-2…….. 69

4.10 Gain in strength and ductility due to confinement…….. 70

4.11 Effect of transverse steel configuration on column behavior……. 71

4.12 Effect of transverse steel amount on column behavior……... 72

4.13 Effect of strain rate on behavior of column type A1…….. 78

4.14 Effect of strain rate on behavior of column type B2……... 78

4.15 Cyclic behavior of column A1-5 subjected to cyclic loading……. 80

4.16 Cyclic behavior of column B1-5 subjected to cyclic loading …… 80

4.17 Cyclic behavior of column B3-5 subjected to cyclic loading …… 81

4.18 Cyclic behavior of column C1-5 subjected to cyclic loading …… 81

4.19 Cyclic behavior of column C2-5 subjected to cyclic loading …… 82

LIST OF FIGURES
(Continued)

Figure **Page**

4.20 Cyclic behavior of column C3-5 subjected to cyclic loading …… 82

5.1a Experimental and predicted stress-strain curves for plain RAC …… 85

5.1b Experimental and predicted stress-strain curves for plain RAC …… 85

5.1c Experimental and predicted stress-strain curves for plain RAC …… 86

5.1d Experimental and predicted stress-strain curves for plain RAC …… 86

5.1e Experimental and predicted stress-strain curves for plain RAC …… 87

5.2 Variation of n with respect to RAC compressive strength……..….. 90

5.3 Variation of σ_f with respect to RAC compressive strength…….. 90

5.4 Proposed model for compressive stress-strain behavior of plain RAC…….. 91

5.5 Shape of arching action……... 93

5.6 Unconfined areas at tie level…….. 94

5.7 Arching action along the column height……. 94

5.8 Experimental stress-strain curve for column A1-1……. 100

5.9 Power regression to determine β and γ …….. 101

5.10 Approximation of ε_{cc} ……. 105

5.11 Approximation of η and λ values……... 105

5.12 Proposed RAC model versus proposed models for normal concrete …… 108

6.1 Cross-sectional properties of the RAC beams…… 112

6.2 Stress-strain behavior of the materials used in the numerical analysis …….. 113

6.3 Beam divisions for numerical calculation…….. 115

LIST OF FIGURES
(Continued)

Figure **Page**

6.4 Analytical moment-curvature diagram……... 116

6.5 Beam test setup: (top) Beam-1, (bottom) Beam-2…….. 117

6.6 Development of cracks and crushing: (top) Beam 1, (bottom) Beam 2……. 118

6.7 Calculated and experimental load-deformation of the RAC beams …….. 119

7.1 Proposed model for compressive stress-strain behavior of plain RAC…….. 123

7.2 Proposed model for compressive stress-strain behavior of confined RAC…… 125

A.1 Failure of Column A1-1 under static loading……. 127

A.2 Failure of Column A1-2 under static loading……. 127

A.3 Failure of Column A2-1 under static loading……. 128

A.4 Failure of Column A2-2 under static loading……. 128

A.5 Failure of Column A3-1 under static loading……. 129

A.6 Failure of Column A3-2 under static loading……. 129

A.7 Failure of Column B1-1 under static loading……. 130

A.8 Failure of Column B1-2 under static loading……. 130

A.9 Failure of Column B2-1 under static loading……. 131

A.10 Failure of Column B2-2 under static loading……. 131

A.11 Failure of Column B3-1 under static loading……. 132

A.12 Failure of Column B3-2 under static loading……. 132

A.13 Failure of Column C1-1 under static loading……. 133

A.14 Failure of Column C1-2 under static loading……. 133

LIST OF FIGURES
(Continued)

Figure **Page**

A.15 Failure of Column C2-1 under static loading……. 134

A.16 Failure of Column C2-2 under static loading……. 134

A.17 Failure of Column C3-1 under static loading……. 135

A.18 Failure of Column C3-2 under static loading……. 135

B.1 Determination of concrete contributions for Columns A1-1 and A1-2…….. 137

B.2 Determination of concrete contributions for Columns A1-1 and A1-2…….. 137

B.3 Determination of concrete contributions for Columns A1-1 and A1-2…….. 138

B.4 Determination of concrete contributions for Columns A1-1 and A1-2…….. 138

B.5 Determination of concrete contributions for Columns A1-1 and A1-2…….. 139

B.6 Determination of concrete contributions for Columns A1-1 and A1-2…….. 139

B.7 Determination of concrete contributions for Columns A1-1 and A1-2…….. 140

B.8 Determination of concrete contributions for Columns A1-1 and A1-2…….. 140

B.9 Determination of concrete contributions for Columns A1-1 and A1-2…….. 141

C.1 Experimental stress-strain curve for column A1-1……. 143

C.2 Experimental stress-strain curve for column A1-2……. 143

C.6 Experimental stress-strain curve for column A2-1……...…….. 144

C.4 Experimental stress-strain curve for column A2-2……. 144

C.5 Experimental stress-strain curve for column A3-1…….… 145

C.6 Experimental stress-strain curve for column A3-2……. 145

C.7 Experimental stress-strain curve for column B1-1……. 146

LIST OF FIGURES
(Continued)

Figure **Page**

C.8 Experimental stress-strain curve for column B1-2……. 146

C.9 Experimental stress-strain curve for column B2-1……...…….. 147

C.10 Experimental stress-strain curve for column B2-2……. 147

C.11 Experimental stress-strain curve for column B3-1…….… 148

C.12 Experimental stress-strain curve for column B3-2……. 148

C.13 Experimental stress-strain curve for column C1-1……. 149

C.14 Experimental stress-strain curve for column C1-2……. 149

C.15 Experimental stress-strain curve for column C2-1……...…….. 150

C.16 Experimental stress-strain curve for column C2-2……. 150

C.17 Experimental stress-strain curve for column C3-1…….… 151

C.18 Experimental stress-strain curve for column C3-2……. 151

LIST OF SYMBOLS

b_i	dimension of concrete core
d_i	center-to-center distance between adjacent longitudinal rebars
f	concrete stress
f_1	strength of confined concrete
f_2	lateral hydrostatic pressure
f_{add}	additional strength due to confinement
f_c	strength of confined concrete
f_{cc}	strength of confined concrete
$f_{cc}^{\dot{\varepsilon}}$	enhance compressive strength of confined concrete
f_{ic}	insitu strength of confined concrete
f_s	tie stress
$f_{uc}^{\dot{\varepsilon}}$	enhance compressive strength of unconfined concrete
f_y^{dyn}	dynamic yield stress of steel
f_y^{stat}	static yield stress of steel
f_{yh}	yield stress of tie steel
f_c'	compressive strength of concrete
m	number of perimeter longitudinal rebars
n	a factor corresponding to variation of elastic modulus
s	tie spacing

LIST OF SYMBOLS
(Continued)

A_s	area of longitudinal rebars
A_{cc}	area enclosed by the centerline of outer ties
$A_{e(tie)}$	net concrete area enclosed by the centerline of outer ties
B	width of concrete core
C	center-to-center distance between adjacent longitudinal rebars
E_c	modulus of elasticity
$E_{\sec}$	secant modulus of elasticity
K_e	a factor corresponding to the effective area of concrete core
K_s	the coefficient of effectiveness
P_o	compressive load capacity of concrete column
P_{occ}	design strength of concrete core
P_c	compressive load capacity of net concrete area
P_{cc}	compressive load capacity of concrete core
$P_{c(conf)}$	additional core load strength due to confinement
$P_{conc(\max)}$	maximum contribution of concrete in axial load bearing capacity
$P_{c(unconf)}$	load bearing capacity of the concrete core without confinement effect
$P_{\max}$	experimental load capacity of concrete column
Z_c	slope of descending branch in stress-strain curve of confined concrete
Z_p	slope of descending branch in stress-strain curve of plain concrete

LIST OF SYMBOLS
(Continued)

α^*	a factor that represents the combined effectiveness of the tie configuration and longitudinal rebars
σ_f	stress corresponding to axial strain of 0.0040
α	a factor representing the effect of tie configuration of compressive strength
β	constant
γ	constant
ε	concrete strain
$\dot{\varepsilon}$	straining rate
ε_{oo}	strain corresponding to strength of unconfined concrete
$\varepsilon_{50\%}$	strain corresponding to 50% of confined concrete strength
ε_c	strain corresponding to strength of unconfined concrete
ε_{co}	strain corresponding to strength of unconfined concrete
ε_{cc}	strain corresponding to strength of confined concrete
ε_{s1}	first strain corresponding to strength of confined concrete
ε_{s2}	second strain corresponding to strength of confined concrete
η	constant
ρ_s	volumetric ratio of transverse reinforcement

CHAPTER 1

INTRODUCTION

1.1 Motivation

The earth's natural resources are being consumed at a very high rate for many years. The potential depletion of resources, CO2 emissions and high energy consumption rates in the process of production, increases the necessity of recycling. All sectors of the society are responsible for these concerns, specially the construction industry.

As a major construction material, concrete is increasingly judged by its environmental impacts and reusing the readily available concrete is becoming very important. Considering that much of the US infrastructures and urban buildings now require renovation and replacement, the concrete left behind can be a valuable source of aggregate for new concrete. Such a concrete is usually called Recycled Aggregate Concrete (RAC). Through cost analyses, it is shown that recycling concrete as aggregate for new concrete production can be a cost-effective method for construction (Tam, 2008).

1.1.1 Saving Natural Resources

There are significant ecological advantages in recycling the waste concrete left behind from construction and demolition into aggregates, including protecting the natural resources as well as saving ecological environment.

Figure 1.2 shows the US annual production of sand and gravel in the past 18 years. The data was compiled from the annual U.S. Geological Survey Mineral Commodity report. More than one billion tons of construction sand and gravel valued at $7.6 billion was produced in 2008, 44% of which was used as concrete aggregates. On

the average, there is 38 million tons annual increase in sand and gravel production. Continuation of such a dramatic use of natural resources can certainly have environmental impacts.

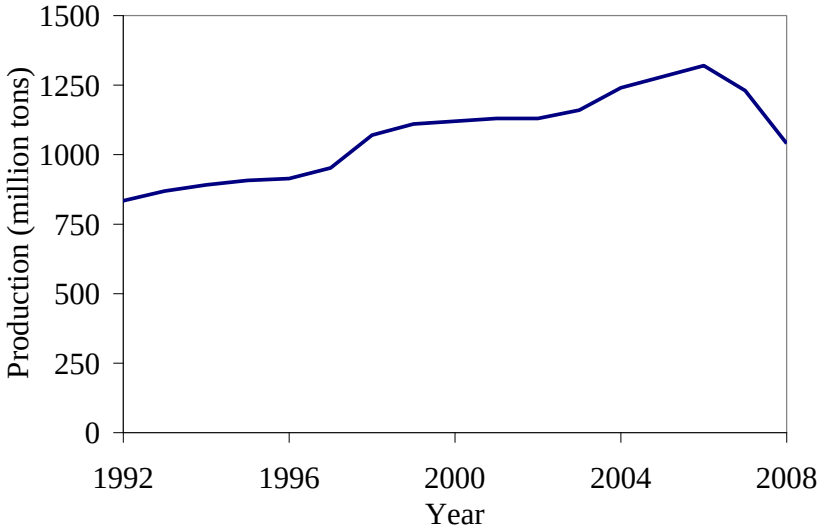

Figure 1.1 The US annual production of sand and gravel.
Source: U.S. Geological Survey Mineral Commodity report, 2009.

1.1.2 Landfills and Generation of Construction and Demolition Debris

Another significant benefit of recycling concrete and building materials is elimination of the need for landfills. According to the US Environmental Protection Agency (EPA530-R-95-019 report) in 1994 there were 1889 Construction and Demolition (C&D) waste landfills across the US. In 2004 this number dropped to 1500 (Simmons, 2006). Some states including Iowa, New Hampshire and Rhode Island have no or as low as only one available C&D waste landfill. Sometimes landfill tipping fees can be as high as $100 per ton.

A significant amount of C&D debris is annually generated in the US. Tables 1.1 and 1.2 present the amount of building-related debris generated in 1996 and 2003, respectively. In 1996, only 20 to 30 percent of the generated C&D waste was recycled

(Franklin Associates, 1998) while in 2003 this number was increased to 48% (EPA530-R-09-002, 2009). Although there is an obvious trend toward increasing the C&D recovery, 52% of the generated waste is still expensively discarded into landfills. A considerable part of the C&D debris is concrete as shown in Figure 1.2.

Table 1.1 Building-related C&D Debris Generation in 1996

Source	Residential		Nonresidential		Total (Million tons)	Percent
	Million tons	Percent	Million tons	Percent		
Construction	7	11%	4	6%	11	8%
Renovation	32	55%	28	36%	60	44%
Demolition	20	34%	45	58%	65	48%
Total	59	100%	77	100%	136	100%
Percent	43%		57%		100%	

Source: Franklin Associates, 1998.

Table 1.2 Building-related C&D Debris Generation in 2003

Source	Residential		Nonresidential		Total (Million tons)	Percent
	Million tons	Percent	Million tons	Percent		
Construction	10	15%	5	5%	15	9%
Renovation	38	57%	33	32%	71	42%
Demolition	19	28%	65	63%	84	49%
Total	67	100%	103	100%	170	100%
Percent	39%		61%		100%	

Source: EPA530-R-09-002, 2009.

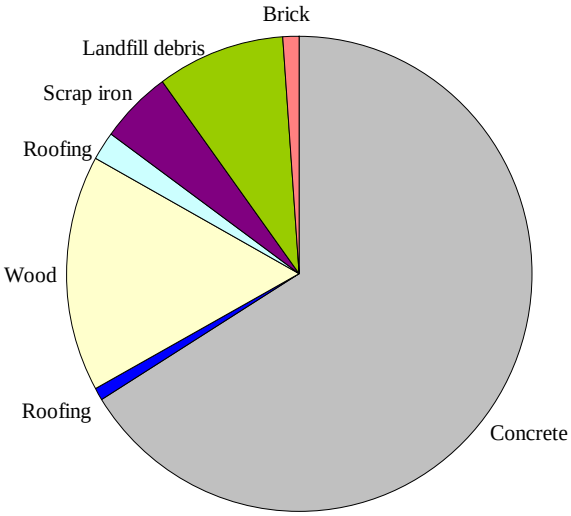

Figure 1.2 Composition of demolition debris.
Source: Franklin Associates, 1998.

1.2 Current Applications of RAC

Within the past 25 years, the use of RAC for base or sub-base applications has been widely accepted by many highway agencies. In 2004, the Federal Highway Administration (FHWA) conducted a national review on RAC. This survey showed that that in many states RAC was primarily used as fill or sub-base materials and less often as aggregates in pavement concrete, as shown in Figure 1.3.

There are many suppliers of ready rubble across the country that receive considerable demand for recycled aggregates as fill and base for construction projects such as buildings, parking lots, roads and drain ducts. Other potential uses include ballast, sub-ballast, drainage, erosion control and filter material. However, the use of recycled concrete as aggregate in structural concrete has until now been restricted by the lack of experience and knowledge on RAC behavior.

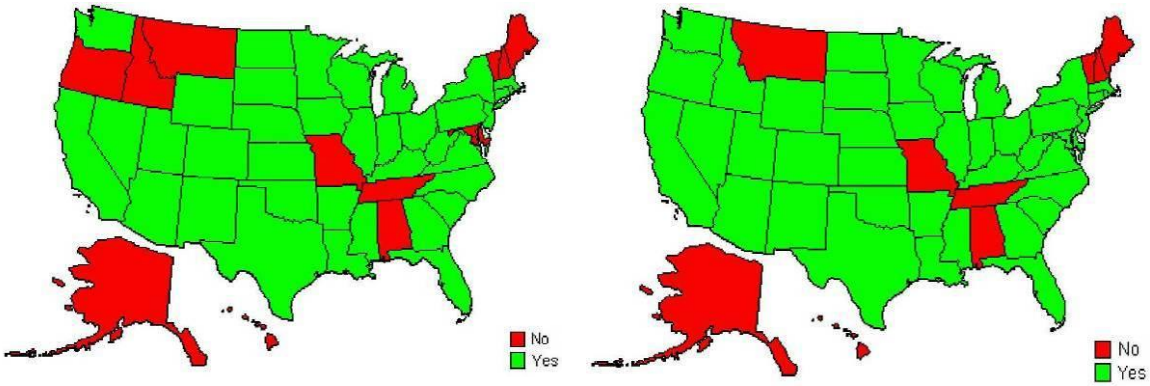

Figure 1.3 (left) States recycling concrete as aggregate, (right) States recycling concrete as aggregate base.

1.3 Significance of Research and Objective

RAC is generally acknowledged to be slightly less strong than NAC due to its higher porosity resulted from old cement mortar adhered to the surface. This has created

hesitations in the use of RAC as a structural material, confining its use to low-grade applications like road work sub-base, embankments, drainage and at the best in pavements. Widespread application of RAC, such as seismic, requires knowledge on behavioral characteristics such as ductility, material behavior under biaxial and triaxial state of stresses, loading rate, strength degradation, etc. which have not yet been sufficiently investigated.

One of the most important factors that can strongly affect the seismic response of a RAC structural member is the stress-strain characteristics. Knowledge on the behavior of RAC under different confinement configurations and derivation of a stress-strain model is very essential to analysis and design of a RAC structural member. The main objective of this research was characterizing seismic properties of RAC by developing a stress-strain model that can reasonably describe the behavior under unconfined and confined conditions.

1.4 Scope

To achieve the research objective, an experimental approach was employed. Forty-four reinforced RAC columns, 10 inches by 10 inches in section and 32 inches in height with different reinforcement configurations were built. These columns were instrumented and tested under monotonic and cyclic loading at New Jersey Institute of Technology. There were numerous parameters influencing the behavior of confined RAC, including steel and unconfined concrete strengths and lateral reinforcement pattern, size and distribution. This created unlimited experimental possibilities. Therefore the parameters were limited to square columns with normal strength RAC and rectilinear tie configurations.

1.5 Contents

Chapter 2 reviews the literature on durability and mechanical properties of plain RAC as well as the very limited research work on behavior of RAC beams. Some of the widely used stress-strain models for normal concrete are also reviewed. The experimental program is described in Chapter 3 in details. Chapter 4 summarizes the experimental results and observations as well as analysis of the effects of different variables on the behavior of RAC. Chapter 5 is dedicated to development of a model for predicting the behavior of unconfined RAC under uniaxial compression, followed by detailed presentation on developing a stress-strain model for confined RAC. Chapter 6 examines the proposed models for plain and confined RAC in flexure where predicted load-deformation of RAC beams is compared with experimental results. Conclusions and recommendations for future research are presented in Chapter 7.

CHAPTER 2

LITERATURE REVIEW

2.1 Properties of Plain RAC

Within the past several decades various researchers have studied the durability and mechanical properties of plain RAC. In this section, the available findings on properties of plain RAC is presented.

2.1.1 Compressive Strength

In general, the majority of researchers have reported 5% to 30% decrease in the compressive strength of concrete made of coarse recycled aggregate, depending on the quality of the parent concrete and mix design (Hansen and Narud 1983, Ravindrarajah and Tam 1985, Topcu and Guncan 1995, Yamato et al. 1998, Ajdukiewicz and Kliszczewicz 2002, Topcu and Sengel 2004, Rahman et al. 2009). Buck (1977) performed one of the earliest investigations on RAC properties. He used concrete from different sources as aggregates in new concrete. Keeping the water/cement ratio (w/c) constant, he observed an average of 20% less strength in the RAC. The use of water reducing admixture and higher cement content was reported to be effective in producing a stronger concrete. Rahal (2007) found 10% decrease in the compressive strength of coarse aggregate RAC while Yamato et al. (1998) observed 20%, 30% and 45% decrease in compressive strength of RAC made using 30%, 50% and 100% of coarse aggregate replacement, respectively. Not many researchers have found higher compressive strength for RAC as compared to its parent concrete. Hansen and Narud (1983) made different grades of RAC with high-strength concrete (w/c = 0.40), medium-strength concrete (w/c

= 0.70) and low-strength concrete (w/c = 1.20) as aggregate. The RAC specimens were prepared with the same mix proportions and aggregate grading as the three original concretes. All the specimens were then cured under the same conditions as the original concretes (i.e. in water at 40 degrees Celsius and tested for compressive strength after 28 days). It was shown that RAC specimens gained approximately the same strength as the corresponding parent concretes, as shown in Table 2.1 except for high-strength concrete made with low-grade recycled aggregates. They, therefore, concluded that the compressive strength of recycled concrete depends on the strength of the original concrete, and that it is largely influenced by a combination of the w/c ratio of the original concrete and that of the RAC. Poon et al. (2004) also stated that recycled aggregate has more angular shape and rough surface texture compared to natural aggregate that can lead to better bond and higher strength of RAC. They stated that to increase the compressive strength, recycled aggregates should be oven dried to create the interfacial bond between cement paste and aggregate particles.

Table 2.1 Compressive Strengths of Recycled Concrete

Series	compressive strength (MPa)											
	H	H/H	H/M	H/L[1]	M	M/H	M/M	M/L[2]	L	L/H	L/M	L/L
1	56.4	61.2	49.3	34.6	34.4	35.1	33	26.9	13.8	14.8	14.5	13.4
2	61.2	60.7			36.0		36.2		14.5			13.6
3	58.5	60.6			33.2		36.0		15.0			12.8

1 High-strength concrete made with low-strength recycled aggregates
2 Medium-strength concrete made with low-strength recycled aggregates
Source: Hansen and Narud, 1983.

The use of recycled fine aggregates is not usually favorable as it can reduce the workability and strength. Khatib (2005) observed only 10% reduction in the compressive strength of RAC when 100% of the natural sand was replaced with recycled fine

aggregates. Evangelista and de Brito (2007) found out that 30% replacement of the fine natural aggregates with recycled aggregates did not jeopardize the strength. It is also shown that blends of 50% natural and 50% recycled sands produced strengths up to 20% less than recycled concrete made with all natural sands, as shown in Table 2.2. In general, it should be noted that the use of fine recycled aggregate in RAC requires extra prudence.

Table 2.2 Compressive Strengths of Original and Recycled Concrete

	compressive strength (ksi)			
w/c	natural coarse and fine aggregate (original concrete)	recycled concrete aggregate and 100% natural sand	recycled coarse aggregate, 50% recycled fine aggregate and 50% natural sand	recycled coarse aggregate and 100% recycled fine aggregate
0.45	5.44	5.36	4.93	4.35
0.55	4.19	4.13	3.62	3.12
0.68	3.19	3.04	2.54	1.88

Source: ACI555R-01.

Rahman et al. (2009) studied the effect of recycled coarse aggregate size on compressive strength and physical properties (including water absorption and specific gravity) of RAC. They found that the compressive strength is reduced upon increasing the size of recycled coarse aggregates. Tam et al. (2009) studied the physio-chemical reactions of cement paste around aggregate for normal concrete and RAC. They found out that because of the large amount of mini-cracks in the recycled aggregate, the concrete samples with recycled aggregate substitution had lower values of physio-chemical reactions than those without recycled aggregate replacement. The mini-cracks absorb some of the required water and reduce water amount for mixing; thus hinder the hydration and reduce the concrete strength. On the contrary, Domingo-Cabo et al. (2009) reported increase in the compressive strength of RAC upon increasing the percentage of

recycled coarse aggregate. It was argued that this phenomenon was possibly caused by the greater water absorption of the dried recycled aggregates produced a smaller effective water/cement ratio. Corinaldesi and Moriconi (2009) studied the effect of silica fume and fly ash on improving compressive strength of RAC. They observed that the strength can be improved to equal or even exceed those of normal aggregate concrete by adding fly ash or silica fume to the mixture.

2.1.2 Modulus of Elasticity

Usually the modulus of elasticity of a RAC made of recycled fine and coarse aggregates is approximately 25% to 40% less that of parent concrete while for a concrete made with only recycled coarse aggregates, it is approximately 10% to 33% less, as shown in Table 2.1. For RAC made with recycled coarse aggregate, Sri Ravindrarajah and Tam (1985) observed a reduction in modulus of elasticity up to 30% while Topcu and Guncan (1995) reported 20% reduction and Domingo-Cabo et al. (2009) noticed approximately 15% reduction in the modulus of elasticity compared to the one of the parent concrete. It is concluded that the reduction in RAC modulus of elasticity with the increase of recycled aggregate content is inevitable. Berndt (2009) studied the effect of blast furnace slag and fly ash on improving mechanical properties of RAC. They suggested that concrete mixes with 50% replacement of cement with blast furnace slag may show better modulus of elasticity. Corinaldesi and Moriconi (2009) studied the effect of silica fume and fly ash on improving modulus of elasticity of RAC. They observed that the strength can be improved to equal or even exceed those of normal aggregate concrete by adding fly ash or silica fume to the mixture.

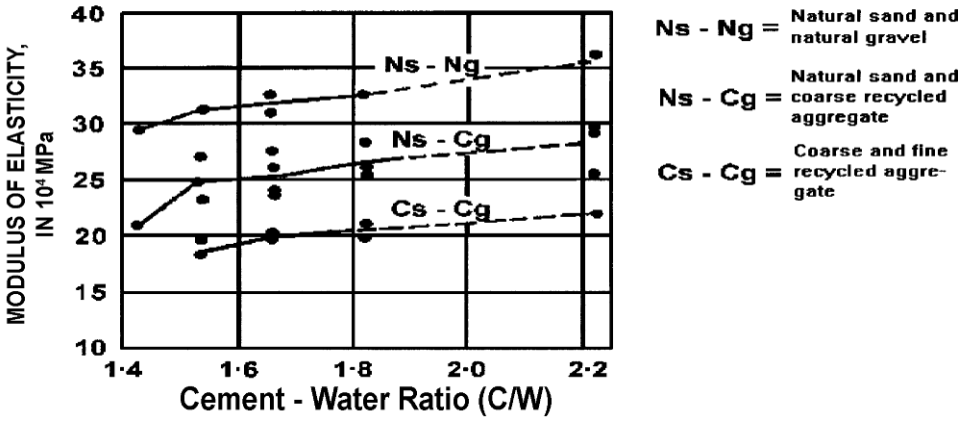

Figure 2.1 Modulus of elasticity as a function of cement/water ratio.
Source: ACI-555R-01.

2.1.3 Tensile and Flexural Strength

The effect of recycled aggregates on tensile and flexural strengths of RAC has been investigated in various studies. The majority of findings indicate that RAC made with recycled coarse aggregate and natural fine aggregate exhibits less than 10% reduction in tensile strength. RAC made with recycled coarse and fine aggregates experiences reductions in tensile strengths of 10-20% (Hansen 1986). The effect of recycled aggregate in tensile strength of concrete appears to be insignificant.

2.1.4 Bond Strength

Xiao and Falkner (2007) examined the behavior of bond between reinforcement and RAC. They reported that, for equivalent mix proportions, bond strength between RAC and reinforcement was similar to that of normal concrete, irrespective of the recycled aggregate replacement. For the case of similar compressive strength of RAC and the parent concrete, the bond strength of the RAC is even higher than the bond strength of the NAC. Eguchi et al. (2007), Etxeberria et al. (2007) and Corinaldesi and Moriconi (2009) studied the bond strength of reinforced RAC and observed no specific issues.

2.1.5 Creep and Shrinkage

According to Building Contractors Society of Japan (1978), RAC made with recycled coarse aggregate and natural sand experienced shrinkage of 20% to 50% greater than concrete made with all natural aggregates. However, RAC made with recycled coarse and fine aggregates experienced shrinkage of 70 to 100% greater than that of corresponding NAC. Sri Ravindrarajah and Tam (1985) showed that RAC creep is approximately 30% to 60% higher than that of its parent concrete. This was attributed to the higher paste content of RAC as creep of concrete is proportional to the content of paste or mortar in concrete. Domingo-Cabo et al. (2009) studied the creep and shrinkage variations in RAC with different substitution percentages (20%, 50% and 100%) of coarse aggregates, keeping cement and cement/water ratio constant. It was observed that 50% replacement of coarse aggregate caused more than 40% increase in creep and 20% increase in shrinkage. In the case of complete replacement of coarse aggregate, more than 50% increase in creep and 70% increase in shrinkage was observed.

Kou et al. (2007) showed that the 25% to 35% cement replacement with fly ash can considerably reduce the creep of RAC, as shown in Figure 2.2. This behavior was attributed to the greater long term strength development due to the pozzolanic reaction of fly ash. They also studied the effect of fly ash on shrinkage of RAC. At the age of 16 weeks, free shrinkage of the original concrete and the RAC made with 35% cement replacement with fly ash were almost identical, as shown in Figure 2.3.

2.1.6 Freeze-Thaw Resistance

Buck (1977) observed that the freeze-thaw resistance of RAC is higher than the corresponding original concrete as presented in Table 2.3. Some studies showed that

there is almost no difference between freeze-and-thaw resistances of RAC and its parent concrete (Hansen 1986).

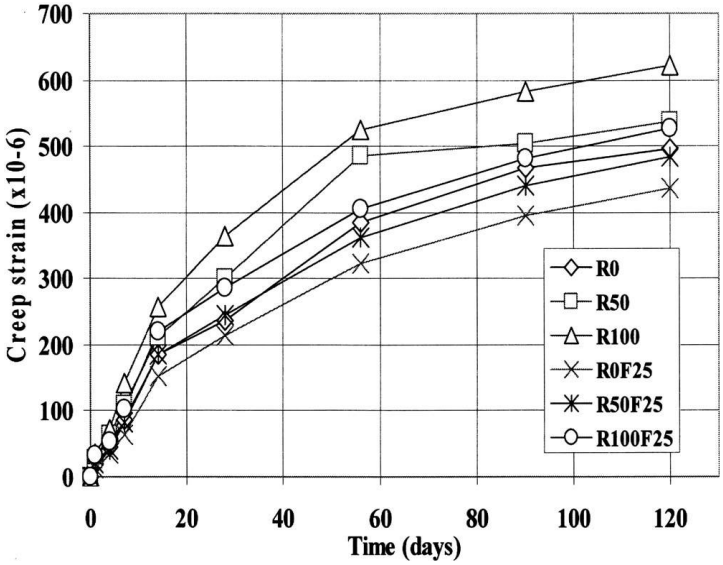

Figure 2.2 Effect of fly ash on creep of RAC.
Source: Kou et al., 2007.

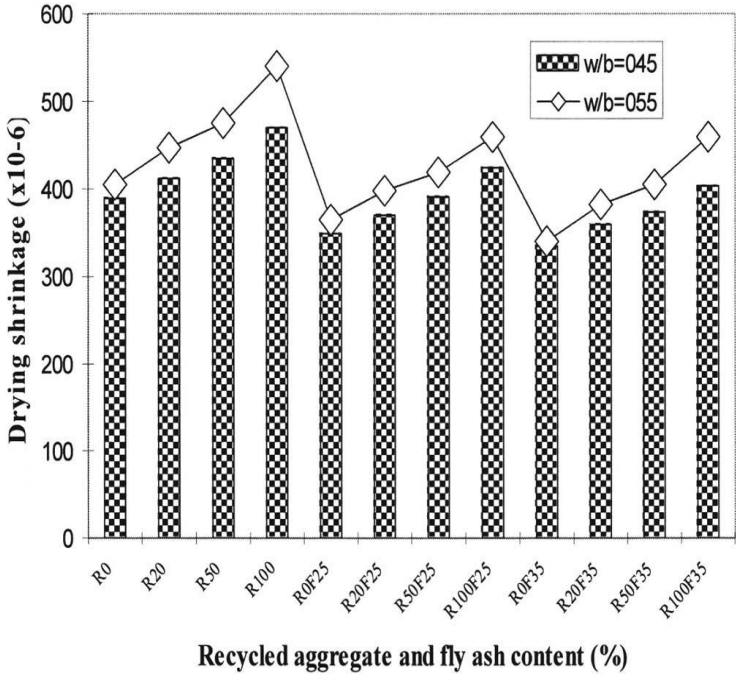

Figure 2.3 Effect of water/binder ratio and fly ash on RAC shrinkage.
Source: Kou et al., 2007.

Table 2.3 Frost Resistance of RAC

type of aggregate	No. of Cycles	Durability Factor
natural gravel and sand	300	4
coarse recycle aggregate and natural sand	300	28
coarse and fine recycle aggregate	300	30

Source: Buck, 1977.

2.1.7 Permeability, Carbonation and Chloride Ion Penetration

Due to the absorption of the old cement mortar attached to the aggregate particles, RAC is generally acknowledged to posses higher water absorption compared to normal concrete. For example, Hansen (1986) reported that concrete made of recycled aggregates with water/cement ratio of 0.5 to 0.7 shows permeability of two to five times more than normal concrete.

Levy and Helene (2004) showed that in general, the high alkaline reserve in RAC compared to normal concrete, helped the reinforcement remain passive (PH>7) much longer which can significantly delay the corrosion of the reinforcement compared to normal concrete. Corinaldesi and Moriconi (2009) also reported that RAC prepared with lower water/cement did not present evidence of corrosion danger. This observation was attributed to the low permeability of the concrete, even if a porous aggregate, such as recycled aggregate was used.

The reinforcement corrosion in concrete exposed to a chloride ion (sea water, de-icing salt, etc.) is usually of a great concern. In general, RAC has higher chloride ion penetration depth. Khan (1984) showed that the reduction in water/cement ratio can significantly improve the corrosion resistant of RAC, as shown in Figure 2.4. Kou et al. (2007) also showed that 25-35% fly ash as a substitute for cement was very effective in

reducing chloride penetration depth. Increasing curing time was also reported to be very beneficial, as shown in Figure 2.5.

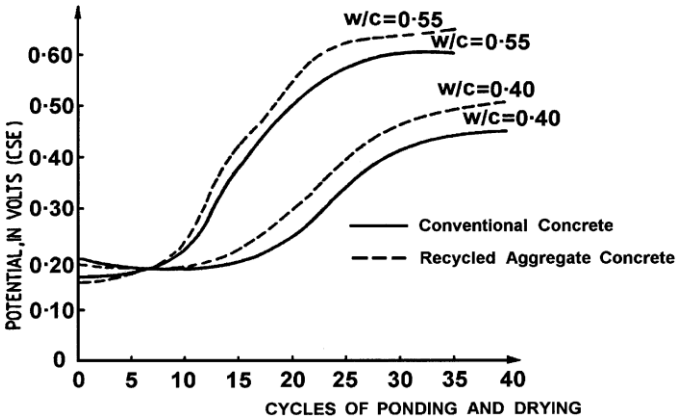

Figure 2.4 Half-cell potentials of rebars in RAC and normal concrete.
Source: Khan, 1984.

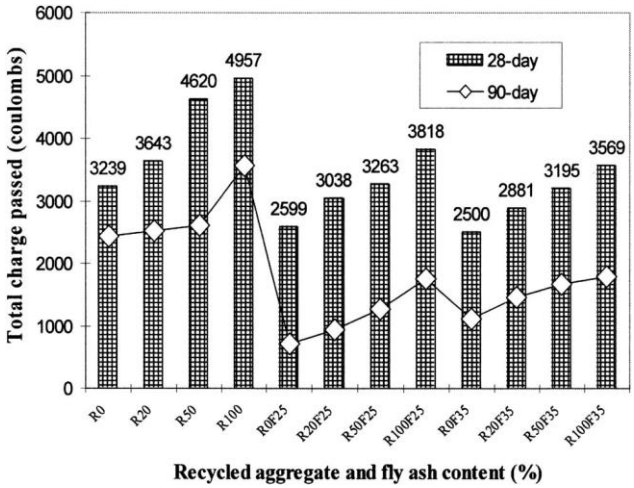

Figure 2.5 Chloride Ion penetration in normal concrete and RAC.
Source: Kou et al., 2007.

2.1.8 Density and Workability of RAC

As a result of the low density of the old cement mortar that remains adhered to the aggregate, recycled aggregate generally has a density slightly less than that of its parent concrete, as presented in Table 2.4.

Table 2.4 Specific Gravity of Natural and Recycled Aggregates

Type of aggregate	Size (mm)	SSD* Specific Gravity
Original natural gravel	4-8	2.50
	8-18	2.62
	16-32	2.61
Recycled aggregate (From high-strength concrete)	4-8	2.34
	8-18	2.45
	16-32	2.49
Recycled aggregate (From low-strength concrete)	4-8	2.34
	8-18	2.42
	16-32	2.49

*Saturated Surface-Dry
Source: Hansen and Narud, 1983.

As the recycled aggregate content of RAC increases, its workability decreases. This may also be attributed to the rougher surface texture, greater angularity and presence of mortar residue adhered to the crushed recycled aggregates compared with the smooth, rounded natural stone (Hansen and Narud 1983). In improving the workability, sometimes the use of dry-surface saturated aggregates is suggested (Hansen 1992). On the contrary, Poon et al. (2004) believed that air-dried recycled aggregate is more preferred because RAC made of saturated aggregate may bleed its excess water. For the same slump, ACI555R-01 recommends adding 5% more free water for RAC than that of conventional concrete with the same slump. In general, the use of plasticizers is always recommended.

2.1.9 Summary of RAC Properties

The compressive strength of RAC made with recycled coarse aggregate is 5-30% smaller than that of normal concrete. The use of recycled fine aggregate in RAC is usually not recommended because it can significantly reduce the workability of RAC as well as the compressive strength. Modulus of elasticity of RAC is usually 10-33% smaller than that

of normal concrete. RAC made with recycled coarse aggregate experiences up to 50% higher shrinkage and creep compared with normal concrete. The use of small water/cement ratio, flyash, silicafume on other pozzolans can significantly reduce the creep and shrinkage of RAC. The use of small water/cement ratio and pozzolans improves the durability of RAC as well. The mechanical properties and durability of plain RAC are summarized in Table 2.5.

Table 2.5 Summary of RAC Properties

property	range of expected changes from NAC
compressive strength	5% to 30% less
tensile strength	0% to 10% less
modulus of elasticity	10% to 33% less
bond strength	almost the same
drying shrinkage	20% to 50% more
creep	30% to 60% more
permeability	up to 5 times more
freeze-thaw durability	Higher
carbonation	up to 65% more
corrosion	might be slightly more

2.2 Behavior of RAC Beams

A limited number of studies on behavior of RAC beams were identified. These studies were mostly concerned about the load bearing capacity of RAC beams compared to NAC.

Mukai and Kikuchi (1988) conducted one of the earliest studies on the effect of recycled aggregates on load-bearing capacity and deformation of concrete beams. They

replaced 30% of the natural gravel with recycled coarse aggregate. The ultimate load-bearing capacity and deformation of the RAC beams were the same of reference normal concrete beam. They concluded that the use of 30% recycled coarse aggregate may be warranted for “structural concrete”.

Concrete aggregate has a significant influence on the shear behavior of reinforced beams. Thus, the shear behavior of RAC beams has been studied more than other behavioral parameters, such as flexural behavior. Fonteboa and Abella (2007) studies the shear behavior of full-size simply supported RAC beams with 50% recycled coarse aggregate. They compared the shear load-bearing capacity and deflections with those of normal concrete beams. Both RAC and normal concrete beams had the same compressive and tensile splitting strength. Although significant splitting cracks along the tension side was observed in RAC beams, there was no significant difference in the ultimate load capacities, as shown in Figure 2.6. Fathifazl et al. (2009) investigated the effect of span/depth ratio and beam size on the shear strength of RAC beams without shear reinforcement. Using the proposed mix proportioning method, several beams were made and tested. The results showed that the shear strength of RAC beams can be comparable or even superior to that of beams made entirely with natural aggregates. They did not find any major difference between the failure modes and cracking pattern of RAC and normal concrete beams. Etxeberria et al. (2007) studied the shear load-bearing capacity of RAC beams. They made 100% recycled coarse aggregate concrete beams as well as normal concrete beams. Under ultimate loads, the 100% unreinforced RAC beams showed 16% less strength than that of normal unreinforced concrete beams. They tested reinforced beams with 25% and 50% recycled coarse aggregate replacement. No reduction in the

load-bearing capacity was observed.

Ajdukiewicz and Kliszczewicz (2007) performed experimental study on bearing capacity of full-scale simply supported RAC beams under bending. They observed that on the average, the load-bearing capacity of RAC beams was almost equal to that of the corresponding normal concrete beams, as shown in Figure 2.7. The mid-span deflection under service loads, however, was up to 100% higher than that of the companion normal concrete beams. The crack patterns and failure modes were similar.

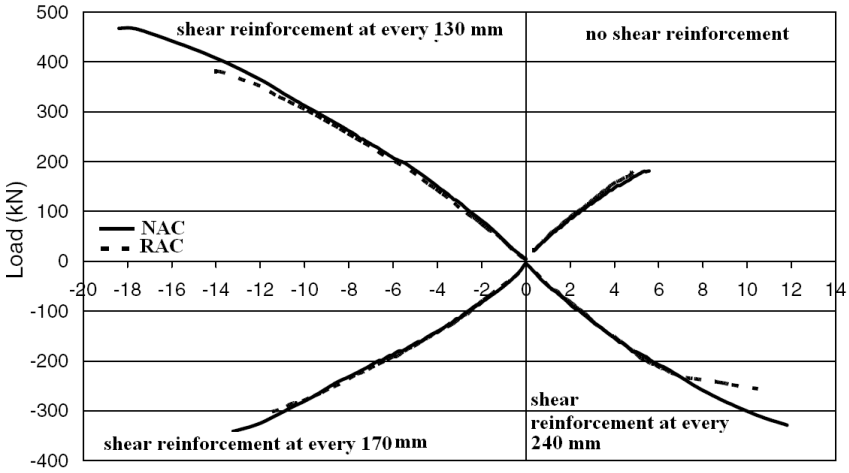

Figure 2.6 Load-deformation of RAC versus NAC beams.
Source: Fonteboa and Abella, 2007.

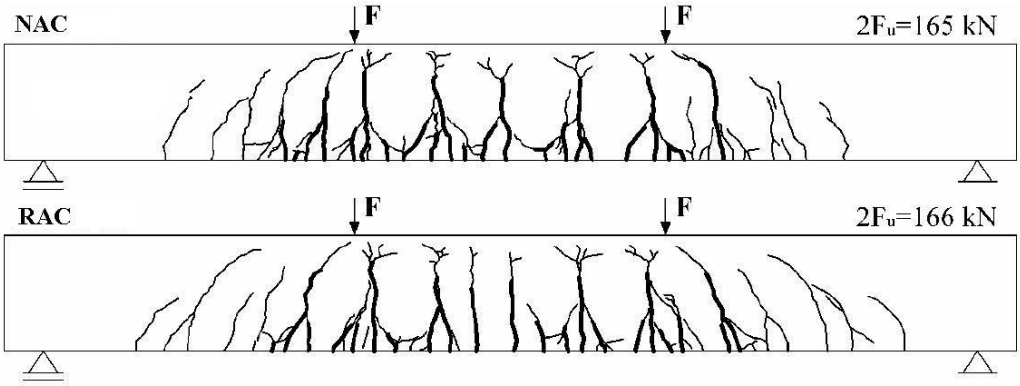

Figure 2.7 Cracking of RAC and NAC beams.
Source: Ajdukiewicz and Kliszczewicz, 2007.

Although the available research work on plain RAC mechanical properties as well as the behavior of RAC beams do not refute the use of RAC as a structural material, widespread application of RAC, such as seismic, requires knowledge on behavioral characteristics such as ductility, material behavior under biaxial and triaxial state of stresses due to lateral confinement, loading rate, strength degradation, etc. The available literature does not address these variables.

2.3 Behavior of Confined Concrete

In this section an introduction to the behavior of unconfined and confined concrete is presented. Both active and passive confinement of concrete are discussed. A summary of some of the previous experimental work on concrete confinement is presented as well.

2.3.1 Behavior of Unconfined Concrete under Monotonic Load

The compressive strength of concrete is usually obtained from cylinders with a height to diameter ratio of 2. Figure 2.8 shows the typical stress-strain behavior of concrete cylinders under axial compression. The strain at the maximum strength is approximately 0.002 in all the curves. Concrete tested in load-control setup usually fails abruptly because it can not absorb the release in strain energy from the testing machine when the load drops after the maximum stress. A displacement-control setup is therefore necessary to trace the falling branch of the stress-strain curve.

For plain concrete in compression, a ductile behavior can not be achieved because the concrete can not maintain the maximum stress with increasing deformation. However, as long as the reduction in stress is gradual (usually for low and normal strength concrete) some approximation of ductility is possible.

Ductility in reinforced concrete in compression requires ductile behavior of both reinforcement and concrete. Ductility in the reinforcement is achieved if local buckling is prevented. In concrete, the ductility can be achieved by close spacing of lateral reinforcement and proper distribution of longitudinal reinforcement around the core perimeter. Ductility is achieved when yielding of all reinforcements can be developed prior to occurrence of crushing in concrete.

2.3.2 Behavior of Unconfined Concrete under Cyclic Load

While behavior of materials and members under cyclic loading is of a prime interest in seismic design, the general load-deformation relationship under monotonic loading can give an indication of strength and ductility under cyclic loading, as shown in Figure 2.9. Since Sinha et al. (1964) it is well established that the envelope curve under repeated loading is almost identical to the curve obtained from monotonic loading. While cyclic loading tends to reduce the stiffness of the reinforced concrete structural member, the strength and ductility should not be adversely affected (Park and Paulay, 1975).

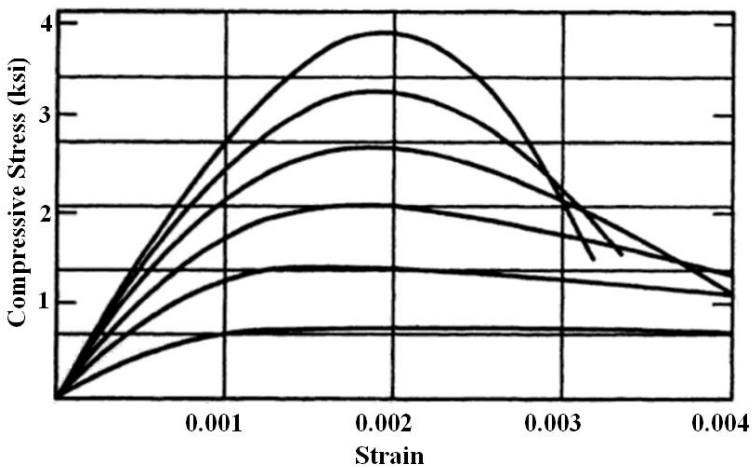

Figure 2.8 Typical monotonic stress-strain behavior of concrete.
Source: Park and Paulay, 1975.

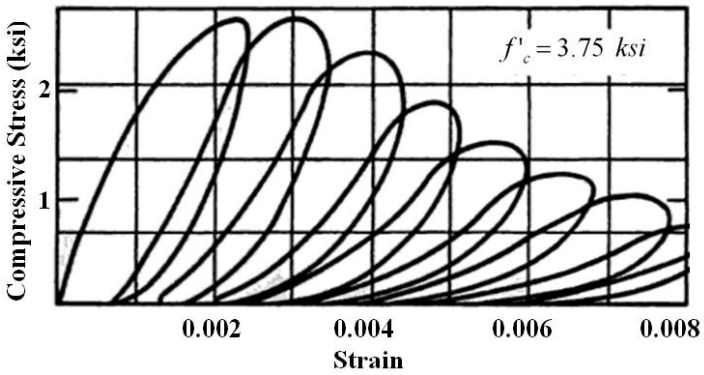

Figure 2.9 Typical cyclic stress-strain behavior of normal concrete.
Source: Sinha et al., 1964.

2.3.3 Behavior of Confined Concrete

The main factor influencing the seismic behavior of concrete is lateral confinement. The term confinement refers to the restraining effect of lateral reinforcement (in the form of hoops, spirals or hydrostatic pressure) which causes a change in the state of stresses from uniaxial to multiaxial.

Mahgoub (1997) investigated two innovative confinement techniques for columns: corrugated steel jacketing and flat steel jacketing with expansion anchors. Four large scale concrete column-base models were tested under cyclic loading. Experimental results showed that confinement enhanced the column ductility. Mechanism of confinement can be simply explained as follows: due to application of the axial compressive load, concrete expands laterally. This expansion causes internal cracking in the concrete. Lateral pressure that confines the concrete controls the extent of internal cracking and permits further axial deformation and increase in the volume prior to failure, resulting in significant enhancement in ductility and appreciable increase in strength. Confinement can be provided in either active or passive forms, as defined in the following sub- sections.

2.3.3.1 Active Confinement. Richart et al. (1928) conducted one of the earliest studies on the failure of concrete under combined stresses due to presence of confining fluid pressure and found the following relationship for the strength:

$$f_1 = f_c' + k' f_2 \tag{2.1}$$

where f_1 is the enhanced strength, f_c' is unconfined strength, f_2 is the lateral hydrostatic pressure and k' is lateral stress coefficient. The average value of k' for the tests they conducted was 4.1, as shown in Figure 2.10. Improvement in strength and ductility can be seen from Figure 2.11.

2.3.3.2 Passive Confinement. In practice, concrete is usually confined by transverse reinforcement in the form of either spirals or rectangular ties. At low levels of concrete axial strain, the transverse reinforcement is hardly stressed, meaning the confinement is not in action yet. As the transverse strains become so high that the concrete bears against the lateral reinforcement, the confinement action comes into play. Therefore, lateral reinforcement provides a passive confinement.

In passive confinement, if the confinement comes to action before the concrete reaches its maximum stress, then the stress gain may be substantial. Upon yielding of the lateral reinforcement, it can not provide additional confinement. When the confinement is delayed (due to presence of shrinkage gap at lateral reinforcement-concrete core interface or small Poisson ratio), its contribution maintains the ductility but the stress gain may be negligible.

2.3.4 Mechanism of Confinement

Figure 2.12 qualitatively illustrates the effects of different types of confinement. The

amount of lateral reinforcement in each case is such that its yield force is equal to the lateral hydrostatic pressure. Continuing effectiveness of lateral reinforcement appears to depend upon its shape. The reason for the considerable difference between the confinement by spirals and rectangular ties is illustrated in Figure 2.13 and 2.14. Due to their shape, circular spirals are in axial hoop tension and provide a continuous confining pressure around the circumference, which at large transverse strains approximates fluid confinement. Ties however, can apply confining pressure only near the corners of the section, because the concrete pressure in the lateral direction will tend to bend the ties outward. The bending resistance of the ties may restrain the concrete to some degree but this usually requires a large outward deflection, thus a significant portion of the cross section may be unconfined. In the space between the ties, the confined area of the concrete may even be further reduced due to the arching of concrete between the ties, as shown in Figure 2.14.

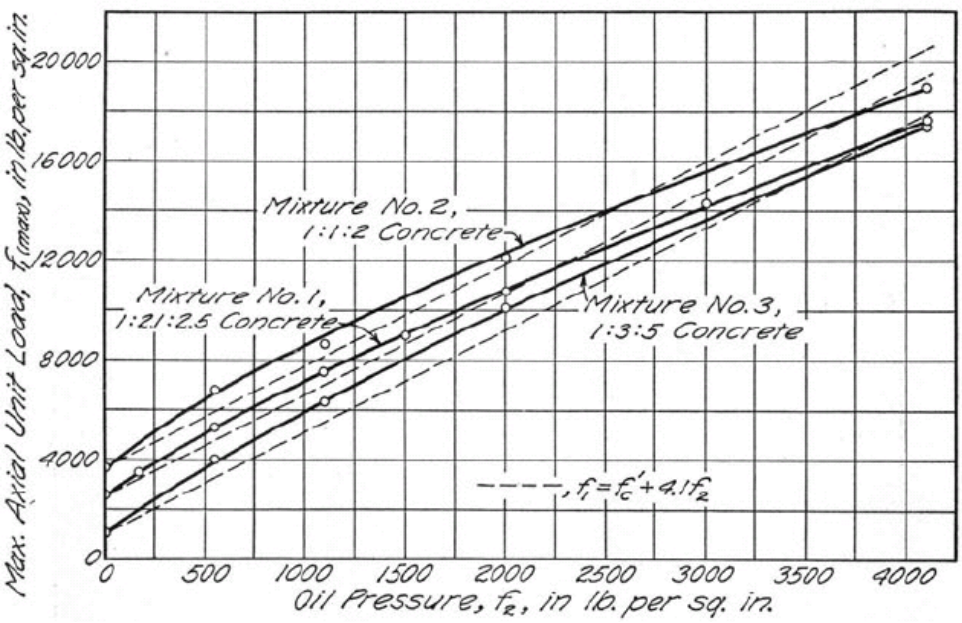

Figure 2.10 Effect of hydrostatic pressure on concrete strength.
Source: Richart et al., 1928.

2.3.5 Parameters Influencing Rectangular Confinement

As illustrated in Figure 2.12, confinement by rectangular lateral reinforcement has a little effect on the stress-strain curve until the uniaxial strength of the concrete is approached. The behavior of confined concrete at high strains depends upon the state of lateral confining pressure (Sheikh and Uzumeri, 1982). There is a number of factors determine this state of pressure, some of which are discussed in the following sub-sections.

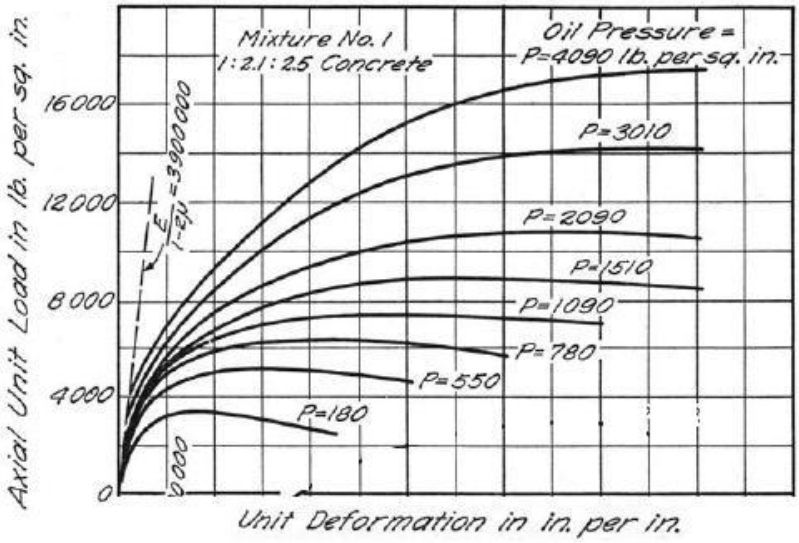

Figure 2.11 Stress-strain curves from triaxial compression tests.
Source: Richart et al., 1928.

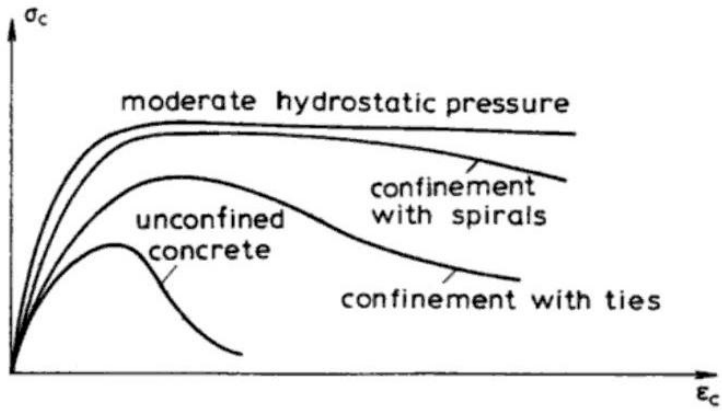

Figure 2.12 Effect of confinement on strength and ductility.
Source: Penelis and Kappos, 1997.

Figure 2.13 Confinement by circular spirals.
Source: Park and Paulay, 1975.

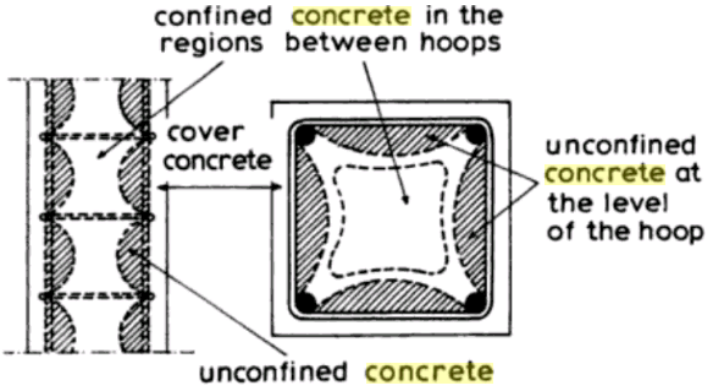

Figure 2.14 Confinement by rectangular ties.
Source: Park and Paulay, 1975.

2.3.5.1 Volumetric Ratio of Transverse Reinforcement. The ratio of the volume of lateral reinforcement to the volume of concrete is an important factor which determines the extent of lateral pressure on concrete. A high lateral reinforcement content creates high confining pressure capability and consequently can result in higher strength and ductility of the confined concrete.

2.3.5.2 Characteristics of Transverse Reinforcement. The yield strength and stress-strain relation of the tie reinforcement determines the state of confining pressure and specifies the maximum confining pressure possible. For steel with pronounced flat yield plateau, when the yielding occurs, it permits the concrete to expand without providing further confinement. The internal cracking of the concrete core then starts to

progress, resulting in drop of the strength. Transverse reinforcement with round-house stress-strain shape, on the other hand, can keep providing restraints to the concrete expansion at high lateral strains until either it fails in tension or the core concrete fails to carry any load. This results in a concrete behavior which is more ductile than the one obtained by using lateral reinforcement with flat yield plateau.

2.3.5.3 Tie Spacing. In a confined concrete member under compression, the clear distance between the ties should theoretically approach zero to achieve a uniform confinement throughout the length of the member. In a compressive member, the effectively confined zone tends to arch between the ties as previously shown in Figure 2.14. If the tie spacing is large, a significant volume of the concrete can not be confined. The area of the effectively confined concrete, therefore, seems to be directly influenced by the spacing of lateral reinforcement; the larger the spacing the smaller would be the confined core. Tie spacing also controls the local buckling of the longitudinal rebars.

2.3.5.4 Longitudinal Reinforcement. Longitudinal rebars are usually large in diameter. The ratio of rebar diameter to the tie spacing is a measure of how the rebars can effectively confine the concrete. However, the longitudinal rebars must be placed tightly against the transverse reinforcement so that they can provide the confining reactions to it. This would require each rebar to be supported by a bend of tie exactly conforming to the its size. If the rebars are spread around the perimeter of the confined core, they will help reduce the spalling of the concrete core. Close distance between each two adjacent longitudinal rebars reduces the arch effect which leads to increase the effectively confined area of the core.

2.3.5.5 Size of Ties. A larger size for lateral reinforcement should lead to more effective confinement for a given unsupported length of a tie. If the flexural stiffness of the tie bar is small, concrete pressure can easily bend the ties outward and the ties will not effectively confine the concrete. Therefore this parameter is very significant, specially if there are no longitudinal rebars to help the lateral reinforcement.

2.3.5.6 Other Factors. In addition to the variables discussed above, there are several other factors such as concrete strength, Poisson ratio, loading rate, shrinkage, creep, etc. which to less extent affect the behavior of the confined concrete. During experimental work, the effect of these variables can be eliminated through using a uniform mix, curing and loading procedure.

2.3.6 Concrete Models

No research work been carried out in order to determine the properties of confined RAC. Although it may not be directly applicable, it would be very beneficial to review some of the proposed models for confined normal concrete.

Various models for unconfined and confined concrete were proposed. Kent and Park (1971) proposed one of the earliest models for concrete confined by rectangular transverse reinforcement. Although this model did not capture any increase in the strength due to the presence of transverse reinforcement, it showed an increase in ductility. This work was the basis of further improvements by Scott et al. (1982) in which an increase in the strength was noticed. Different investigators such as Sheikh and Uzumeri (1982), Dilger et al. (1984), Ahmad and Shah (1985) and Mander et al. (1988) carried out numerous experiments on small-scale or nearly full-size confined specimens. It was observed that strength, as well as ductility of concrete substantially increase

whenever multiaxial state of stress is used, as shown in Figures 2.15 and 2.16.

The most commonly used models, among different proposed models, are those suggested by Sheikh and Uzumeri (1982) and Mander et al. (1988). This is possibly because they were based on adequate number of reliable experiments. The Sheikh and Uzumeri (1982) set of equations is applicable to rectangular sections. The equations express the gain of strength in terms of the effectively confined. The Sheikh and Uzumeri (1982) proposed equations are as follows:

$$K_s = 1 + \frac{2.73B^2}{P_{occ}}\left[\left(1 - \frac{\sum C^2}{5.5B^2}\right)\left(1 - \frac{s}{2B}\right)^2\right]\sqrt{\rho_s f_s} \tag{2.2}$$

$$P_{occ} = 0.85 f_c \times \left(B^2 - A_s\right) \tag{2.3}$$

$$\varepsilon_{s1} = 0.55 K_s f_c \times 10^{-6} \tag{2.4}$$

$$\varepsilon_{s2} = \varepsilon_{oo}\left[1 + \frac{0.81}{C}\left(1 - 5.0\left(\frac{s}{B}\right)^2\right)\frac{\rho_s f_s}{\sqrt{f'_c}}\right] \tag{2.5}$$

$$Z = \frac{0.5}{\frac{3}{4}\rho_s\sqrt{\frac{B}{s}}} \tag{2.6}$$

where n is the number of longitudinal bars, ρ_s is the volumetric ratio of the transverse reinforcement and f_s is the tensile strength of the transverse reinforcement (usually taken as the yield strength), f_c is the compressive strength of unconfined concrete and A_s is the area of longitudinal reinforcement. Other parameters are demonstrated in Figure 2.15. Due to sudden failure of the specimen or due to failure of instrumentation devices, it is difficult to obtain the curve beyond ε_{s85}. Because of lack of reliable data after this point, the region proposed by their equation may not be really reliable.

The model proposed by Mander et al. (1988) is applicable to both rectangular and circular cross sections with any transverse reinforcement type (i.e. spiral or rectangular ties). This model can be expressed by the following equations:

$$f_{cc} = f_c\left(-1.254 + 2.254\sqrt{1+\frac{7.94K_e\rho_s f_{yh}}{2f_c}} - \frac{K_e\rho_s f_{yh}}{f_c}\right) \tag{2.7}$$

$$K_e = \frac{\left(1-\sum\frac{C'^2}{6B^2}\right)\left(1-\frac{s'}{2B}\right)^2}{1-\frac{A_s}{B^2}} \tag{2.8}$$

$$\varepsilon_{cc} = \varepsilon_{co}\left[1+5\left(\frac{f_{cc}}{f_c}-1\right)\right] \tag{2.9}$$

where ρ_s is the volumetric ratio of the transverse reinforcement, A_s is the area of longitudinal rebars, f_{yh} is the yield strength of the transverse reinforcement and f_c is the strength of unconfined concrete. Other parameters are shown in Figure 2.16.

Although various researchers have proposed different models for confined concrete (Table 2.6), they all agree that the strength and ductility can be improved if:

- The lateral reinforcement bars are placed at a relatively close pitch;
- The longitudinal rebars are well distributed around the perimeter;
- The volume of lateral rebars to the volume of the concrete core is increased;
- The yield strength of the transverse reinforcement is increased.

The monotonic stress-strain curve of concrete is assumed to practically coincide with the envelope of cyclic loading stress-strain response (Kappos 1997), with some discrepancies in the range of large inelastic deformation in which the monotonic curve is

assumed to be the enveloping curve. For practical purposes, usually the most important aspect in modeling concrete under compression is the envelope curve rather than the detailed shape of the reloading and unloading curves. The test results for confined concrete by Mander et al. (1984) and other researchers support this assumption.

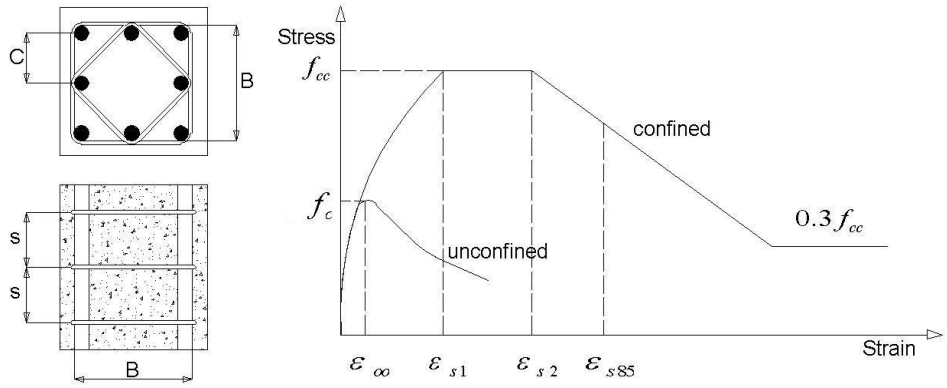

Figure 2.15 Concrete stress-strain model proposed by Sheikh and Uzumeri, 1982.

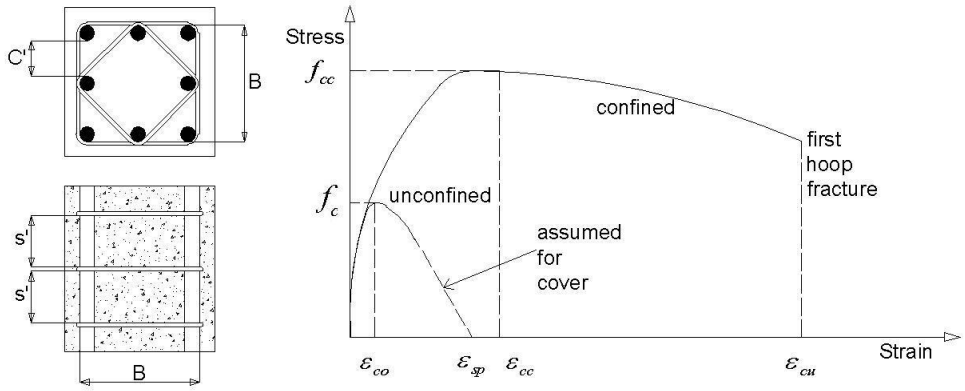

Figure 2.16 Concrete stress-strain model proposed by Mander et al., 1988.

The monotonic stress-strain curve of concrete is assumed to practically coincide with the envelope of cyclic loading stress-strain response (Kappos 1997), with some discrepancies in the range of large inelastic deformation in which the monotonic curve is assumed to be the enveloping curve. For practical purposes, usually the most important

aspect in modeling concrete under compression is the envelope curve rather than the detailed shape of the reloading and unloading curves. The test results for confined concrete by Mander et al. (1984) and other researchers support this assumption.

2.4 Summary

Earlier investigations on mechanical properties and durability of RAC are reviewed. Plain RAC with 100% aggregate replacement has 30% less strength than NAC but with the use of low water/cement ratio and pozzolans like fly ash, the strength can significantly be enhanced. Although durability is not a major issue in RAC, the use of pozzolans can enhance it. The very limited literature on behavior of RAC members is presented as well. RAC beams can exhibit load-carrying capacities comparable to normal concrete beams.

Table 2.6 Proposed Models for Confined Normal Concrete

Constitutive Model	Rising Branch	Softening Rate	$\frac{f_{residual}}{f_{cc}}$
Park et al. (1982)	$Kf_c\left[\frac{2\varepsilon_c}{\varepsilon_{cc}}-\left(\frac{\varepsilon_c}{\varepsilon_{cc}}\right)^2\right]$	$\frac{0.5}{\varepsilon_{50}-\varepsilon_{cc}}$	0.2
Sheikh and Uzumeri (1982)	$Kf_c\left[\frac{2\varepsilon_c}{\varepsilon_{s1}}-\left(\frac{\varepsilon_c}{\varepsilon_{s1}}\right)^2\right]$	$\frac{0.5}{0.75\rho_s\sqrt{\frac{b_c}{s}}}$	0.3
Kappos (1991)	$Kf_c\left[\frac{2\varepsilon_c}{\varepsilon_{cc}}-\left(\frac{\varepsilon_c}{\varepsilon_{cc}}\right)^2\right]$	$\frac{0.5}{\varepsilon_{50}-\varepsilon_{cc}}$	0.25
Saatcioglu and Razvi (1992)	$(1+K)f_c\left[2\left(\frac{\varepsilon_c}{\varepsilon_{cc}}\right)-\left(\frac{\varepsilon_c}{\varepsilon_{cc}}\right)^2\right]^{1/(1+2K)}$	$\frac{0.15f_{cc}}{\varepsilon_{85}-\varepsilon_{cc}}$	0.2
Hoshikuma et al. (1997)	$E_c\varepsilon_c\left[1-\frac{1}{n}\left(\frac{\varepsilon_c}{\varepsilon_{cc}}\right)^{n-1}\right];n=\frac{E_c\varepsilon_{cc}}{E_c\varepsilon_{cc}-f_{cc}}$	$\frac{11.2}{\rho_s\frac{f_{yh}}{f'^2_c}}$	0.5

CHAPTER 3

EXPERIMENTAL WORK

3.1 General

To study different variables influencing the behavior of confined RAC, an extensive experimental investigation was carried out. Forty-four reinforced RAC columns, 10 inches by 10 inches in section and 32 inches in height, were tested under concentric axial loading. The core dimensions (measured from center to center of the exterior ties) were kept constant at 8 x 8 inches for all column specimens.

3.2 Materials

3.2.1 Original Concrete and Recycled Coarse Aggregate (RCA)

The RCA was obtained from five cubic yards of a discarded concrete mass. To ensure easy flow of fresh RAC through the reinforcements, the maximum RCA size was limited to 3/8 inch.

Figure 3.1 briefly shows the crushing machinery utilized to produce the RCA. The crushing process was the same as crushing natural stones. The waste concrete was fed to rotary crushers and the product was passed through stacks of shaking screens to obtain the size of interest. Larger aggregates were automatically fed back to the crushers

The RCA stockpile was further screened to separate the fines (i.e., smaller than #8). Sieve analysis was carried out to make sure that the gradation of the RCA conforms to the ASTM C33-3 requirements for size of coarse aggregates, as presented in Table 3.1. Several 4 x 8 inch cylinders were sampled from the original concrete. The specimens

were cured for 7 days under standard laboratory conditions. At the age of 21 and 28 days the cylinders were tested for compressive strength where average strengths of 4.24 and 4.42 ksi were obtained, respectively, as shown in Figure 3.2 and Table 3.2. The maximum strength was almost achieved at the age of 21 days, the age at which the RCA was produced. Fast strength gain was due to the use of accelerator in concrete mix design.

Figure 3.1 Weldon Materials crushing facilities, New Jersey.

Several 4 x 8 inch cylinders were sampled from the original concrete. The specimens were cured for 7 days under standard laboratory conditions. At the age of 21 and 28 days the cylinders were tested for compressive strength where average strengths of 4.24 and 4.42 ksi were obtained, respectively, as shown in Figure 3.2 and Table 3.2. The maximum strength was almost achieved at the age of 21 days, the age at which the RCA was produced. Fast strength gain was due to the use of accelerator in concrete mix.

Table 3.1 Results of RCA Sieve Analysis

Sieve designation	Percent passed[1]	ASTM C33 requirement
3/8”	93	85-100
#4	16	10-30
#8	1	0-10
#16	0	0-5

[1] average of three samples of 1000 grams

Table 3.2 Compressive Strength of the Original Concrete

Specimen number	21-day compressive strength (ksi)	28-day compressive strength (ksi)
1	4.27	4.42
2	4.32	4.49
3	4.24	4.35
4	4.12	4.40
Average	4.24	4.42

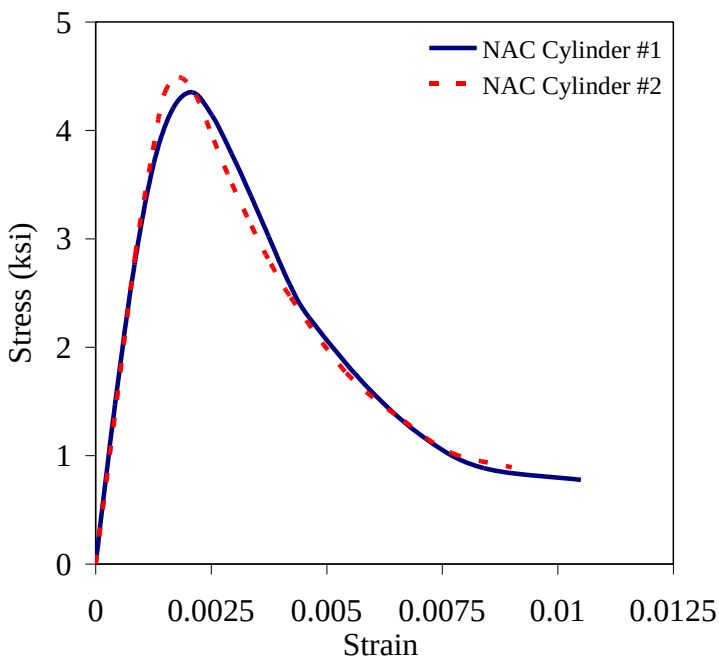

Figure 3.2 Stress-strain curves of the original concrete.

3.2.2 Column RAC mix

A small laboratory-scale 6 CF electric concrete mixer was used for mixing. To ensure homogeneity of the concrete, only 2.25 CF concrete was mixed in each load, enough to cast one column and a few 4 x 8 inch cylinder specimens at a time.

In order to improve the quality of RAC, the "Two-Stage Mixing Approach (TSMA)" recommended by Tam et al. (2005) was employed, as shown in Figure 3.3. Through experiments, Tam et al. (2005) showed that their proposed mixing procedure improved the strength of aggregate-paste Interfacial Transition Zone (ITZ), as illustrated in Figure 3.4, and hence improved the strength. During the first stage of mixing, TSMA uses half of the required water for mixing leading to formation of a thin layer of cement slurry on the surface of RCA which will permeate into the porous old cement mortar, filling up the old cracks and voids. At the second stage of mixing, the remaining water is added to complete the concrete mixing process.

The RAC mix proportions and physical properties of the constituent materials are presented in Tables 3.3 and 3.4, respectively. The mix design was obtained through a trial-and-adjustment procedure such that a 21-day compressive strength of 4.25 ± .25 ksi can be achieved while the slump remains about 5 inches. This slump was necessary to ensure easy flow of the fresh RAC through the reinforcement. In the absence of high early strength cement, 20% of the cement content was replaced by silica fume. With the use of accelerators, most of the concrete strength was achieved within the first two weeks, as shown in Figure 3.5. An average compressive strength of 4.3 ksi was obtained which was very close to the strength of original concrete. Figure 3.6 shows the mixing arrangement.

Table 3.3 RAC Mix Proportions

Cement Type I (lb)	Silica Fume (lb)	RCA (lb)	Sandclay (lb)	Water (lb)	Accelerator[1] (oz)	Water reducer[2] (oz)
12.25	3.25	60.50	53.00	10.25	4	6

[1]PRO-SET® CaCl, [2] Sikament® 86

Table 3.4 Physical Properties of Recycled Aggregates

Property	Bulk Specific Gravity	SSD Specific Gravity	Apparent Specific Gravity	Water Absorption
Quantity	2.32	2.37	2.49	5.67%

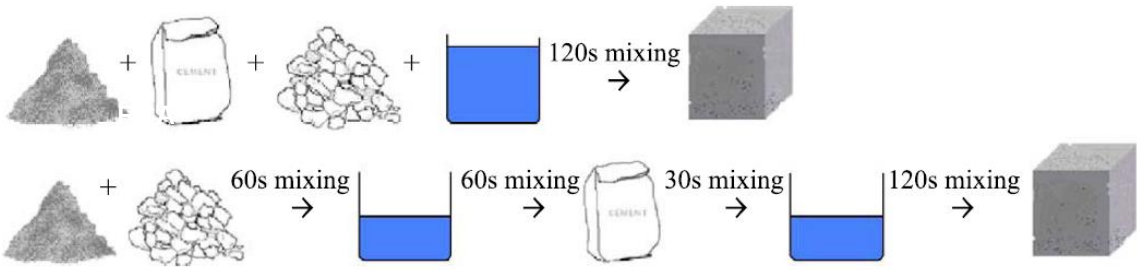

Figure 3.3 "TSAM" and normal mixing approach.
Source: Tam et al., 2005.

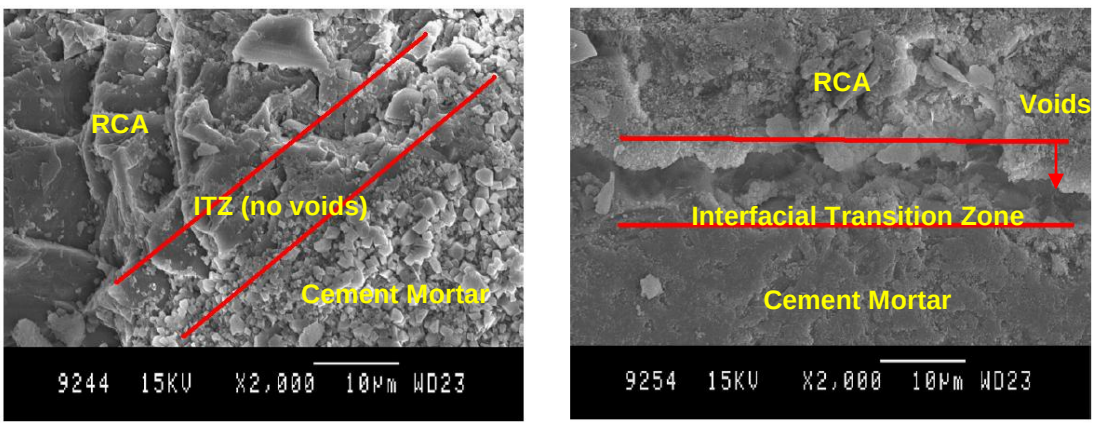

Figure 3.4 Improvement of ITZ by employing "TSMA".
Source: Tam et al., 2005.

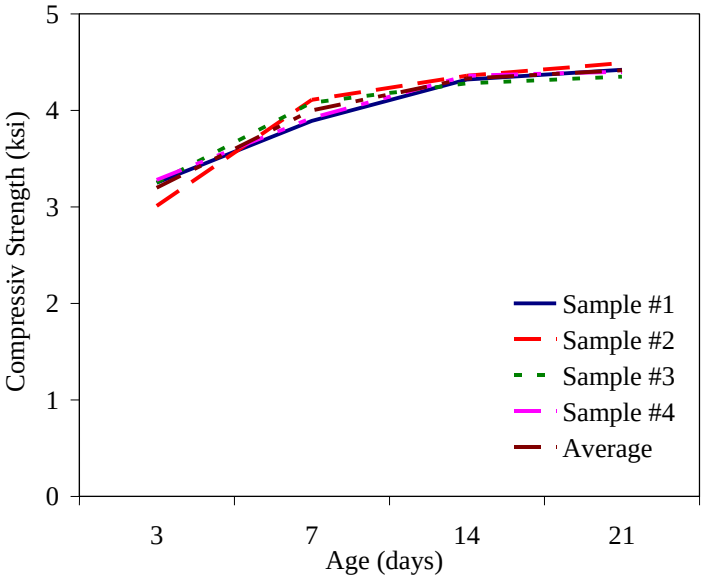

Figure 3.5 Compressive strength of the finalized RAC mix.

Figure 3.6 Mixing arrangement.

3.2.3 Plain RAC Strength

On the average, three 4 x 8 inch cylinder samples were sampled from each column batch. The samples were cured under standard condition and about seven days after testing each column, their stress-strain curves were obtained using the same MTS815 loading. It was not possible to obtain the stress-strain curves on the same day that the column was tested

because the MTS815 machine could not conveniently be setup for cylinder testing frequently. The delay in obtaining stress-strain curves, however, could not make a significant difference because most of the strength had been achieved due to the use of accelerator and silica fume. This is shown in Table 3.5 where the average compressive strengths on the day of column testing and on the day of obtaining stress-strain curves are compared. A Forney QC 50 machine, as shown in Figure 3.7, was used to solely measure the strength of RAC cylinders while the stress-strain curves were later obtained using the MTS815 loading unit. Typical stress-strain curves of the plain RAC cylinders are shown in Figure 3.8. The column designations are described in section 3.3.4.

Table 3.5 Compressive Strengths of Cylinder Samples on the Day of Column Testing vs. the Strengths on the Day of Obtaining Stress-Strain Curves

Column	Strength (ksi)		Percent difference (%)
	On the day of column testing	On the day of obtaining stress-strain curves	
A1-1	4.31	4.26	-1
A2-1	4.16	4.12	-1
A3-1	4.41	4.26	-4
B1-1	4.12	4.23	3
B2-1	4.22	4.18	-1
B3-1	4.30	4.36	1
C1-1	4.15	4.23	2
C2-1	4.25	4.34	2
C3-1	4.36	4.45	2
A1-2	4.32	4.41	2
A2-2	4.31	4.35	1
A3-2	4.05	4.05	0
B1-2	4.51	4.42	-2
B2-2	4.41	4.32	-2
B3-2	4.11	4.23	3
C1-2	4.10	4.06	-1
C2-2	4.17	4.09	-2
C3-2	4.01	4.13	3

Figure 3.7 Testing machine used for measuring strength of concrete cylinders.

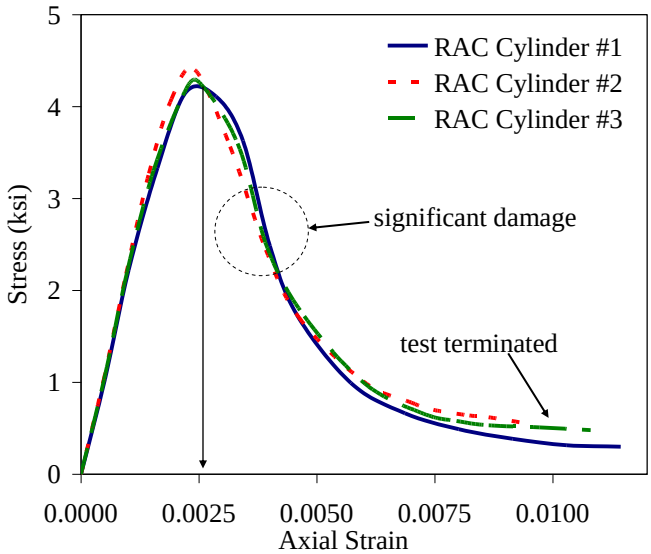

Figure 3.8 Typical stress-strain curves for plain RAC cylinders.

3.2.4 RAC Cylinders for Developing Stress-Strain model

RAC cylinders with wide range of strength were made, cured and tested to obtain their stress-strain curves, as presented in Chapter 4. Target strengths from 2500 psi to 7000 psi were considered. The proportions of these mixes were obtained by modifying the

cementitious material as well as the water, without changing the quantity of aggregate. Sufficient Water Reducer admixture was used to obtain the desired workability, as shown in Table 3.6.

Table 3.6 Mix Proportions for Target Strengths of 2500 psi to 7000 psi

Cylinder Designation	Cement Type I (lb)	Silica Fume (lb)	RCA (lb)	Sandclay (lb)	Water (lb)	Accelerator[1] (oz)	Water reducer[2] (oz)
A1 and A2	12.25	--	60.50	53.00	14.00	6	--
A3 and A4	12.25	--	60.50	53.00	13.00	6	--
A5 and A6	12.25	--	60.50	53.00	12.00	6	--
A7 and A8	12.25	--	60.50	53.00	11.00	6	4
A9 to A11	12.25	3.25	60.50	53.00	10.25	4	6
A12 and A13	14.00	3.25	60.50	53.00	10.25	4	6
A14 and A15	15.00	3.25	60.50	53.00	10.25	4	6
A16 and A17	17.00	3.25	60.50	53.00	11.00	4	8
A18 and A19	18.00	4.00	60.50	53.00	12.00	4	10
A20 and A21	21.00	4.00	60.50	53.00	12.00	4	12
A22 and A23	24.00	4.00	60.50	53.00	13.00	4	12

[1]PRO-SET® CaCl, [2] Sikament® 86

3.2.5 Longitudinal and Lateral Reinforcement

Grade 60 deformed steel rebars of #3 through #6 were used to provide a constant longitudinal reinforcement content of approximately 1.7% of the columns gross cross-sectional area. This value represent what usually is utilized in construction practice. Twelve 8-inch long samples of #3, #4 and #5 of the longitudinal rebar were tested for tension using a MTS 810 servo-hydraulic uniaxial loading unit, as shown in Figure 3.9. It is worth mentioning that steel has a very similar behavior in tension and compression.

Therefore, the results obtained for the steel under tension were assumed to be the same for compression. Some important mechanical properties of the longitudinal reinforcement samples are presented in Table 3.7. The stress-strain curves of the longitudinal reinforcement samples are shown in Figure 3.10.

Smooth 3/16-inch cold-rolled galvanized steel bars were used for the tie reinforcement. The 3/16-inch bar is relatively easy to bend which is a significant advantage over using larger sizes. Twelve 8-inch long samples were randomly taken from the wire bundles (Figure 3.9). Based on ASTM E8, tension tests were then carried out on these samples using the servo-hydraulic uniaxial MTS 810 loading unit. Some important mechanical properties of the transverse steel samples are presented in Table 3.8. The stress-strain curves of the tie steel are shown in Figure 3.10.

Figure 3.9 (left) Longitudinal rebars samples, (right) Tie steel samples.

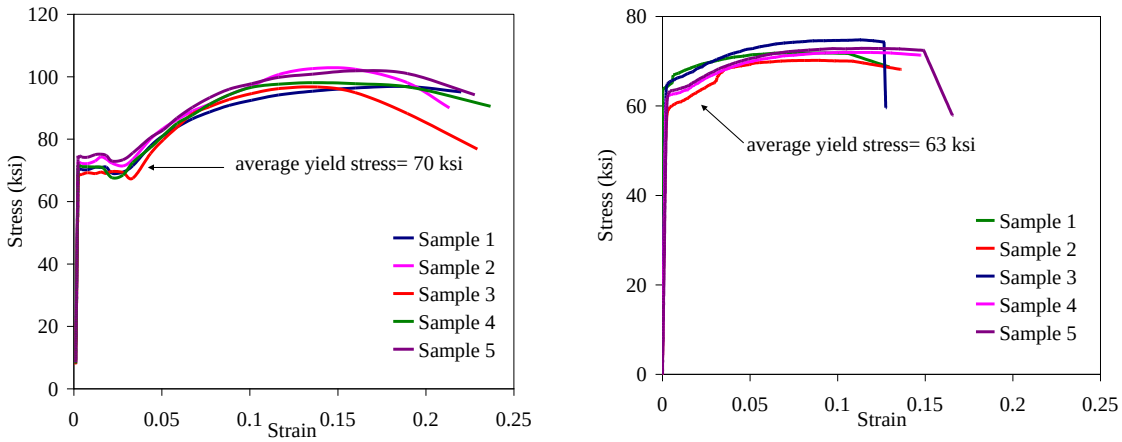

Figure 3.10 Tensile behavior of longitudinal rebars (left) and tie steel (right).

Table 3.7 Mechanical Properties of Longitudinal Reinforcement

Sample	Elastic Modulus (ksi)	Yield Stress (ksi)	Maximum Stress (ksi)	Yield Strain (ksi)	Maximum Strain
1 (bar #3)	29700	70	97	.0021	>.225
2 (bar #3)	30400	71	103	.0021	>.225
3 (bar #3)	29600	68	97	.0020	>.225
4 (bar #4)	29400	70	98	.0021	>.225
5 (bar #4)	30200	72	102	.0020	>.225
average	29900	70	99	.0210	>.225

Table 3.8 Mechanical Properties of Tie Reinforcement

Sample	Elastic Modulus (ksi)	Yield Stress (ksi)	Maximum Stress (ksi)	Yield Strain (ksi)	Rupture Strain (ksi)
1	30200	64	72	.0025	>.12
2	29800	59	70	.0025	>.12
3	29000	65	75	.0023	>.12
4	29100	62	72	.0024	>.12
5	30100	63	74	.0022	>.12
average	29600	63	73	.0024	>.12

3.3 Fabrication of Columns

Forty-four columns were cast in sets of five. In order to obtain a uniform distribution of stresses in the instrumented region and to provide adequate length for the development of failure mechanism, a width-to-length ratio of 1/3 was considered. The columns were 32 inches high and had square cross section of 10 inches by 10 inches.

3.3.1 Forms

15/32-inch plywood was used to make the forms, as shown in Figure 3.11. For easy removal of the forms, the walls were first covered in 6 mil plastic sheet. Through practice it was found that the plastic sheet may not be appropriate as it would get ripped by the cages during placement. Painting and oiling the plywood was a better alternative.

Figure 3.11 Plywood forms.

3.3.2 Casting and Curing

Each column was cast vertically in six layers. A concrete vibrator was used to thoroughly consolidate the core and the cover concrete. The columns were kept under laboratory conditions for 24 hours. The forms were then removed and the columns were properly

covered by plastic sheets. After four days the covers were removed and the columns were exposed to laboratory condition. The age of the columns at the time of testing varied between 21 days to 28 days. The forms were sufficiently painted prior to each use.

3.3.3 Reinforcing Cages

Three different lateral reinforcement configurations shown in Figure 3.12 were under consideration. Such configurations are frequently used in construction practice. Configuration “A” had four longitudinal rebars and one tie while configuration “B” had 8 longitudinal rebars with two ties at the same level. Configuration “C” had 12 longitudinal rebars with three ties. These uppercase letters were used to designate the columns. For all of the columns, the size of cages from center to center of the outer tie was 8 x 8 inches. The length of the longitudinal rebars was 30 inches. A one-inch thick concrete cover was considered for the top and bottom of the columns, as shown in Figure 3.13. This was necessary to ensure that the longitudinal rebars were not in direct contact with the load which may cause local rebar buckling. Details of reinforcement are presented in Table 3.9. From the table, by utilizing three different tie spacings, quite wide range of transverse reinforcement volumetric ratio (i.e., volume of the transverse reinforcement to the volume of the core between two adjacent ties) was achieved. In order to facilitate the development of yield strength of the steel wires, 135-degree hooks with at least 3-inch extension were provided. In total, more than 2300 ties were fabricated. Sample cages are shown in Figure 3.14.

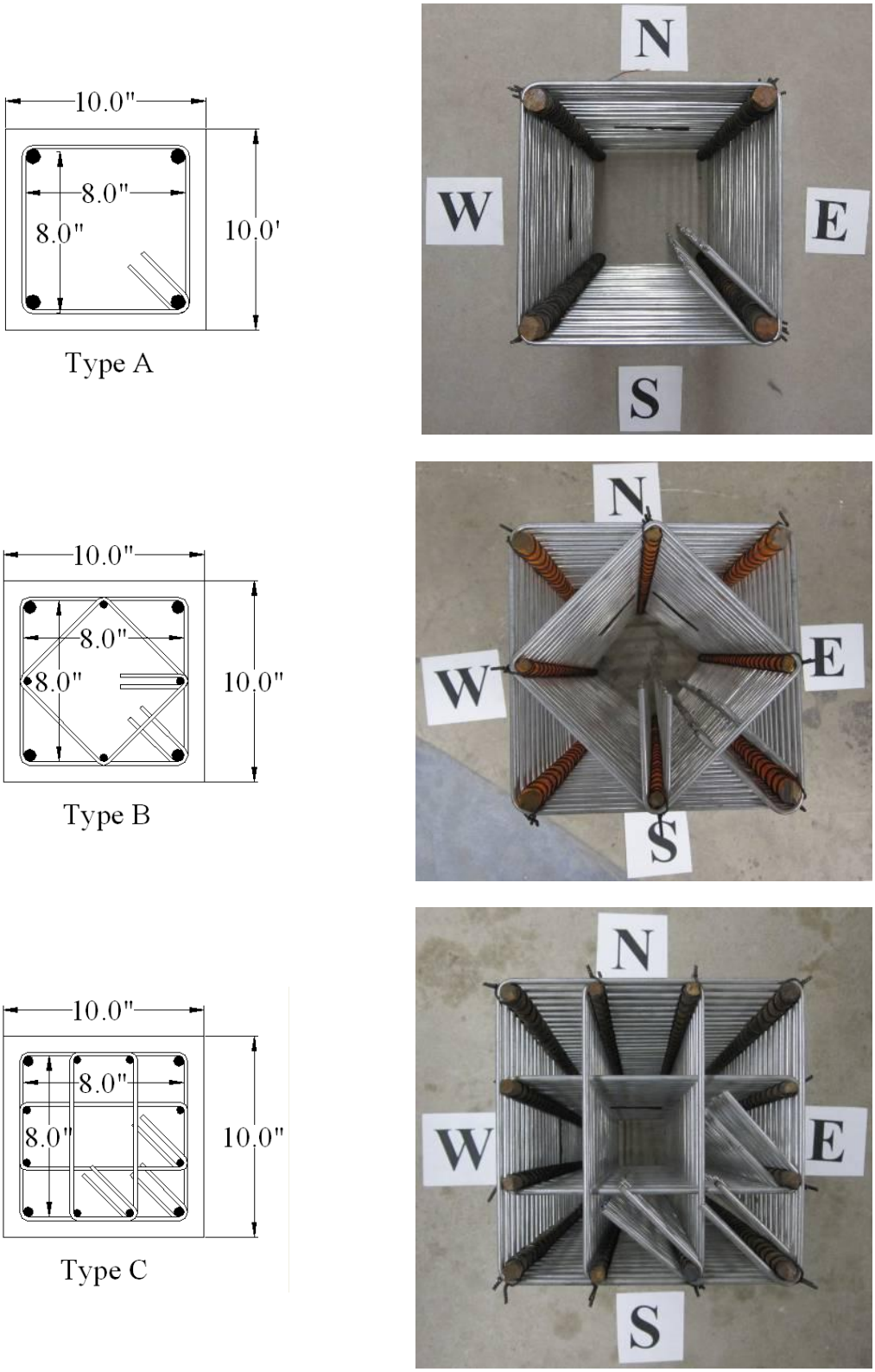

Figure 3.12 Tie configurations.

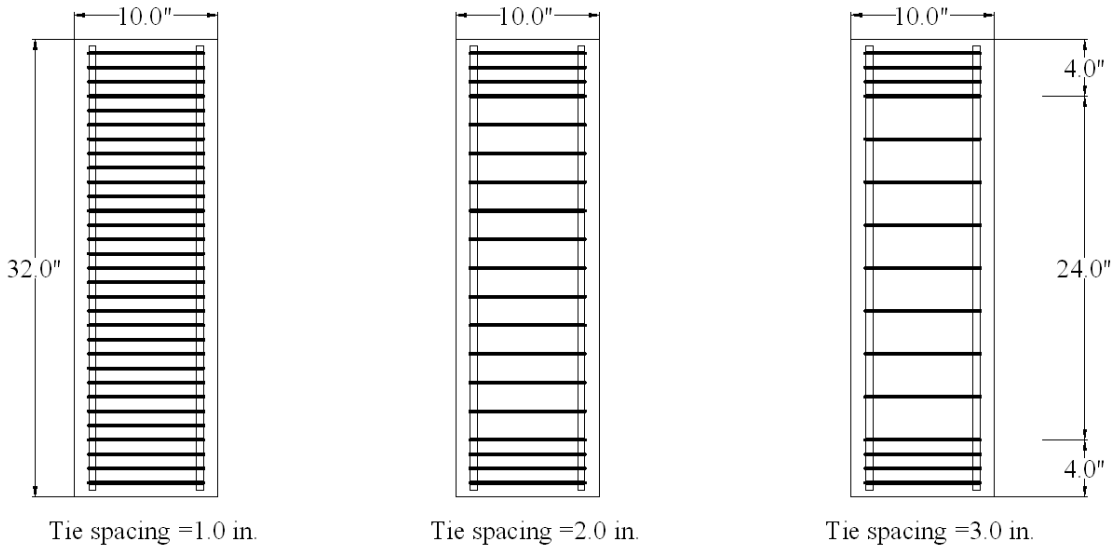

Figure 3.13 Tie spacing and end extra reinforcement.

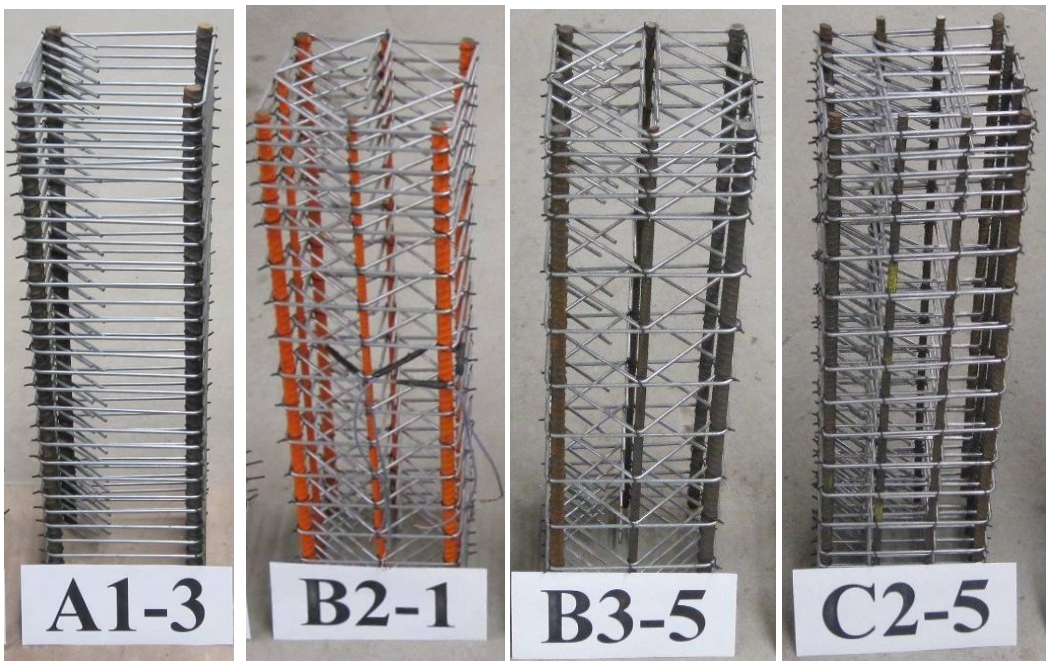

Figure 3.14 Example cages.

3.3.4 Column Designation

In the alphanumeric characters in the titles of the columns (e.g., B2-4) the letter represents the lateral reinforcement pattern (i.e., A, B or C, as previously shown in Figure 3.12). The first number after the letter indicates the tie spacing in inches (i.e., 1, 2 or 3, as shown in Figure 3.13). The number after the dash sign is the specimen sequence number.

Table 3.9 Details of the Specimens

specimen	longitudinal steel			transverse steel		Concrete Strength
	A_s (in^2)	ρ_{gross} (%)	ρ_{core} (%)	s (in)	ρ_s (%)	f_c (ksi)
A1-1	1.76	0.018	.028	1	0.88	4.26
A1-2	1.76	0.018	.028	1	0.88	4.41
A1-3	1.76	0.018	.028	1	0.88	4.17
A1-4	1.76	0.018	.028	1	0.88	4.28
A1-5	1.76	0.018	.028	1	0.88	4.29
A2-1	1.76	0.018	.028	2	0.44	4.12
A2-2	1.76	0.018	.028	2	0.44	4.35
A2-3	1.76	0.018	.028	2	0.44	4.28
A2-4	1.76	0.018	.028	2	0.44	4.46
A3-1	1.76	0.018	.028	3	0.29	4.26
A3-2	1.76	0.018	.028	3	0.29	4.05
A3-3	1.76	0.018	.028	3	0.29	4.24
A3-4	1.76	0.018	.028	3	0.29	4.16
B1-1	1.68	0.017	.026	1	1.51	4.23
B1-2	1.68	0.017	.026	1	1.51	4.42
B1-3	1.68	0.017	.026	1	1.51	4.34
B1-4	1.68	0.017	.026	1	1.51	4.21
B1-5	1.68	0.017	.026	1	1.51	4.39
B2-1	1.68	0.017	.026	2	0.75	4.18
B2-2	1.68	0.017	.026	2	0.75	4.32
B2-3	1.68	0.017	.026	2	0.75	4.18
B2-4	1.68	0.017	.026	2	0.75	4.35
B2-5	1.68	0.017	.026	2	0.75	4.47

Table 3.9 Details of the Specimens (Continued)

specimen	longitudinal steel			transverse steel		Concrete Strength
	A_s (in^2)	ρ_{gross} (%)	ρ_{core} (%)	s (in)	ρ_s (%)	f_c (ksi)
B3-1	1.68	0.017	.026	3	0.50	4.36
B3-2	1.68	0.017	.026	3	0.50	4.23
B3-3	1.68	0.017	.026	3	0.50	4.38
B3-4	1.68	0.017	.026	3	0.50	4.42
B3-5	1.68	0.017	.026	3	0.50	4.16
C1-1	1.68	0.017	.026	1	2.10	4.23
C1-2	1.68	0.017	.026	1	2.10	4.06
C1-3	1.68	0.017	.026	1	2.10	4.26
C1-4	1.68	0.017	.026	1	2.10	4.17
C1-5	1.68	0.017	.026	1	2.10	4.28
C2-1	1.68	0.017	.026	2	1.05	4.34
C2-2	1.68	0.017	.026	2	1.05	4.09
C2-3	1.68	0.017	.026	2	1.05	4.41
C2-4	1.68	0.017	.026	2	1.05	4.27
C2-5	1.68	0.017	.026	2	1.05	4.19
C3-1	1.68	0.017	.026	3	0.70	4.45
C3-2	1.68	0.017	.026	3	0.70	4.13
C3-3	1.68	0.017	.026	3	0.70	4.19
C3-4	1.68	0.017	.026	3	0.70	4.33
C3-5	1.68	0.017	.026	3	0.70	4.25
					Max	4.47
					Min	4.05
					Average	4.27

3.3.5 Glass Fiber Reinforced Polymer (GFRP) confinement

It was intended to localize the failure to the centrally instrumented region of the columns as much as possible. For this purpose additional ties were considered for each end of the column specimens, as shown in Figures 3.13 and 3.14. For Type B and C columns where

spacing was 1 inch, no extra ties were provided because practically there was no sufficient room available for additional ties. The column ends were further confined with two layers of 6-inch wide SikaWrap® GFRP laminates, as shown in Figure 3.15. Depending on the smoothness of the surface, Sikadur Hex 300® or Sikadur Hex 30® epoxies were used to bond the laminates to the column surface. As shown in Chapter 4, the utilized technique was relatively successful and in many columns most of the failures took place within the instrumented region. The epoxy used to bond the laminates was a hazardous material and extreme precautions had to be exercised in its application.

Figure 3.15 Additional end confinement using GFRP laminates.

3.4 Instrumentation

3.4.1 External Instrumentation

Direct Current Differential Transformers (DCDTs) were utilized to monitor the axial deformation of the columns. In order to eliminate end effects, only 20 inches of the mid region of the columns was instrumented (Figure 3.16). Individual DCDTs were first assigned to monitor the axial deformation on each side of the columns because it was

thought that the readings might be significantly different. During the first few tests, however, it was observed that the readings are very close so there was no real need for more than one measurement.

A holding frame was fabricated to place the DCDTs in the position of interest. Since the lateral expansion of the column could break the frame or cause disturbance in readings, compressive springs were placed on the frame such that the frame could expand freely upon lateral expansion of the columns. The DCDTs were placed some distance away from the specimen to safeguard them from disturbance of the falling debris. The sensors were frequently calibrated during the experiments.

For monitoring axial deformations of the RAC cylinders, an average measurement obtained by two 4-inch extensometers was used, as shown in Figure 3.16.

Figure 3.16 Measuring axial deformation of cylinder by a pair of extensometers.

3.4.2 Internal Instrumentation

In the absence of more resilient and environment-tolerant measurement gauges, some of the ties were instrumented using Vishay Micro-Measurements CEA-06-240UZ-120

electrical strain gauges, as shown in Figure 3.17. CEA strain gauges are a general-purpose family of strain gauges encapsulated in polyimide which are widely used in advance experimental stress analysis. This type of strain gauges are very delicate and may not be really appropriate for use in concrete work where it is exposed to hard objects (coarse aggregates, rod and vibrator for proper consolidation, etc).

Surface preparation and installation of the electrical strain gauges on the small surface of 3/16-inch ties required utmost precision and experience. The small diameter of ties compared to the width of strain gauges could create bonding issues. The strain gauge edges were trimmed as much as possible. Some trial installations on 8-inch long specimens were conducted and tested under the MTS 810 loading unit, at a slow rate of 15 lb per second. The data was collected using a Micromeasurement P3® Strain Indicator, as shown in Figure 3.18. In some of the trial specimens, premature failure of the soldering tabs or delamination of the strain gauge occurred. To avoid losing data during testing the RAC columns due to such incidents, one additional strain gauge was installed on each tie. Figure 3.19 shows the location of strain gauges on the ties. In each column one tie was instrumented. In practice, it was found that this type of strain gauges was not suitable for the purpose as installation and handling was difficult. Only columns with sequence number “1” were instrumented.

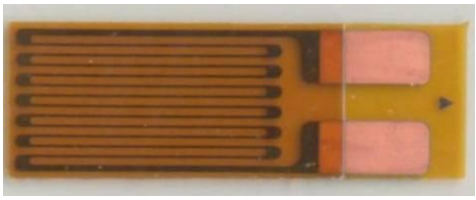

Figure 3.17 CEA-06-240UZ-120 electrical strain gauge.

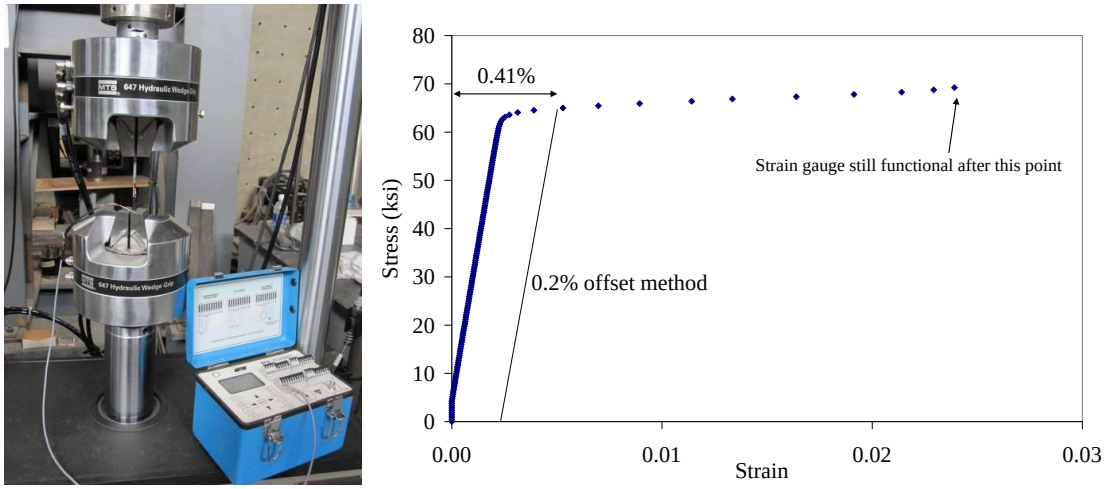

Figure 3.18 Examination of bond quality of a strain gauge installed on 3/16" steel wire.

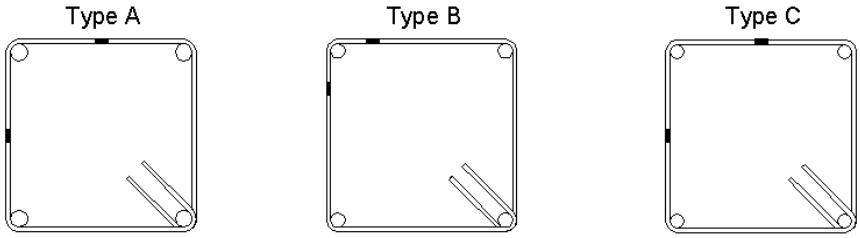

Figure 3.19 Location of strain gauges on ties.

3.5 Test Setup

3.5.1 Capping

To ensure good contact with the loading heads, the column ends were capped with hydro-stone® gypsum cement, as shown in Figure 3.20. This product is self-leveling when poured and its strength can exceed 10,000 psi after only few hours. The concrete cylinders were capped with Sulphur.

3.5.2 Positioning

Ceiling crane was used to lift the column specimens, which weighed approximately 320 lbs each. To ensure uniform load applications, one-inch thick steel plates were placed

between the column and the MTS815 upper head.

3.5.3 Loading Unit and Data Acquisition System

All concrete specimens were concentrically loaded in the 1000-kips MTS815 servo-hydraulic loading unit, as shown in Figure 3.20. All test loads and actuator positions were controlled via MTS TestStar® digital controller. Automatic loading processes were also programmed and introduced to the MTS machine through TestWare® software.

Figure 3.20 Application of hydro-stone® gypsum cement.

The load and displacement generated by the loading unit as well as the DCDT and the internal sensor data were fed to a System 5000® data acquisition hardware which was programmed using StrainSmart® software. The data were recorded at 10-second and 0.01-second intervals for the low-rate and fast-rate loadings, respectively.

3.6 Loading Procedure

A 2000 lb compressive load was initially applied on each column and all the sensors zeroed. Then at a rate of 1000 lb per second, up to 25% of the expected strength, a loading-unloading loop was applied on each column to further consolidate the hydro-

stone caps. The main loading stage then was conducted. In order to obtain the full range of load-displacement curves, a displacement-control loading approach was utilized. In the case of static loading, the columns were pushed to failure at a strain rate of 1.6×10^{-5} in/in/s. The repeatability of test results was verified by testing two columns of each type. Monotonic tests were also conducted using higher straining rate of 1.6×10^{-2} in/in/s. Similar to static loading, two columns of the same type were tested to ensure the repeatability of the results.

Figure 3.21 1000-kip MTS815 servo-hydraulic loading unit and other hardware.

In the case of cyclic loading, the MTS815 unit was programmed to apply five cycles such that the loading-unloading loops were uniformly distributed across the axial deformation range. The cycles were applied at a rate of 1.6×10^{-1} in/in/s that is the strain rate normally used in seismic testing (Kappos, 1997). Seven columns were tested under cyclic loading: A1-5, B1-5, B2-5, B3-5, C1-5, C2-5 and C3-5. Testing of column B2-5 had to be prematurely terminated due to technical difficulties with the MTS loading unit.

CHAPTER 4

ANALYSIS AND DISCUSSION OF TEST DATA

Results of the experimental work are presented in this chapter, primarily in the form of force-deformation and stress-strain curves. Both behaviors of cover and core concrete are discussed in details and their individual contributions to the load bearing are calculated.

4.1 Test Observations

4.1.1 Plain RAC Cylinders

Figure 4.1 shows the typical stress-strain curve of RAC cylinders versus a few widely used models for normal concrete. By comparing the RAC experimental stress-strain curve and the theoretical curve for normal concrete the following statement can be made:

- RAC cylinders demonstrate relatively smaller modulus of elasticity;
- The strain corresponding to the maximum strength is approximately 0.0025 for RAC that is appreciably more than the average value of 0.002 for normal concrete;
- Compared to normal-strength normal aggregate concrete, the change in modulus of elasticity (i.e., variation in the slope of the ascending branch) is less significant;
- The cracking and compressive failure of the plain RAC cylinders were not different from those of normal concrete under compression. Most often shear-type failure was observed for both, as shown in Figure 4.2.

4.1.2 Reinforced RAC Column

Separate DCDTs were used to measure the axial deformations on each side of the columns. The differences between the readings were insignificant, as shown in Figure 4.3 for column B1-2. This was primarily due to the concentric nature of the loading,

precision in fabrication of the reinforcement cage and thorough consolidation of the concrete. Due to the fear of damaging the DCTDs, they were removed at relatively small axial deformations.

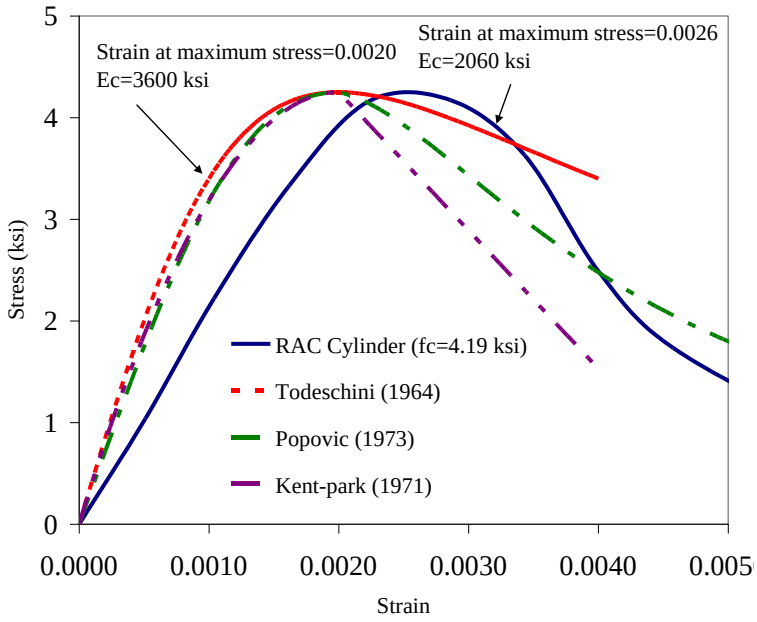

Figure 4.1 RAC stress strain curves vs. models for normal concrete.

Figure 4.2 Typical failure of RAC and normal concrete cylinders.

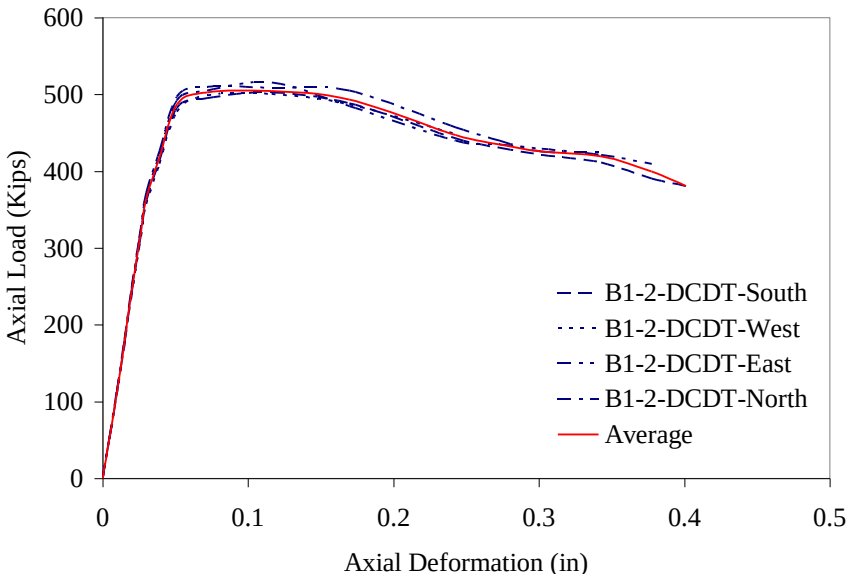

Figure 4.3 Axial deformation of column B1-2.

Typical failure and load-deformation of the columns under static loading were similar to those shown in Figures 4.4 to 4.6 for columns A1-1, B2-2 and C3-2 tested. The behavior of the RAC columns was continuously observed during the testing, particularly for development of cracks in vertical direction. The general behavior of the RAC columns was similar to that of normal reinforced concrete columns under axial load, reported by various researchers (Sargin 1971, Kent and Park 1971, Vallenas et al. 1977, Sheikh and Uzumeri 1982, Mander 1984). The first visual indication of distress in the columns was the development of vertical cracks in the corners. Very similar to the reported value of 0.0015 to 0.0020 for normal concrete, the vertical cracks started appearing at all four corners of the columns at a longitudinal strain of approximately 0.0020. As the loading proceeded, faster growth of the vertical cracks occurred. These cracks, however, started widening at a longitudinal strain of approximately 0.0030 and large slabs of the cover concrete gradually started spalling off in a rather simultaneous

manner on all sides. The maximum load reached at an average strain of 0.0035.

Up to the maximum load, the transverse reinforcement added very little to the strength of the columns. Shortly after the maximum load was reached, the columns with smaller tie spacing and higher volumetric ratio of lateral reinforcement immediately failed, accompanied by crushing of the concrete, buckling of the longitudinal rebars and slippage/fracture of the tie steel. The columns with larger tie spacing and smaller volumetric ratio of lateral reinforcement, however, exhibited a significant ductility and started to fail only when they achieved a significant axial deformation.

The nature and sequence of compressive failure of RAC columns were not different with that of normal concrete reported by various researchers (Sargin 1971, Kent and Park 1971, Vallenas et al. 1977, Sheikh and Uzumeri 1982, Mander 1984): the cover spall off, crushing of the concrete core and buckling of longitudinal rebars followed by fracture and possibly hook slippage of the lateral reinforcement. The majority of the columns failed in the mid-height. However, some column failed on top, mainly due to inadequate bonding strength of the GFRP laminates.

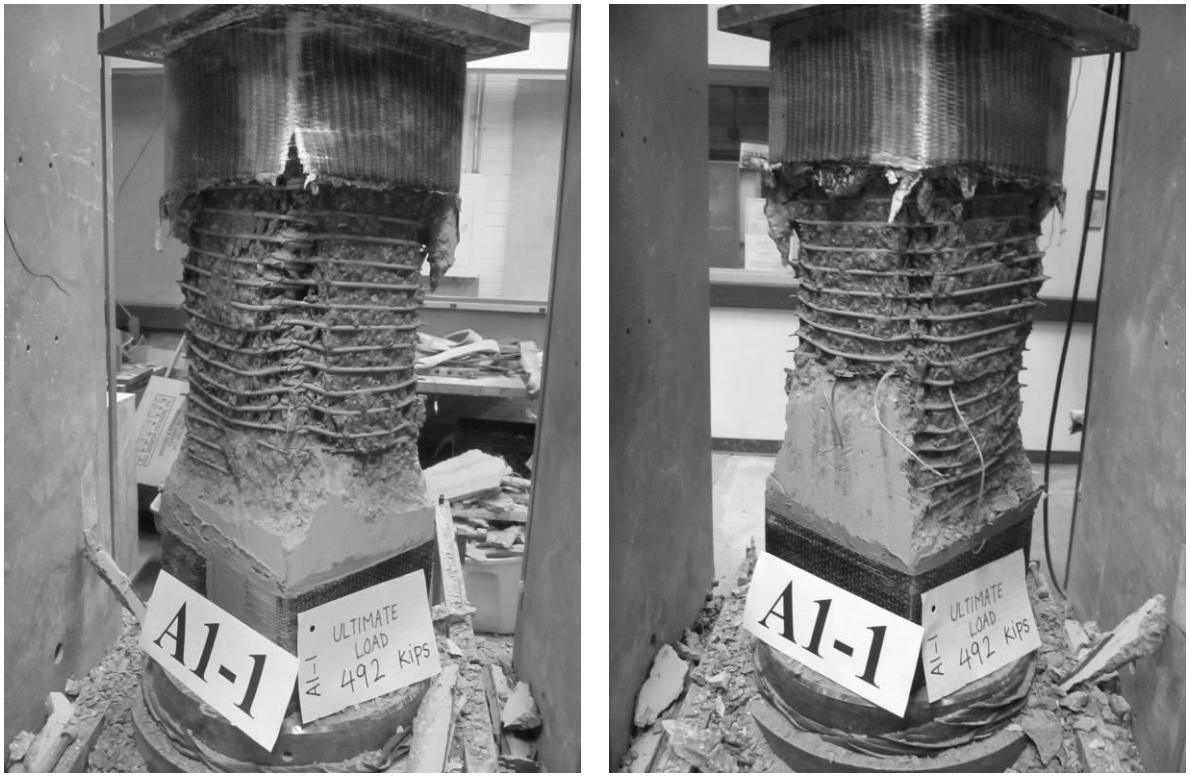

South and East sides

North and West sides

Figure 4.4 Failure of Column A1-1 under static loading.

South and East sides

North and West sides

Figure 4.5 Failure of Column B2-2 under static loading.

South and East sides

North and West sides

Figure 4.6 Failure of Column C3-2 under static loading.

4.2 Contribution of Cover and Core Concrete

4.2.1 Spalling Mechanism

While the cover is still in place, it can be assumed that the longitudinal strains in the cover and the core are equal (Kent and Park 1971, Vallenas et al 1977, Sheikh and Uzumeri, 1982). In the early stages of loading where the longitudinal strains are very small, due to small Poisson's ratio of concrete the lateral expansion of the column is consequently very small. Therefore, the lateral confinement provided by the transverse reinforcement at this stage is insignificant and the column behaves as if there is no lateral reinforcement. With the increase in the longitudinal strain, the lateral strain of the column starts increasing. Since the core is restrained against expansion by the transverse reinforcement, a gradual separation occurs at the core-cover interface. After this point, the core and cover start behaving differently. The cover behaves like a brittle-slender component under compression. It starts unloading until its contribution to carrying the load completely diminishes. From this point onward, the load is entirely carried by the core and the behavior is primarily influenced by the lateral reinforcement.

4.2.2 Transition of Stresses

Determining the axial strain at which the cover was no longer effective required continuous visual monitoring, tapping the column with a small hammer and interpretation of the strain in lateral reinforcements. For normal concrete columns, Park and Paulay (1975) suggested that the cover can be assumed ineffective at ε_{50u}, the strain at which the stress drops to 50% of the maximum stress in concrete cylinders. The ε_{50u} of the normal-strength RAC cylinders tested in this study was around 0.0050 while the strain at which

the complete cover spalled off was in a wider range of 0.0040 to 0.0070. For normal concrete, various researchers reported quite different values for strain at which the cover becomes completely ineffective. While Vallenas et al. (1977) reported a strain approximately 0.0100, Sheikh and Uzumeri (1982) observed a strain between 0.004 and 0.005.

Table 4.1 presents the axial strains corresponding to different cracking conditions of the RAC columns: the strains at which first vertical crack started appearing and the strains at which the cover became completely ineffective. The cracking strains are in fact the axial strains at which the strain in the outer ties started increasing. The strains were obtained by interpretation of the strain history of columns shown with * sign in Table 4.1. For other columns, it was assumed that the strains are the same. The tie strains are plotted against column longitudinal strains in Figure 4.7. From the figure, an average of 0.0020 can be assumed as the strain at which the ties undergo tensile stresses which means the onset of passive confinement action. Before this stage, it can be assumed that the axial stresses are uniformly carried by the core and cover concrete. After the complete spall, the core is completely responsible for carrying the axial stresses. Between the strains corresponding to “hair cracking” and “complete spall”, there is a “transition” zone where the stresses are carried by a complicated combination of the core and the cover. Since the exact shape of the transition is not possible to determine, conservatively, a simple linear shape may be assumed. Figure 4.8 schematically illustrates the stress transition mechanism and the stress-strain behavior of the confined RAC (curve OABC).

Table 4.1 Strains Corresponding to Cracking Condition of RAC Columns

Column	f_c (ksi)	ρ_s (%)	Crack Initiation	Complete Spall
A1-1*	4.26	0.88	0.0019	0.0037
A1-2	4.41	0.88	0.0019	0.0035
A2-1*	4.12	0.44	0.0021	0.0033
A2-2	4.35	0.44	0.0021	0.0036
A3-1*	4.26	0.29	0.0018	0.0031
A3-2	4.05	0.29	0.0018	0.0033
B1-1*	4.23	1.51	0.0022	0.0058
B1-2	4.42	1.51	0.0022	0.0053
B2-1*	4.18	0.75	0.0019	0.0052
B2-2	4.32	0.75	0.0019	0.0048
B3-1*	4.36	0.50	0.0016	0.0042
B3-2	4.23	0.50	0.0016	0.0038
C1-1*	4.23	2.10	0.0023	0.0070
C1-2	4.06	2.10	0.0023	0.0053
C2-1*	4.34	1.05	0.0019	0.0047
C2-2	4.09	1.05	0.0019	0.0043
C3-1*	4.45	0.70	0.0021	0.0043
C3-2	4.13	0.70	0.0021	0.0046
		Average:	0.0020	$.00397 \cong .0040$

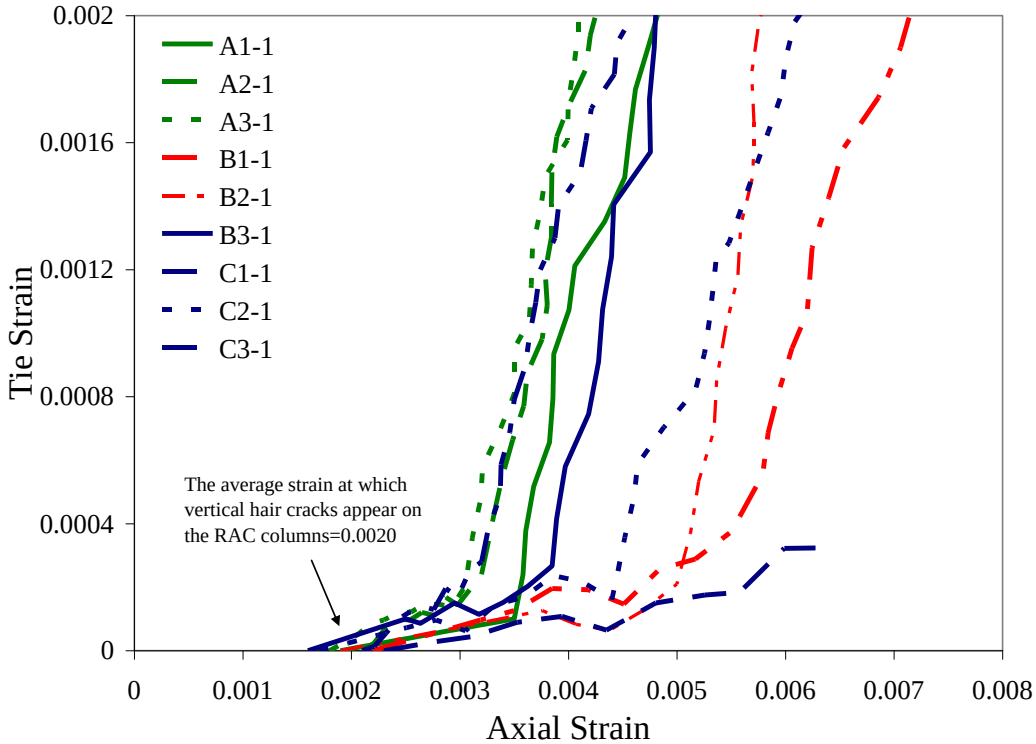

Figure 4.7 Tie strain versus longitudinal strains.

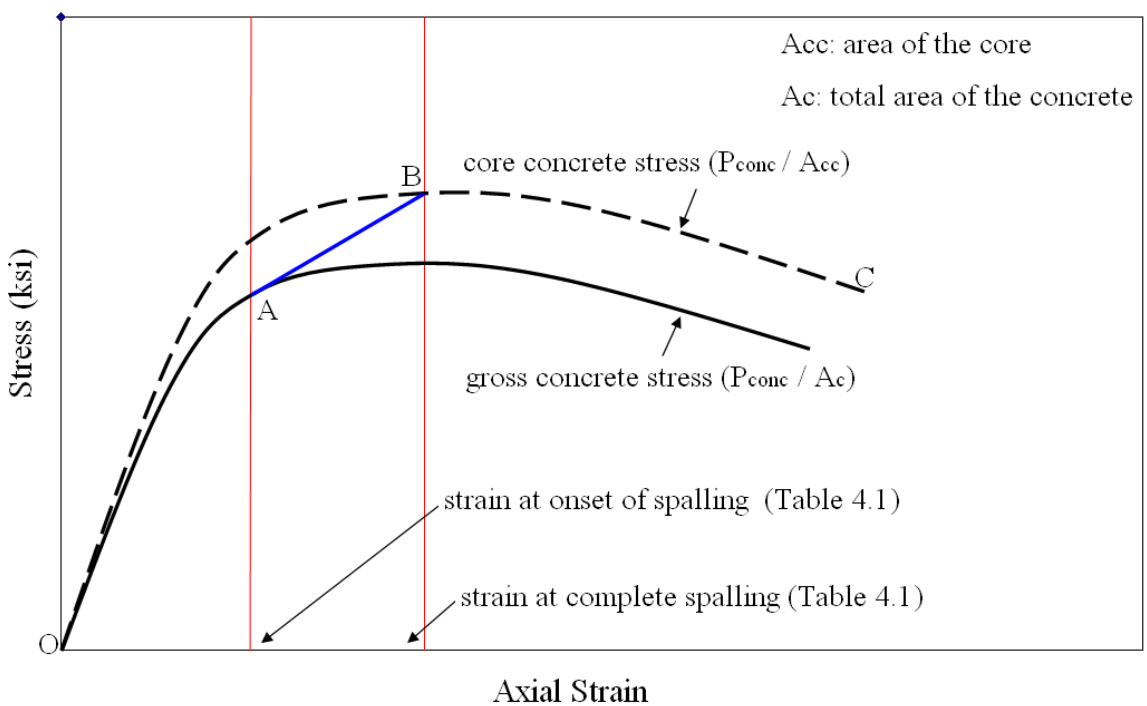

Figure 4.8 Concrete contribution and stress transition zone.

4.2.3 Concrete Contribution

In order to obtain the stress-strain relationship for RAC under axial compression rather than that of the composite section, it was necessary to obtain the concrete contribution in carrying the axial load. Figure 4.9 shows the concrete contribution in columns A1-1 and A1-2 as an example. For these columns, the concrete contributions were obtained by subtracting the contribution of longitudinal steel from the total load. It was assumed that the strains in steel and concrete were equal and the longitudinal steel has an elasto-plastic behavior. Repeatability of the test results can also be easily verified from the figure.

Table 4.2 presents the maximum values of contributions as well as design values. The table includes $(P_{conc})_{\max} / P_c$ values which roughly indicate the gain in concrete strength due to confinement. Based on ACI, the design values are obtained as follows:

$$P_0 = 0.85 f_c A_c + A_s f_y \tag{4.1}$$

$$P_c = 0.85 f_c A_c \tag{4.2}$$

$$P_{cc} = 0.85 f_c A_{cc} \tag{4.3}$$

where f_c is the compressive strength of the concrete, A_c is the total concrete area, A_{cc} is the area of the concrete core and f_y is longitudinal steel yield stress. Due to size effects and uneven consolidation in columns, the real compressive strength of concrete columns is usually less than f_c. The ACI code assumes that the design strength of concrete is $0.85\ f_c$. This assumption is based on the observations and tests results of Karsan and Jirsa (1969).

Table 4.2 Calculated and Experimental Axial Strengths and Contributions

Specimen	Compressive Strength Of Concrete Cylinder (ksi)	Calculated			Experiment				
		Total Load P_0 (kips)	Total Concrete Contribution P_c (kips)	Core Contribution P_{cc} (kips)	Total Load $P_{\max}$ (kips)	Concrete Contribution $(P_{conc})_{\max}$ (kips)	Strain at $P_{\max}$	$\frac{P_0 - P_{\max}}{P_0}$	$\frac{(P_{conc})_{\max}}{P_{cc}}$
A1-1	4.26	478	356	225	492	370	0.0022	3%	1.40
A1-2	4.41	490	368	233	468	346	0.0026	-4%	1.26
A2-1	4.12	466	344	218	449	327	0.0027	-4%	1.28
A2-2	4.35	485	363	230	474	352	0.0026	-2%	1.30
A3-1	4.26	478	355	225	449	327	0.0026	-6%	1.24
A3-2	4.05	460	338	214	427	305	0.0024	-7%	1.21
B1-1	4.23	475	354	224	511	393	0.0057	8%	1.49
B1-2	4.42	491	369	234	536	418	0.0058	9%	1.52
B2-1	4.18	471	349	221	501	383	0.0024	6%	1.47
B2-2	4.32	483	361	228	518	400	0.0028	7%	1.49
B3-1	4.36	486	364	231	495	377	0.0028	2%	1.39
B3-2	4.23	475	354	224	480	362	0.0027	1%	1.37
C1-1	4.23	475	354	224	546	428	0.0092	15%	1.62
C1-2	4.06	461	339	215	520	404	0.0066	13%	1.60
C2-1	4.34	484	362	230	524	406	0.0027	8%	1.50
C2-2	4.09	463	342	217	494	402	0.0031	6%	1.57
C3-1	4.45	493	372	236	518	400	0.0026	5%	1.44
C3-2	4.13	467	345	219	485	367	0.0031	4%	1.42

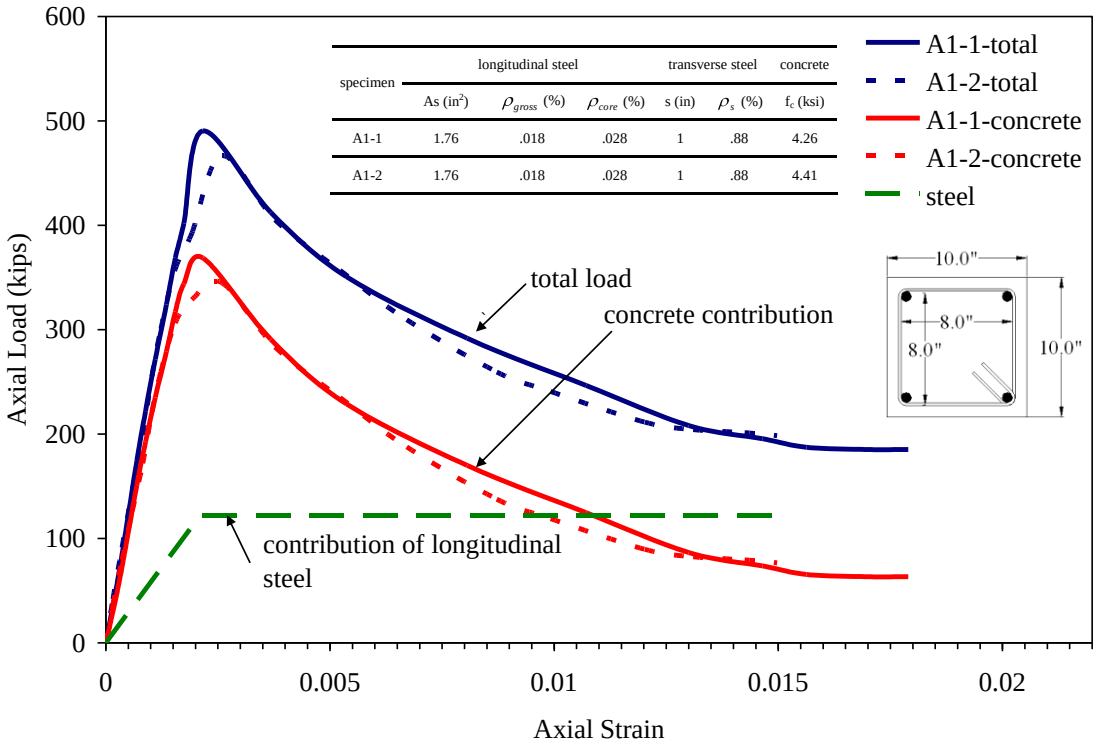

specimen	longitudinal steel			transverse steel		concrete
	As (in^2)	ρ_{gross} (%)	ρ_{core} (%)	s (in)	ρ_s (%)	f_c (ksi)
A1-1	1.76	.018	.028	1	.88	4.26
A1-2	1.76	.018	.028	1	.88	4.41

Figure 4.9 Determination of concrete contributions for Columns A1-1 and A1-2.

4.3 Effects of Reinforcement Variables on Behavior of RAC Columns

The RAC columns exhibited significant gain in ductility and appreciable increase in strength due to the presence of lateral reinforcement. There were different factors corresponding to the lateral reinforcement that affected the RAC load-deformation curves. These factors are described in this section.

4.3.1 Effect of Volumetric Ratio

Volumetric ratio, ρ_s, is defined as the volume of transverse reinforcement to the volume of core. The enhancing effect of volumetric ratio on strength and ductility of normal concrete columns has been well recognized (Vallenas et al 1977, Sheikh and Uzumeri 1982, Mander et al. 1988). In this study, similarly, it was observed that increasing the

amount of transverse reinforcement had a significant effect on improving the strength and ductility of the RAC columns. This observation can be verified by comparing the load-deformation behavior of the RAC columns presented in Figure 4.10. It can be easily noted that the columns with higher volumetric ratio of lateral reinforcement sustain considerable level of load while other columns show a rapid degradation of strength. While the well confined RAC columns (for instance B1-1) showed a definite increase in the maximum load-bearing capacity over that of poorly confined ones (for instance A3-1), the primary increase was in the ductility (i.e., their ability to sustain the applied loads) and energy absorption capacity (i.e., the area under load-deformation curves).

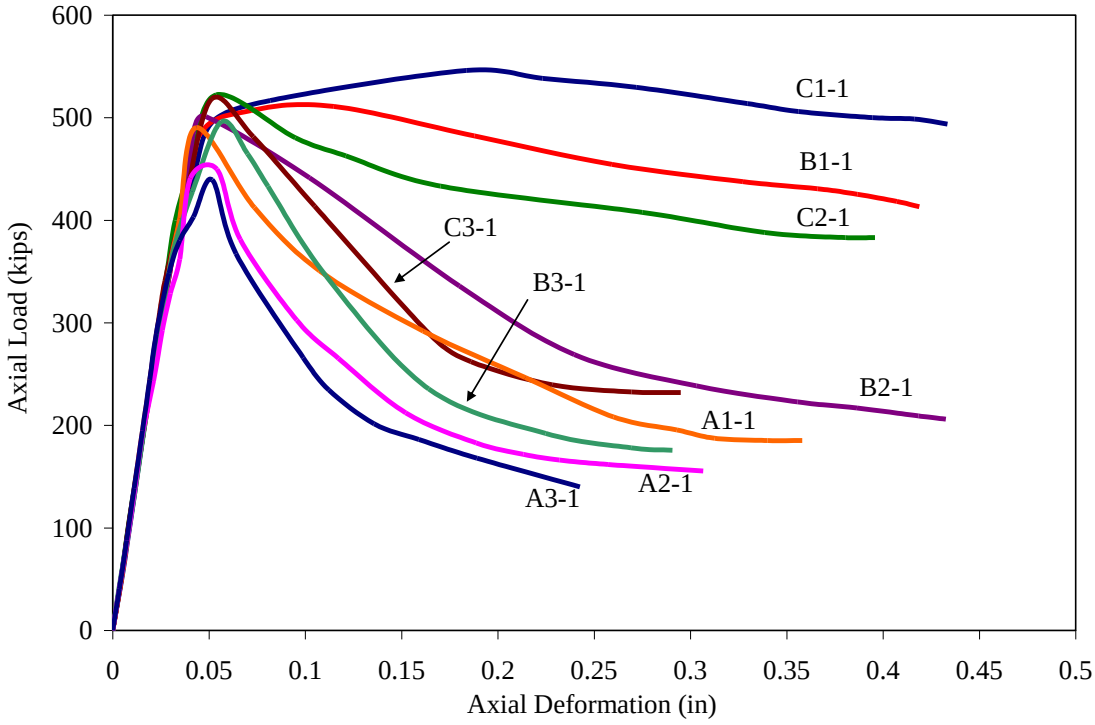

Figure 4.10 Gain in strength and ductility due to confinement.

4.3.2 Effect of Tie Spacing

Tie spacing had a substantial impact on the ductility, and to lesser extent, on the strength of the RAC columns as shown in Figure 4.11. Smaller tie spacing creates a stress condition similar to hydrostatic pressure. The small tie spacing for the RAC columns provided better confinement of the concrete core between the tie levels, as well as avoiding premature buckling of the longitudinal rebars. Larger spacing on the other hand, resulted in a smaller confined area of concrete core and consequently smaller strength gain and poor ductile behavior. Therefore, for an equal amount of volumetric ratio of lateral steel, the use of smaller ties at closer spacing is superior than the use of larger ties at larger spacing.

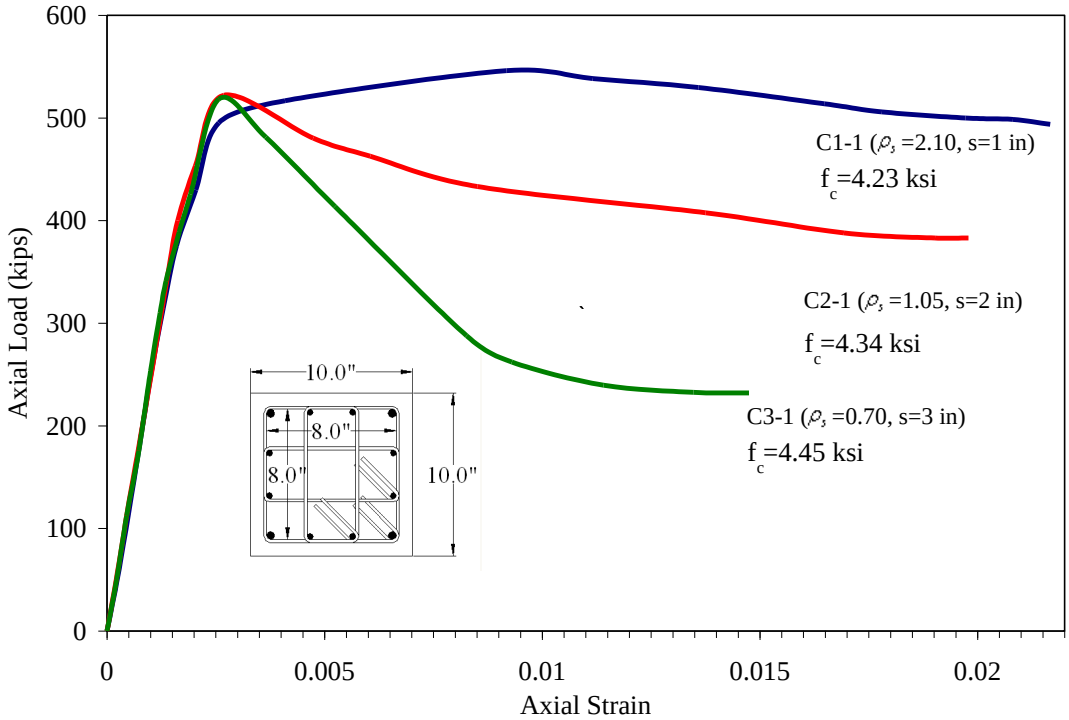

Figure 4.11 Effect of transverse steel spacing on column behavior.

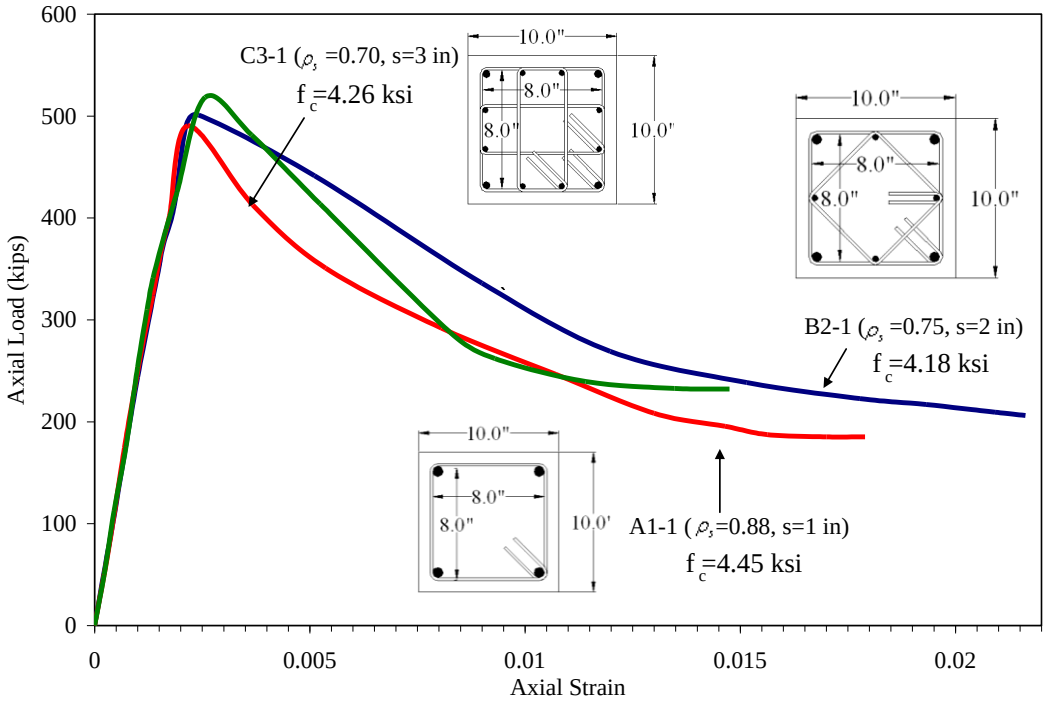

Figure 4.12 Effect of transverse steel configuration on column behavior.

4.3.3 Effect of Tie Configuration

Various researchers have shown that the effectiveness of confining steel primarily depends on the distribution of confining pressure (Vallenas et al. 1977, Sheikh and Uzumeri 1982, Mander 1984) which in turn is affected by the configuration of lateral reinforcement and distribution of the longitudinal rebars. In the columns that were confined with single-perimeter ties (configuration “A”), the cross-sectional area of the core concrete was not efficiently confined. These columns in general showed a relatively poor behavior. On the other hand, in the columns that the longitudinal rebars were all supported by the ties (configuration “B” and “C”) the cross-sectional area of the core concrete was very effectively confined and the columns exhibited superior behavior. Distributing the longitudinal reinforcement has another important role. It provides

additional confinement across the height of the column between adjacent ties and consequently increases the volume of effectively confined core. Figure 4.12 shows the effect of tie configuration on the behavior of RAC columns. As it can be seen, with even smaller amount of volumetric ratio for transverse reinforcement (amount of transverse reinforcement in unit volume of core concrete), the specimens with configuration C exhibited almost equal strength and ductility to that of configuration A. The column with configuration "B" showed even superior behavior, as it can be seen from the figure.

4.4 Effect of Loading Rate on Strength and Ductility of RAC Columns

Various researchers have shown that normal concrete exhibits higher compressive strength under higher straining rates (Dilger et al. 1984, Shuaib and Shah 1985). Typical strain rates induced to structural members by earthquake motions with normal frequency content usually ranges between 0.01 in/in/s and 0.02 in/in/s (Kappos, 1995). In this section, the behavior of RAC column under such strain rate is discussed. Similar to Dilger et al. (1984) and Shuaib and Shah (1985), a straining rate of 0.016 in/in/s was adopted.

4.4.1 Effect of Loading Rate on Strength

Table 4.3 presents the estimated and experimental load bearing capacities of the RAC columns tested under the strain rate of 0.016 in/in/s. In the absence of any equation for RAC, the strength of unconfined (cover) and confined (core) areas were estimated using the equations proposed by Dilger et al. (1984) and Shuaib and Shah 1985, for normal concrete.

For unconfined concrete column, Dilger et al. suggested the following equation:

$$f_{uc}^{\dot{\varepsilon}} = f_{ic}(1.38 + 0.08 \ \log \dot{\varepsilon}) \tag{4.4}$$

where $f_{uc}^{\dot{\varepsilon}}$ is the enhanced unconfined concrete strength due to the high loading rate, $\dot{\varepsilon}$ is the straining per second and f_{ic} is the insitu unconfined strength under static loading. For concrete confined by lateral reinforcement, Shuaib and Shah (1985) suggested the following equation:

$$f_{cc}^{\dot{\varepsilon}} = f_{uc}^{\dot{\varepsilon}} + \frac{6.61}{f_{uc}^{\dot{\varepsilon}}}\left[\frac{\rho_s f_{yt}}{2}(1 - \sqrt{\frac{s}{1.25 b_i}})\right]^{0.04}\left(\frac{\log \ \dot{\varepsilon}}{\log \ \dot{\varepsilon}_s}\right)^{0.30} \tag{4.5}$$

where $\dot{\varepsilon}_s$ is the static strain rate (i.e., 1.6x10^{-5} per second), $\dot{\varepsilon}$ is the high strain rate (i.e., 0.016 per second), ρ_s is the volumetric ratio of lateral reinforcement in percent, f_{yt} is the yield stress of tie steel in ksi, s is tie spacing in inches and b_i is the core dimension in inches.

To calculate to the effect of the strain rate on the strength of longitudinal rebars, Soroushian and Sim (1986) suggested the following equation for estimating the dynamic yiled stress:

$$f_y^{dyn} = f_y^{stat}\left[-6.54\times10^{-4} f_y^{stat} + 1.46 + \left(-1.33\times10^{-4} f_y^{stat} + 0.0927\right)\log \ \dot{\varepsilon}\right] \tag{4.6}$$

where f_y^{dyn} and f_y^{stat} are dynamic and static yield stresses in ksi, respectively. Using the above equations, the load bearing capacities were calculated, as presented in Table 4.3.

Equations 4.4 and 4.5 could reasonably predict the experimental values of the strength. Therefore, in absence of more accurate equations, these equations may be used to estimate the gain in the strength of plain and confined RAC under high-rate loading.

The effect of lateral steel volumetric ratio, ρ_s, on strength gain due to high straining rate can be observed from Table 4.4 where the average values of experimental static (P_{stat}) and dynamic (P_{dyn}) load bearing capacities are presented. Under the high straining rate, RAC columns showed 7% to 26% increase in ultimate axial strength. It can be clearly noticed that the strength gain can be improved by increasing the amount of lateral steel.

4.4.2 Effect of Loading Rate on Ductility

Figures 4.13 and 4.14 show the behavior of A1-3 and B2-3 columns under the high strain rate of 0.016 per second. It is clearly noticed that due to the effect of high straining rate, the strength is considerably increased. The initial stiffness (slope of the ascending branch) also shows an appreciable increase. The ductility, however, was not significantly affected by the loading rate. This behavior is similar to that of normal concrete columns under high strain rates (0.2 in/in/s), observed by Digler et al. They did not notice any noticeable change in the ductility of concrete columns due to the fast loading rate.

Table 4.3 Calculated and Experimental Dynamic Axial Strengths

Specimen	s (in)	ρ_s (%)	f_{ic} (ksi)	$f_{uc}^{\dot{\varepsilon}}$ (ksi)	$f_{cc}^{\dot{\varepsilon}}$ (ksi)	Caclulated				Experimental	Percent Difference
						Cover Strength (kips)	Core Strength (kips)	Steel Strength (kips)	P_{dyn} (kips)	Maximum load (kips)	
A1-3	1	0.88	3.62	4.48	4.69	137	292	146	575	554	-4
A1-4	1	0.88	3.75	4.63	4.84	142	301	146	589	568	-4
A2-3	2	0.44	3.50	4.33	4.41	132	275	146	553	513	-8
A2-4	2	0.44	3.70	4.57	4.65	140	290	146	576	535	-8
A3-3	3	0.29	3.62	4.48	4.52	137	281	146	565	473	-19
A3-4	3	0.29	3.44	4.26	4.30	130	268	146	544	465	-17
B1-3	1	1.51	3.60	4.45	4.81	136	300	141	577	650	11
B1-4	1	1.51	3.76	4.64	5.00	142	312	141	595	631	6
B2-3	2	0.75	3.55	4.39	4.54	134	283	141	558	581	4
B2-4	2	0.75	3.67	4.54	4.68	139	292	141	572	605	6
B3-3	3	0.50	3.71	4.58	4.66	140	290	141	571	552	-4
B3-4	3	0.50	3.60	4.45	4.52	136	282	141	559	557	0
C1-3	1	2.10	3.60	4.45	4.97	136	309	141	587	731	20
C1-4	1	2.10	3.45	4.27	4.81	131	300	141	571	716	20
C2-3	2	1.05	3.69	4.56	4.76	140	297	141	577	634	9
C2-4	2	1.05	3.48	4.30	4.51	132	281	141	554	614	10
C3-3	3	0.70	3.78	4.68	4.78	143	298	141	582	561	-4
C3-4	3	0.70	3.51	4.34	4.45	133	277	141	551	580	5

Table 4.4 Variation of Static-to-Dynamic Axial Strength Ratios with Respect to ρ_s

ρ_s (%)	Specimen	Dynamic Capacity, P_{dyn} (kips)	Average (kips)	Specimen	Static Capacity, P_{stat} (kips)	Average (kips)	Percent Difference
0.88	A1-3	554	561	A1-1	492	480	14
0.88	A1-4	568		A1-2	468		
0.44	A2-3	513	524	A2-1	449	461.5	12
0.44	A2-4	535		A22	474		
0.29	A3-3	473	469	A3-1	449	438	7
0.29	A3-4	465		A3-2	427		
1.51	B1-3	650	640.5	B1-1	511	523.5	18
1.51	B1-4	631		B1-2	536		
0.75	B2-3	581	593	B2-1	501	509.5	14
0.75	B2-4	605		B2-2	518		
0.50	B3-3	552	554.5	B3-1	495	487.5	12
0.50	B3-4	557		B3-2	480		
2.10	C1-3	731	723.5	C1-1	546	533	26
2.10	C1-4	716		C1-2	520		
1.05	C2-3	634	624	C2-1	524	509	18
1.05	C2-4	614		C2-2	494		
0.70	C3-3	561	570.5	C3-1	518	501.5	12
0.70	C3-4	580		C3-2	485		

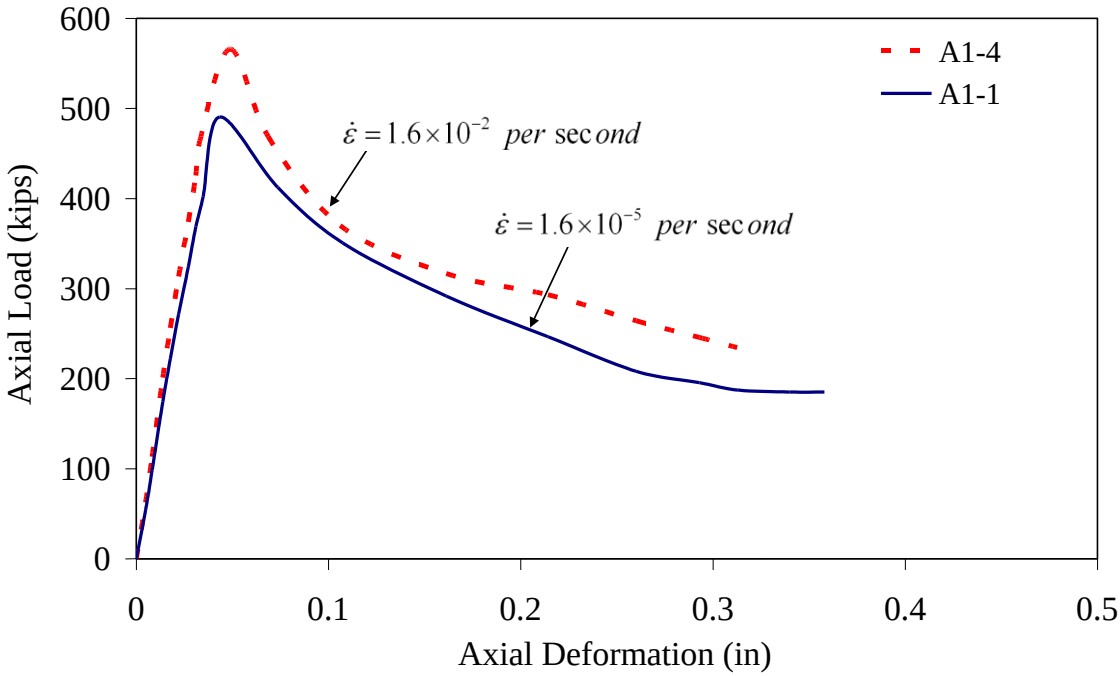

Figure 4.13 Effect of strain rate on behavior of column type A1.

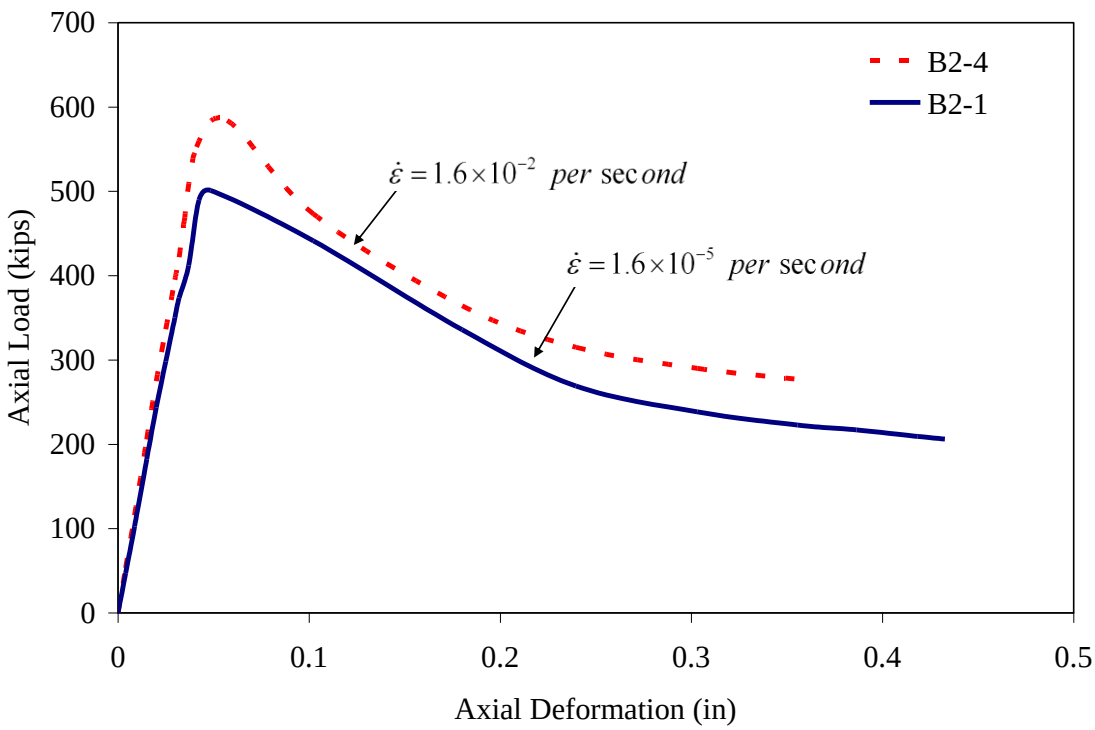

Figure 4.14 Effect of strain rate on behavior of column type B2.

4.5 Effect of Cyclic Loading

The results of uniaxial cyclic tests on unconfined normal concrete have revealed that considerable degradation of stiffness due to cyclic loading can occur (Sinha et al. 1967, Karsan and Jirsa 1969). However, when effectively confined, concrete can maintain its stiffness under cyclic loading conditions (Priestly et al., 1981). Figures 4.15 to 4.20 show the load-deformation diagrams of the RAC columns under cyclic loading. It can be easily noticed that for the columns with higher confinement (i.e., higher volumetric ratio of lateral reinforcement and smaller tie spacing) the strength and stiffness is not adversely affected by the load cycles whereas in the columns with smaller confinement, the slope of the unloading and reloading branches significantly decreases by increasing the number of cycles. This observation indicates that similar to normal concrete, adequate confinement of RAC is essential in order to obtain the desirable ductility under cyclic conditions.

For plain concrete, is well established that the stress-strain envelope curve under cyclic loading is almost identical to the curve obtained from monotonic loading (Sinha et al. 1964, Karsan and Jirsa 1969, Shah et al. 1983 and Mander 1984). Figure 4.15 shows the monotonic and cyclic stress-strain curves of columns A1-4 and A1-5, respectively. It can be seen that the monotonic curve, although not perfectly, approximates the envelope of the cyclic curve.

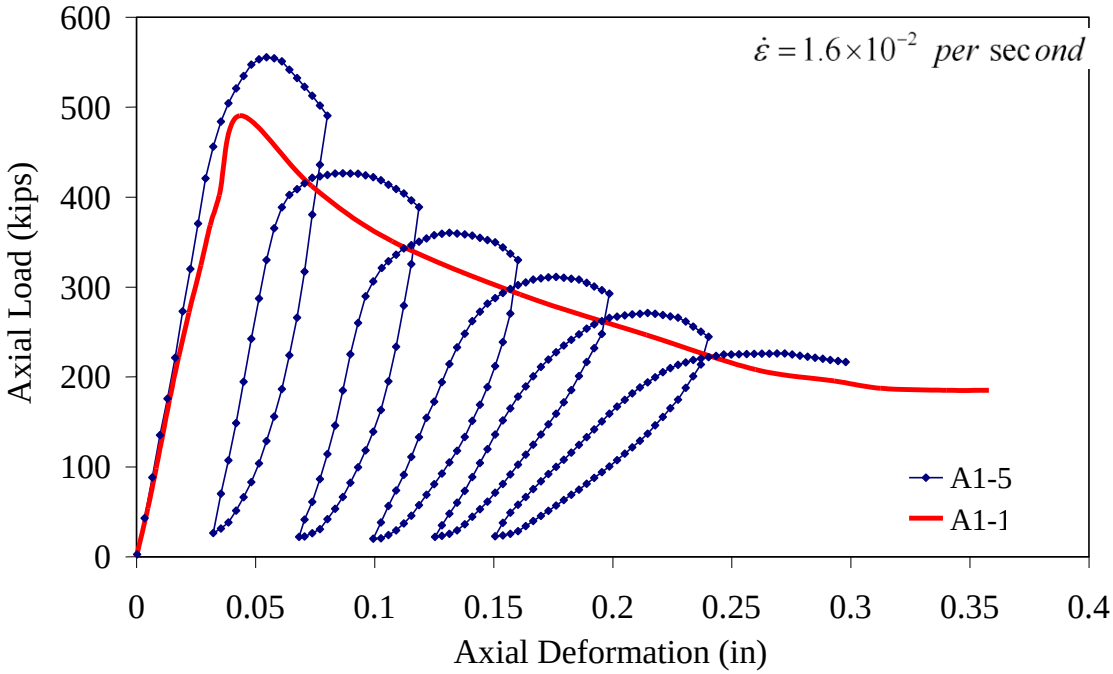

Figure 4.15 Behavior of column A1-5 subjected to cyclic loading.

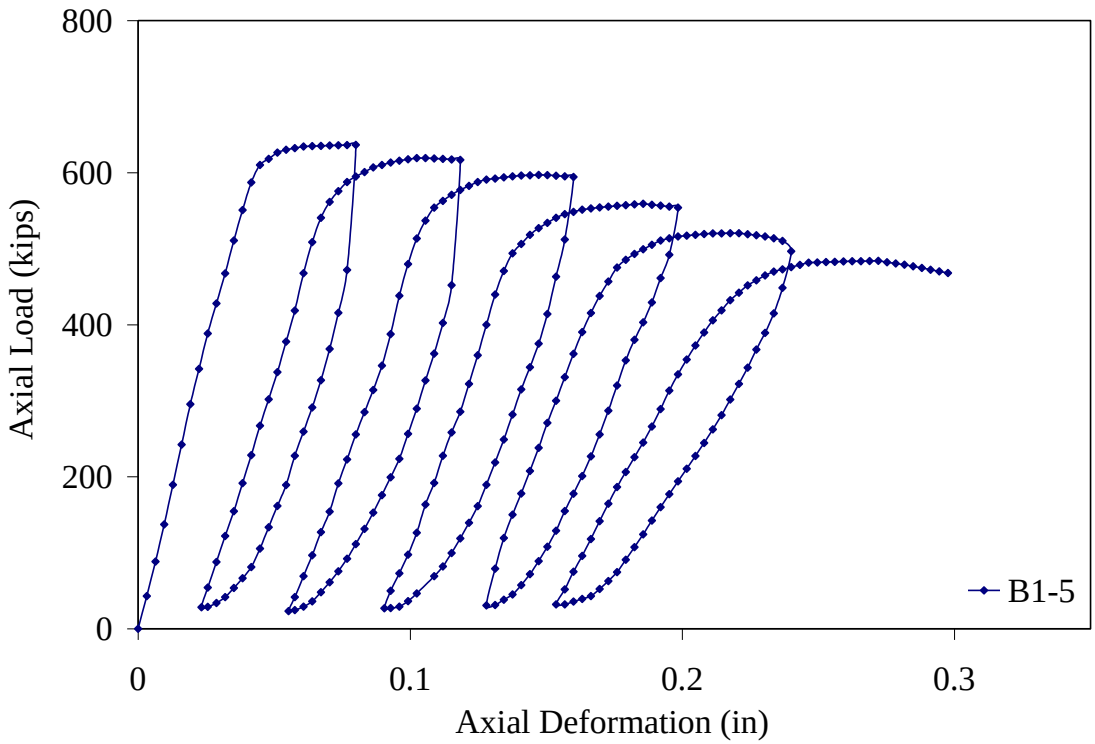

Figure 4.16 Behavior of column B1-5 subjected to cyclic loading.

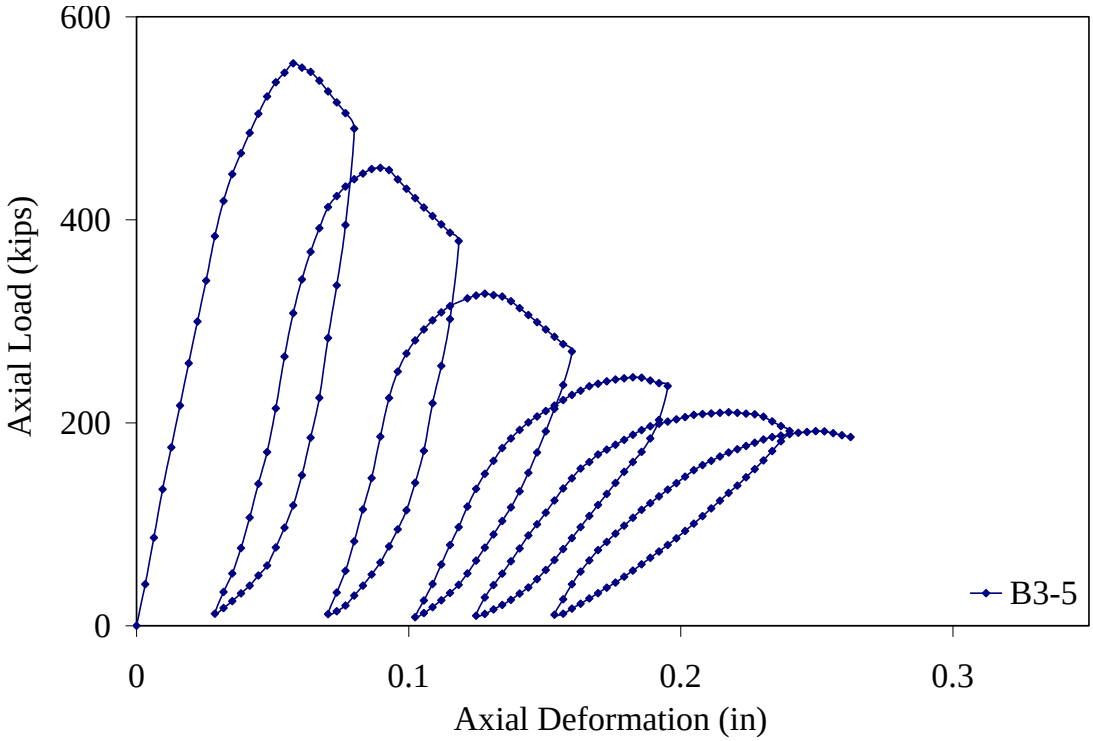

Figure 4.17 Behavior of column B3-5 subjected to cyclic loading.

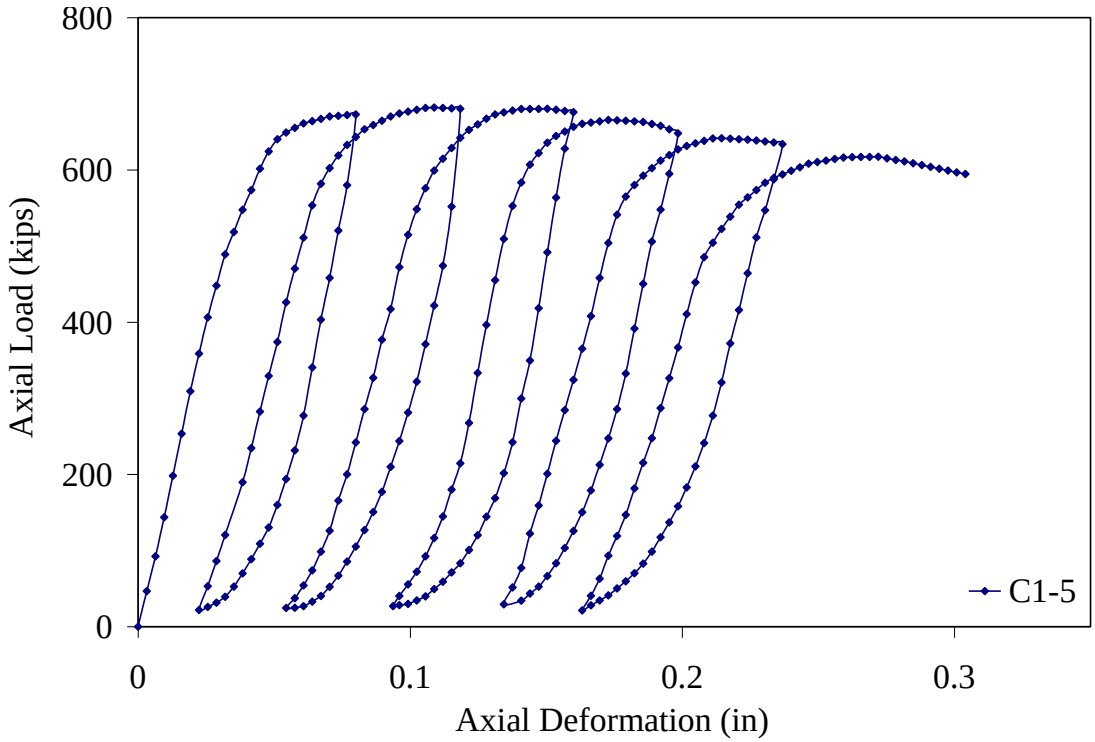

Figure 4.18 Behavior of column C1-5 subjected to cyclic loading.

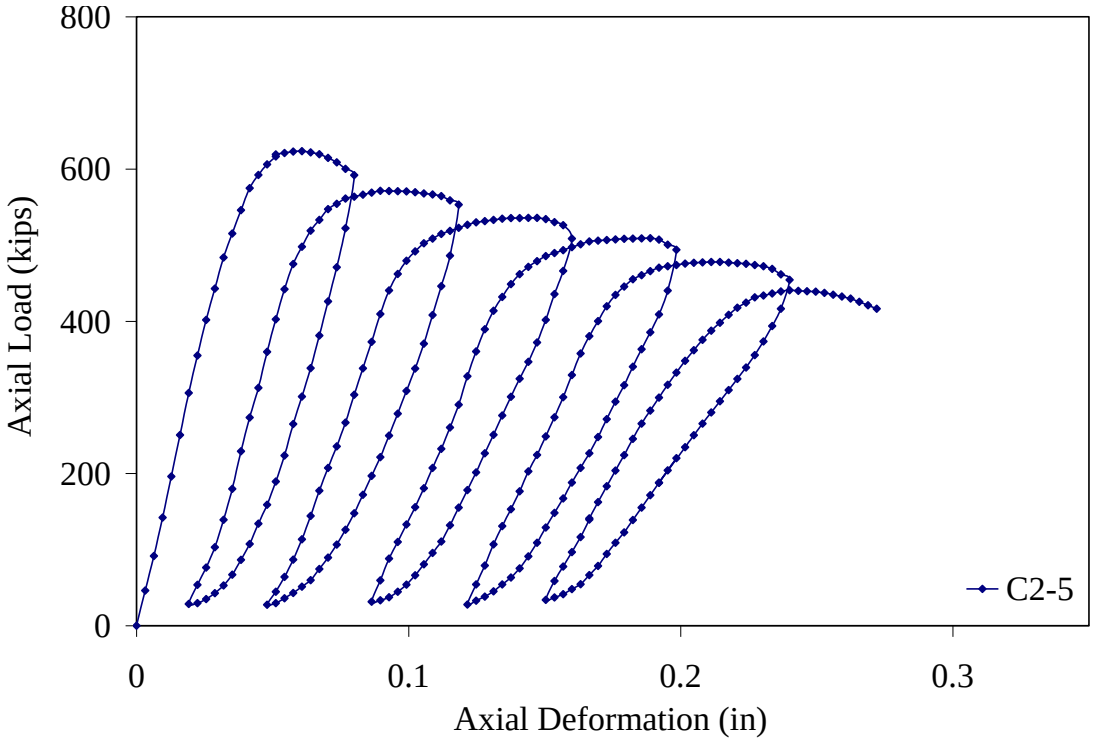

Figure 4.19 Behavior of column C2-5 subjected to cyclic loading.

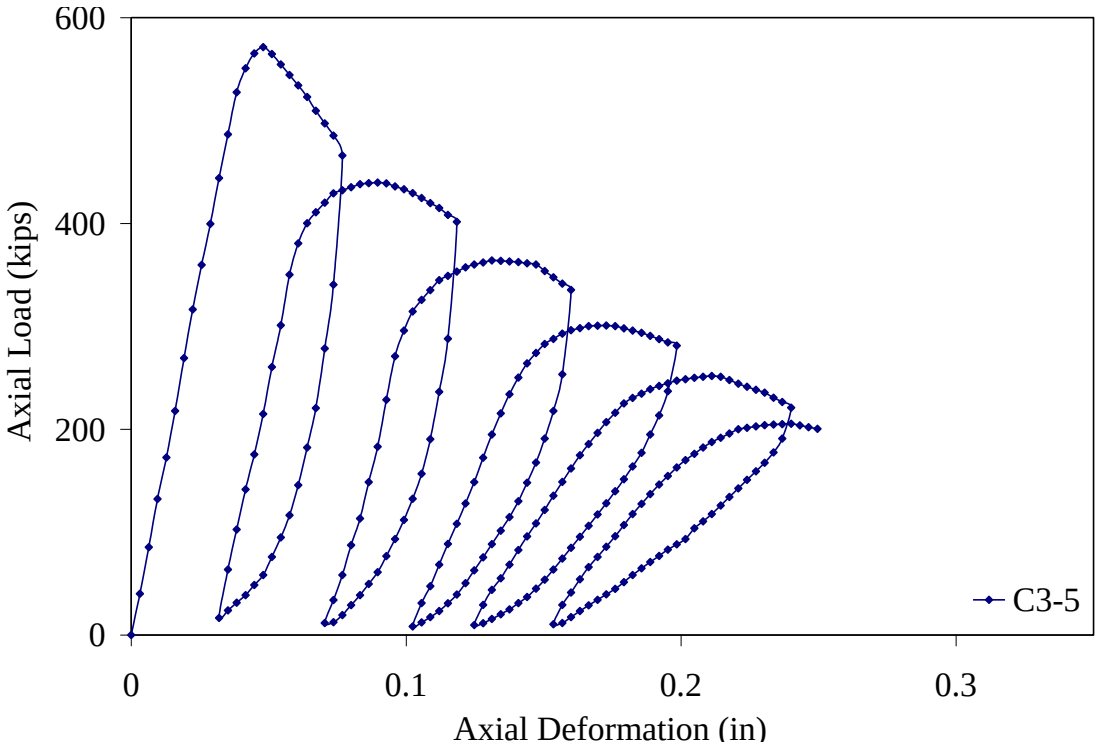

Figure 4.20 Behavior of column C3-5 subjected to cyclic loading.

CHAPTER 5

ANALYTICAL PREDICTION OF RAC STRESS-STRAIN BEHAVIOR

5.1 General

RAC stress-strain formulation is an essential for predicting the behavior of structural members. While there are various formulations for estimating the stress-strain relationship of normal concrete, a model for RAC stress-strain does not yet exist. Since the mechanical properties of RAC are quite different compared to those of normal concrete, the stress-strain equations for normal concrete are not suitable for RAC. This chapter is devoted to developing models for plain and confined RAC.

5.2 Development of Stress-Strain Formulation for Plain RAC

5.2.1 Experimental Stress-Strain Curves

Using an MTS815 loading unit, experimental stress-strain curves for the plain RAC cylinders were obtained. A wide range of compressive strength (2.5 ksi to 7 ksi) was considered, as previously discussed in section 3.2.4. Axial deformation of the RAC cylinders was measured using two individual extensometers. The average of these two reading was considered as the axial deformation of the specimens. During the trial experiments, it was observed that the descending branch of the stress-strain curves of a RAC cylinder is influenced by the location of the extensometers. Therefore, it was necessary to be consistent in positioning the extensometers in order to obtain consistent results.

If the testing of concrete cylinders under axial compression is conducted in a load-control mode, after reaching the maximum load, the cylinder fails abruptly and the descending branch can not be accurately recorded. In a displacement-control mode, however, the failure occurs at the rate of the applied displacement and the descending branch can be easily attained. All of the stress-strain curves in this study were obtained in displacement-control mode with a strain rate of 1.6×10^{-5} per second. Figure 5.1a to 5.1e show the experimental stress-strain curves of the RAC cylinders which compressive strength lies between 2.40 and 7.30 ksi. These figures also include the predicted stress-strain curves which will be later discussed in this chapter.

Referring to Figure 5.1a to 5.1e, it can be seen that similar to that of normal concrete, the stress-strain curve of RAC cylinders has a nonlinear nature. It consists of an ascending branch up to the maximum stress, followed by a descending branch that for the most part is a relatively straight line. The descending branch is then continued by a sustaining branch where the stress remains almost unchanged.

Along the ascending branch of the stress-strain curve and up to the maximum stress, the RAC cylinders did not experience any significant damage. After the maximum strength was reached, however, the specimens started crumbling and the load started dropping. The slope of the descending branch was substantially affected by the strength of the RAC. Usually, the higher the strength of the concrete, the steeper the descending branch was. Therefore any equation to approximate the slope of the descending branch should include the strength as a key variable. Also, the strain corresponding to the peak stress appeared to be independent of the RAC strength. All the cylinders reached their maximum strength at a strain about 0.0025.

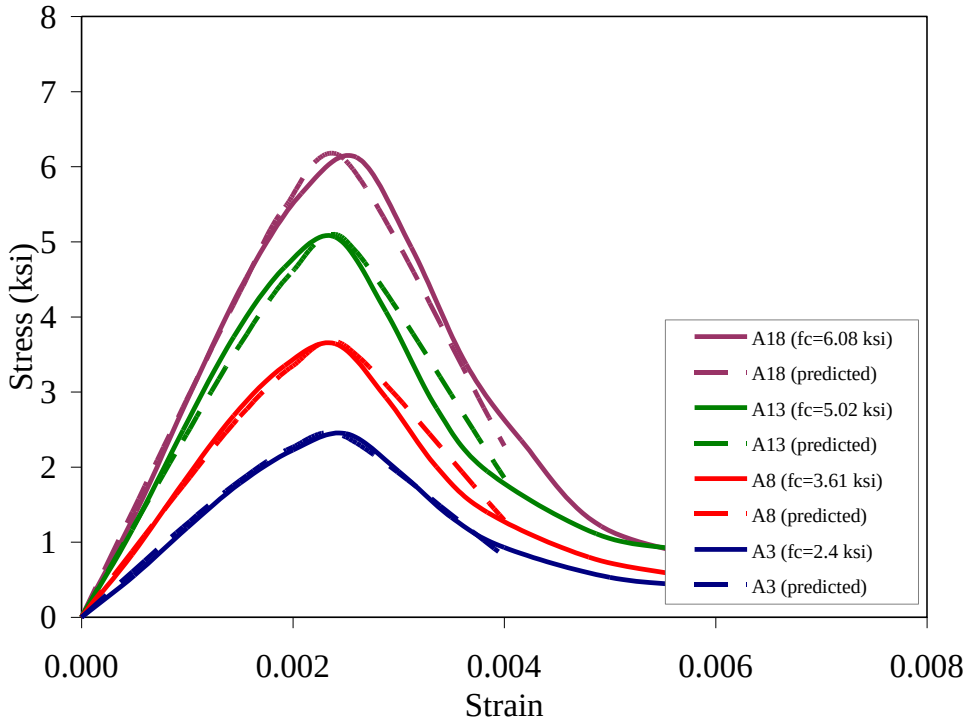

Figure 5.1a Experimental and predicted stress-strain curves for plain RAC.

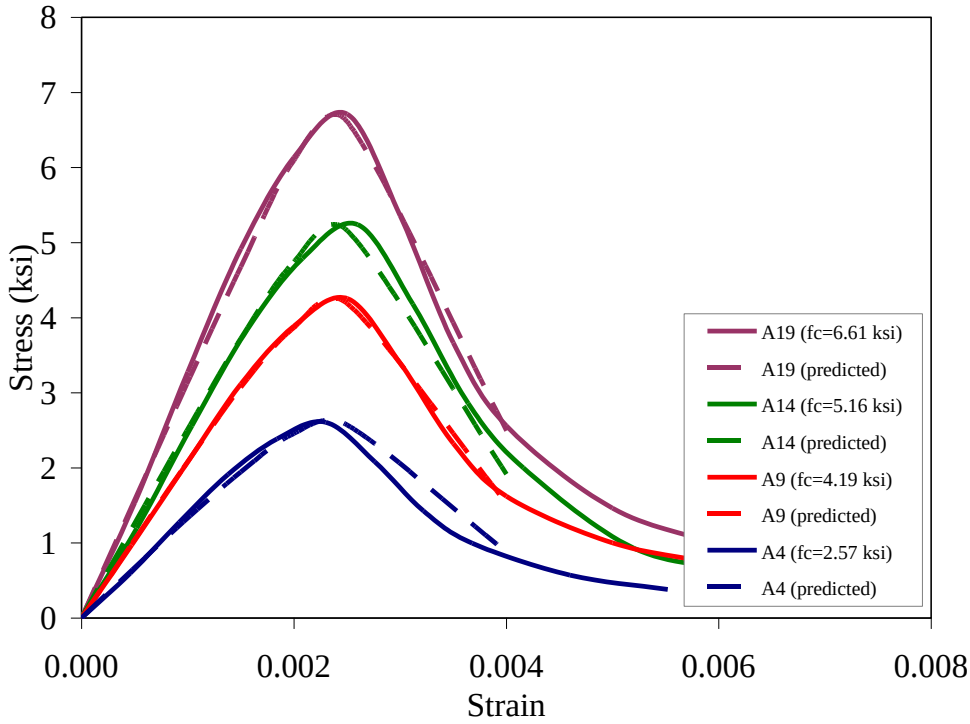

Figure 5.1b Experimental and predicted stress-strain curves for plain RAC.

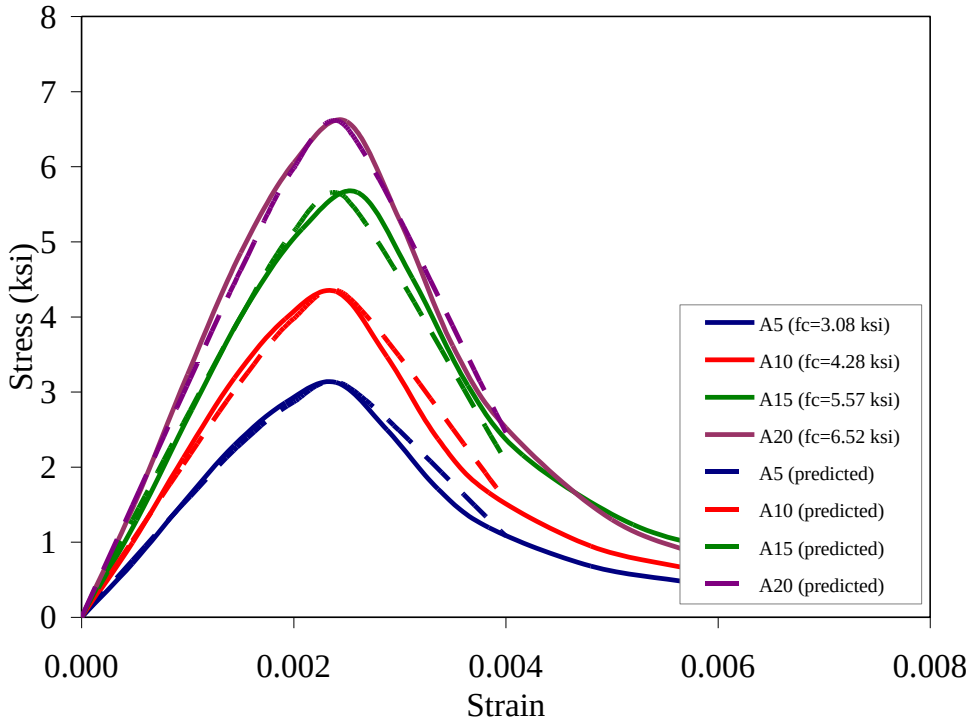

Figure 5.1c Experimental and predicted stress-strain curves for plain RAC.

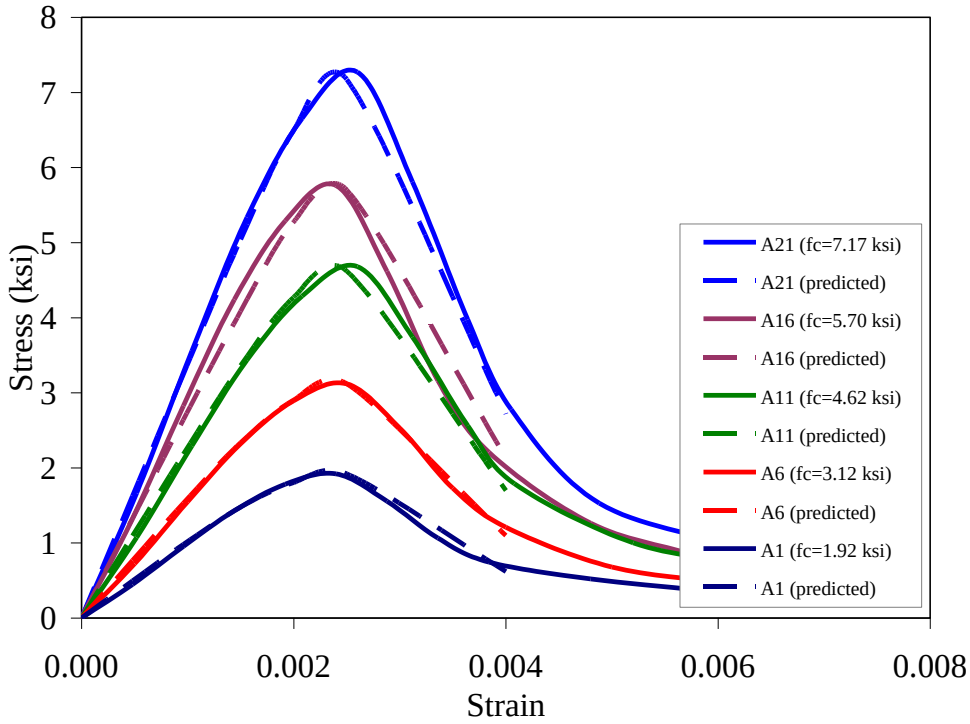

Figure 5.1d Experimental and predicted stress-strain curves for plain RAC.

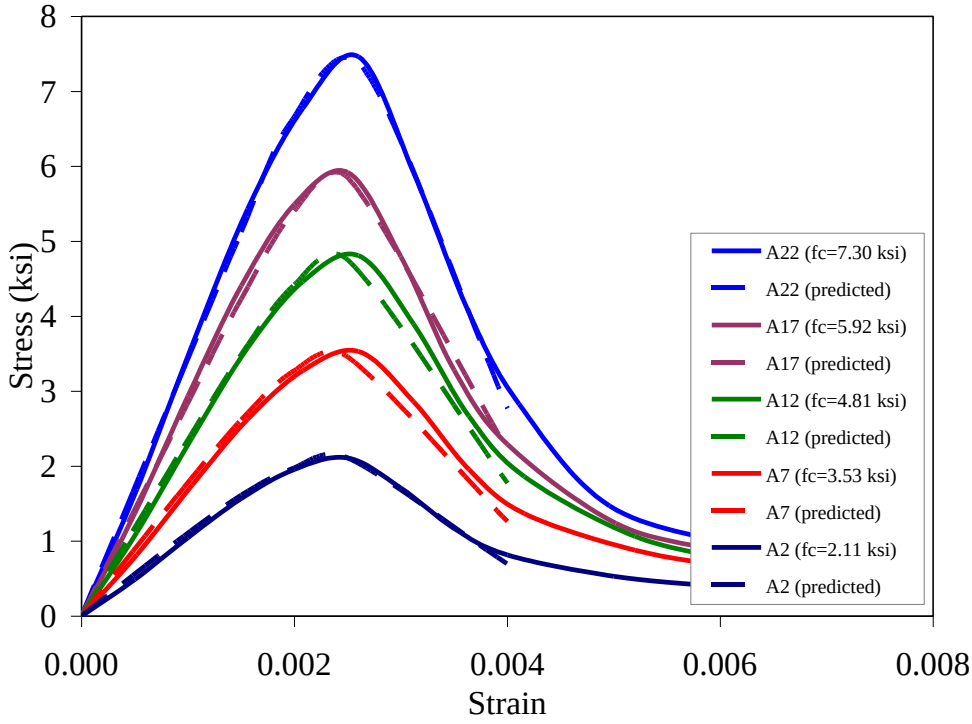

Figure 5.1e Experimental and predicted stress-strain curves for plain RAC.

5.2.2 Proposed Stress-Strain Model for Plain RAC

Various mathematical models for normal concrete were examined and found incapable for predicting the RAC behavior, as previously shown in Figure 4.1. Therefore a new model should be developed.

A stress-strain equation in the form of $\sigma = f(\varepsilon)$ should satisfy the following conditions: (a) $f(\varepsilon = 0) = 0$,(b) $f(\varepsilon = \varepsilon_c) = f_c$, (c) $f'(\varepsilon = 0) = E_c$ and (d) $f'(\varepsilon = \varepsilon_c) = 0$. The proposed model to predict the ascending portion of RAC stress-strain curves follows the equation suggested by Popovic (1973):

$$f = f_c \frac{n\ (\varepsilon / \varepsilon_c)}{(\varepsilon / \varepsilon_c)^n + n - 1} \tag{5.1}$$

where f (in ksi) and ε are stress and strain variables, f_c is the maximum stress (in ksi), ε_c is the strain corresponding to the maximum stress and n is a factor that determines the variation in the slope of ascending branch and is calculated as follows:

$$n = \frac{E_c}{E_c - E_{\sec}} = \frac{E_c}{E_c - f_c / \varepsilon_c} \tag{5.2}$$

where E_c is initial tangent modulus of elasticity and $E_{\sec}$ is the secant modulus.

Variations of the slope of ascending branch, n, with respect to compressive strength is shown in Figure 5.2. The following simple equation is proposed to approximate n:

$$n = \frac{f_c}{2} + 3 \tag{5.3}$$

Visual examination of the experimental stress-strain curves showed that assuming a straight line for the descending branch was reasonable. The slope of descending branch was observed to be primarily a function of σ_f which is the stress corresponding to a strain of 0.004. A linear approximation of the descending branch is as follows:

$$f = f_c - Z_p(\varepsilon - \varepsilon_c) \tag{5.4}$$

where Z_p is the slope of the descending branch. Z_p can be conveniently obtained if σ_f is known. As shown in Figure 5.3, σ_f was found to be a function of f_c (in ksi) where:

$$\sigma_f \cong \frac{f_c}{2.5} - 0.15 \tag{5.5}$$

The slope of the descending branch can be expressed as a function of the compressive strength:

$$Z_p = \frac{f_c - \sigma_f}{0.0015} = \frac{0.6 f_c + 0.15}{0.0015} = 400 f_c + 100 \tag{5.6}$$

As previously discussed in Chapter 2, various researchers observed that normal concrete is capable of sustaining some stresses after the descending branch (Kent and Park 1971, Sheikh and Uzumeri 1982, Mander 1988, Kappos 1997). Similar observations were made laboratory tests in study. In general, it was observed assuming a sustaining stress of $0.1\ f_c$ may not be unrealistic.

Figures 5.1a through 5.1e compare the experimental results with the predicted curves. It can be seen that the agreement between the predicted and experimental curves is satisfactory. The proposed model for plain RAC is summarized in Figure 5.4.

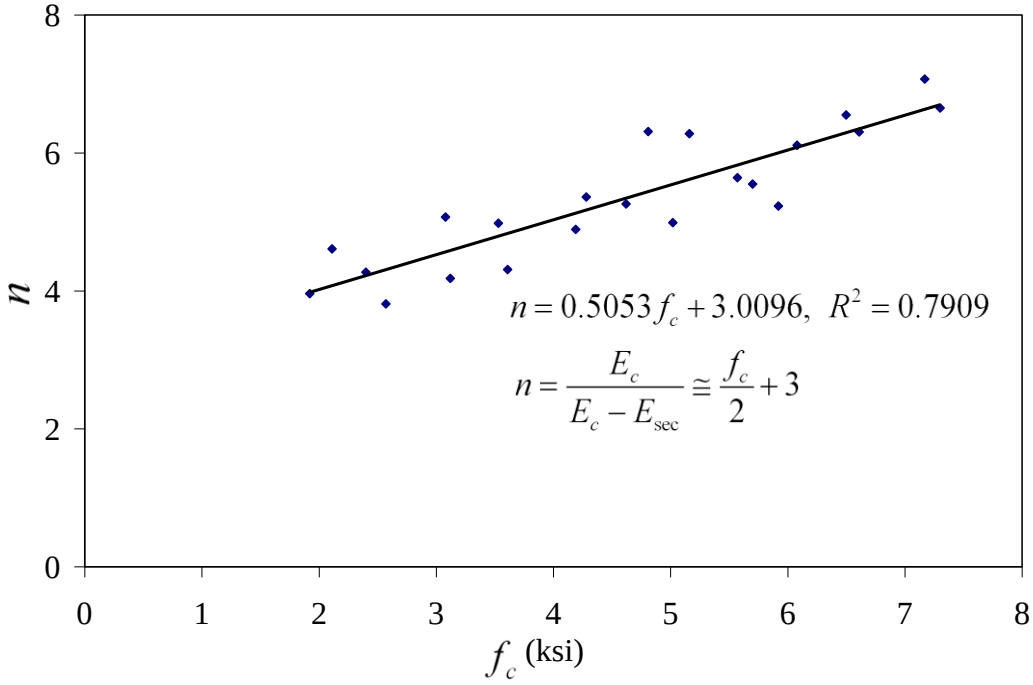

Figure 5.2 Variation of n with respect to RAC compressive strength.

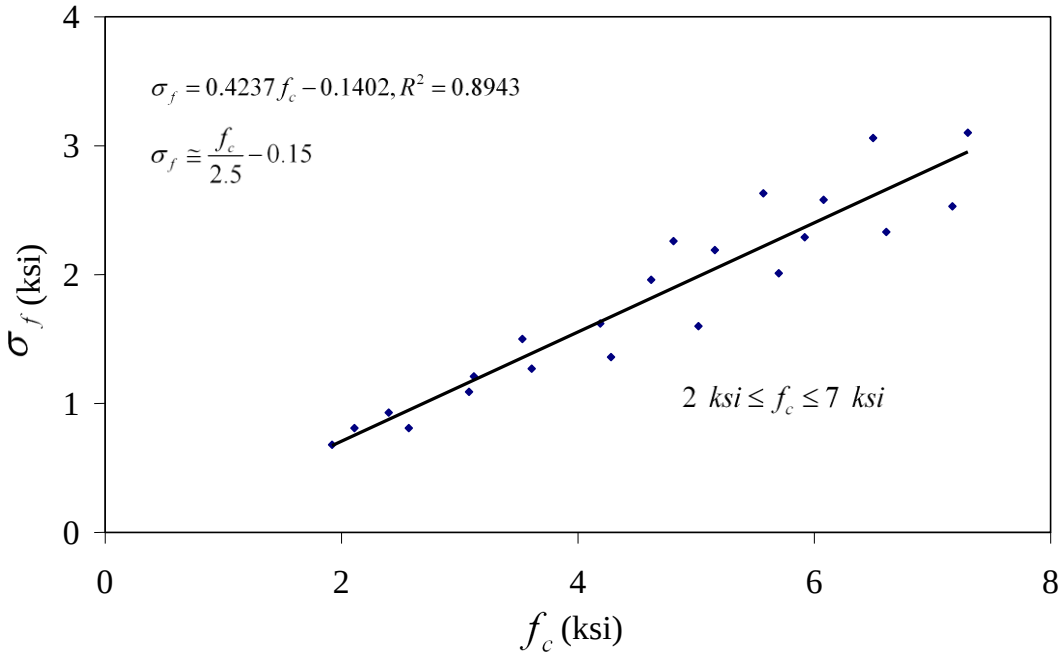

Figure 5.3 Variation of σ_f with respect to RAC compressive strength.

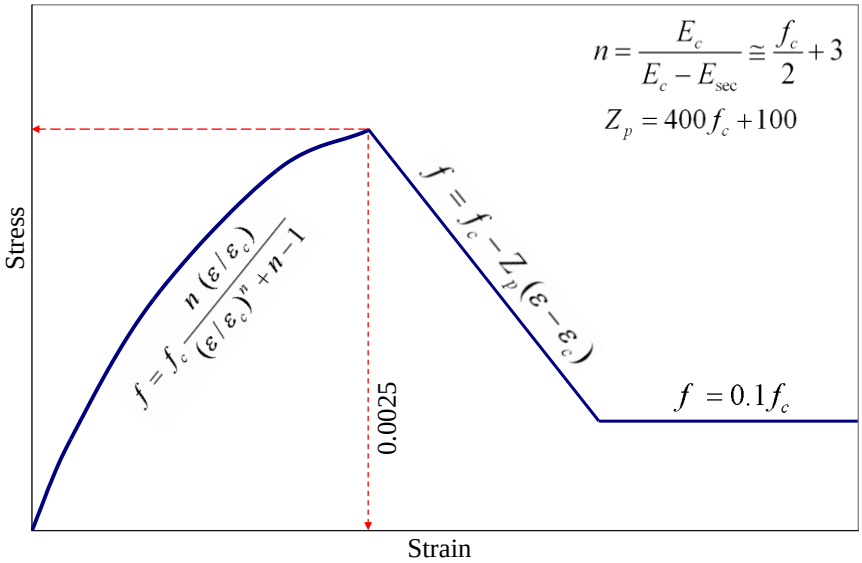

Figure 5.4 Proposed model for compressive stress-strain behavior of plain RAC.

5.3 Model for Confined RAC

5.3.1 Confinement Effectiveness

Similar to the method employed by Sheikh and Uzumeri (1982) and Mander (1984) for normal concrete, the relationship between the strengths of the confined and plain RAC can be expressed as follows:

$$f_{cc} = f_c + f(\rho_s, s, f_s, \alpha) \tag{5.7}$$

where f_{cc} and f_c are strengths of confined and plain RAC, respectively, ρ_s is the volumetric ratio of transverse steel, s is the tie spacing, f_s is the stress in transverse steel, and α is a factor which takes into account the effect of tie configuration and distribution of longitudinal steel.

In rectangular ties the confining pressure is mostly due to the reaction of the ties at the angle bends of the transverse steel as oppose to the uniform lateral pressure of spirals. Due to local effects of the ties, an arching action develops between each two adjacent longitudinal rebars and therefore, part of core remains unconfined. Sheikh and Uzumeri (1982), Mander (1984) and other researchers assumed that the arching action is in the form of a second degree parabola with an initial tangent slope of approximately 45 degrees as shown in Figure 5.5, such that:

$$y = x - \frac{x^2}{d_i} \tag{5.8}$$

where d_i is the center-to-center distance between the adjacent longitudinal rebars. The unconfined area due to one arch, A_i, is:

$$A_i = \int_0^{d_i} (x - \frac{x^2}{d_i})\ dx = \frac{d_i^{\ 2}}{6} \tag{5.9}$$

and therefore the net area at the tie level, $A_{(net)tie}$, can be estimated as follows:

$$A_{e(tie)} = A_{cc} - \frac{1}{6}\sum_{i=1}^{m}(d_i)^2 \tag{5.10}$$

where A_{cc} is the area enclosed by the center line of outer ties and m is the number of

perimeter longitudinal rebars. It is clear that the effectively confined area can be increased by increasing the number of longitudinal rebars. Equation 5.10 can be rewritten as:

$$\alpha = 1 - \frac{1}{6\ A_{cc}} \sum_{i=1}^{n} (d_i)^2 = 1 - \frac{1}{6} \sum_{i=1}^{n} (\frac{d_i}{b_i})^2 \tag{5.11}$$

where α is defined as the ratio of effectively confined core at tie level to the core area. Therefore, the area of effectively confined concrete at the tie level can be written as:

$$A_{e(tie)} = \alpha\ A_{cc} = \alpha\ b_i^{\ 2} \tag{5.12}$$

where b_i is center-to-center distance between opposite sides of external tie, as shown in Figure 5.6.

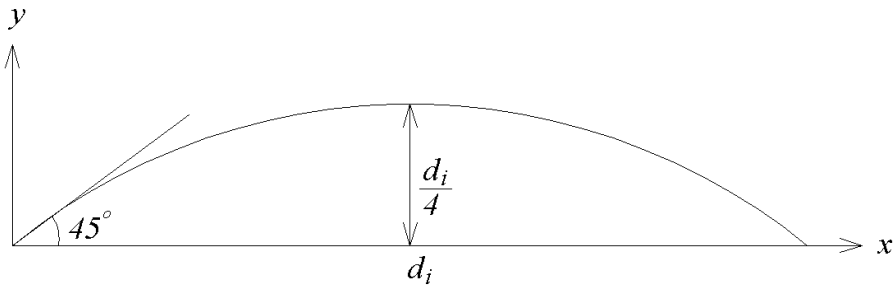

Figure 5.5 Shape of arching action.
Source: Sheikh and Uzumeri, 1982.

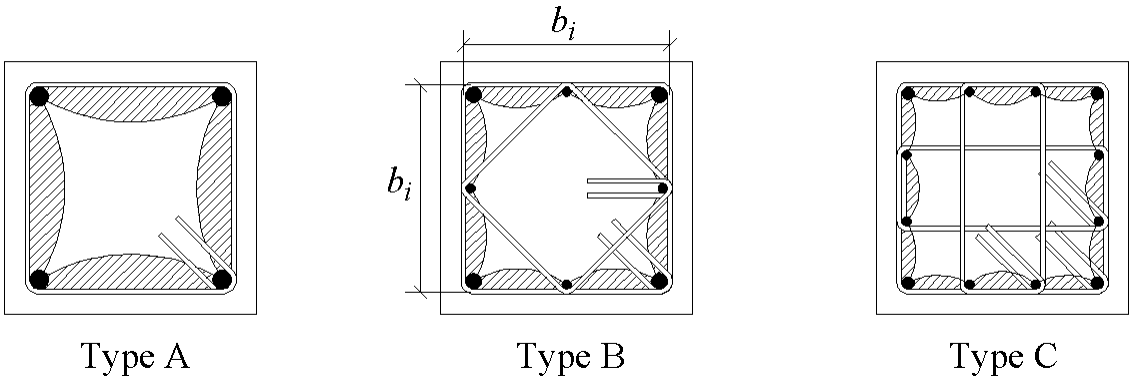

Figure 5.6 Unconfined areas at tie level.

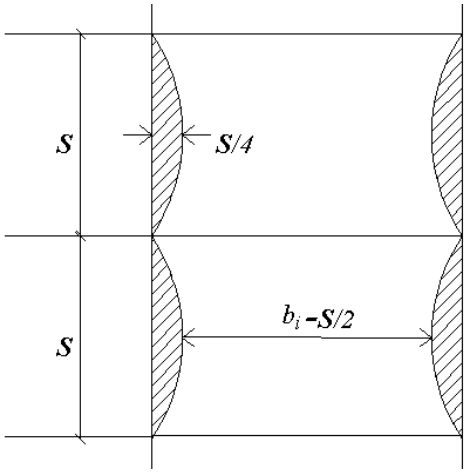

Figure 5.7 Arching action along the column height.

Arching action also happens along the height of the column, midway between the tie levels, as shown in Figure 5.7. The shaded areas in this figure represent the ineffectively confined areas. Similar to confined area at tie level, it is assumed that the curve along which the unconfined and confined concrete separate can be defined by a second degree parabolic equation as defined in Equation 5.8. The exact shape of this curve is not very important because the strength of the compressive concrete is governed by the smallest area of the cross section which is at the center of each two sets of tie. Apparently larger distance between the ties reduces this effective area.

The area of effectively confined area at midway between the ties without considering the horizontal arching action at the tie level can be simply calculated from Figure 5.6:

$$A_{cc(mid)} = (b_i - 0.5\ s)^2 = b_i^{\ 2}(1 - \frac{s}{2b_i})^2 \tag{5.13}$$

and finally, the net area of confined concrete at midway between adjacent ties is calculated using Equations 5.11 through 5.13:

$$A_e = \alpha\ A_{cc(mid)} = \alpha\ b_i^{\ 2}(1 - \frac{s}{2b_i})^2 = \alpha\ (1 - \frac{s}{2b_i})^2\ A_{cc} = \alpha * \ A_{cc} \tag{5.14}$$

where $\alpha *$ is a factor which represents the combined effectiveness of the tie configuration and longitudinal rebar arrangement.

The additional core strength due to confinement effect can be expressed as follows where $P_{conc(\max)}$ is the maximum load carried by the concrete core, $P_{c(unconf)}$ is the load bearing capacity of the concrete core without confinement effect and $P_{c(conf)}$ is the additional core load strength due to confinement:

$$P_{conc(\max)} = P_{c(unconf)} + P_{c(conf)} \tag{5.15}$$

With an insitu strength of f_{ic}, Equation 5.15 can be rewritten as:

$$P_{conc(\max)} = f_{ic}\ A_{cc} + P_{c(conf)} = f_{ic}\ A_{cc} + f_{add}\ A_e \tag{5.16}$$

where f_{add} is the additional strength due to confinement. At this point, K_s factor or the *effectiveness coefficient*, which represents the increase in strength due to the effect of transverse reinforcement, can be obtained through a set of mathematical operations:

$$\frac{P_{conc(\max)}}{A_{cc}} = f_{ic} + \frac{P_{c(conf)}}{A_{cc}} \tag{5.17}$$

$$f_{cc} = f_{ic} + f_{add}\frac{A_e}{A_{cc}} \tag{5.18}$$

$$\frac{f_{cc}}{f_{ic}} = 1 + \frac{f_{add}\ A_e}{f_{ic}\ A_{cc}} \tag{5.19}$$

$$K_s = 1 + \frac{1}{P_{cc}} f_{add}\ A_e \tag{5.20}$$

and finally:

$$K_s = 1 + \frac{1}{P_{cc}} f_{add}\ \alpha * A_{cc} \tag{5.21}$$

Richart et al. (1928) found that the increase in the concrete strength confined by fluid pressure was proportionally higher for lower confining pressure, i.e., they observed higher K_s values for lower fluid pressures. Kent and Park (1971) reported that the strength increasing effect of square lateral reinforcement in normal concrete was

proportional to the square root of volumetric ratio of the steel tie, i.e., $f_{add} \propto (\rho_s)^{1/2}$. Based on these observations, Sheikh and Uzumeri (1982) assumed that the effect of confining pressure in enhancing the strength of the confined normal concrete is equal to $\beta(f_s\ \rho_s)^{1/2}$ where f_s is the stress in lateral reinforcement at the time of the maximum resistance of confined concrete and β is a constant. In this study a similar concept is utilized. The gain in the strength of confined RAC is expressed as:

$$f_{add} = \beta(f_{yt}\ \rho_s)^{\gamma} \tag{5.22}$$

where f_{yt} is the yield stress of the lateral reinforcement, ρ_s is the volumetric ratio of ties and β and γ are constants. Substituting Equation 5.22 in Equation 5.21:

$$K_s = 1 + \frac{1}{P_{cc}} \alpha * A_{cc}\ \beta(f_{yt}\rho_s)^{\gamma} \tag{5.23}$$

In Equation 5.23, the variables β and γ are to be obtained through linear regression of the tests results. It should be noted that when the confinement is fully active, the lateral reinforcement will eventually yield. Therefore, in Equation 5.23 the tie yield stress f_{yt} is used. For normal concrete, Sheikh and Uzumeri (1982) suggested 2.73 and 0.5 for β and γ variables. For RAC these variables are determined in section 5.3.4.

5.3.2 Stress-Strain Curve of Confined RAC

In this section the procedure for determining the stress-strain curve of confined RAC is illustrated. Figure 5.8 graphically shows the entities necessary to determine the stress-strain curve of column A1-1 as an example. In order to establish the stress-strain curve for the confined core, the followings are necessary:

- Stress-strain curve of unconfined RAC;
- "gross" stress-strain curve of RAC column. This curve is obtained by dividing the concrete contribution to the gross area of the concrete. Similar to the example in Figure 4.10 for Column A1-1, for each column, the concrete contribution is obtained. In Appendix B, the concrete contributions of all of the columns tested under static loading are presented;
- Stress-strain curve of "core" concrete. This curve is obtained by dividing the concrete contribution to the area of the concrete core;
- Strain corresponding to the onset of confinement action. As previously described, this is the strain at which the vertical cracks appear. Table 4.1 presents the values of this strain for all the columns. An average value of 0.0020 for this strain is very close to the exact one and consequently is adopted for all of the columns;
- Strain at which the cover is no longer effective in carrying the axial load. Table 4.1 presents the values of this strain.

Using the concept described in Section 4.2 and having the above mentioned entities specified, the stress-strain curve of the confined RAC in column A1-1 (OABC) was determined, as shown in Figure 5.8. In Appendix C, the stress-strain curves of all the columns tested under static loading are presented.

The stress-strain behavior of the confined RAC can be described by four parts: a nonlinear ascending branch which continues up to cracking strain (OA), a straight transition line which is located between the strains corresponding to hair cracks and complete cover spall-off (AB), and linear descending branch followed by the sustaining

branch (BC). An examination of the descending branch of the load-deformation curves (Figure B1 to B9 in Appendix B) shows that between ε_{cc} and $\varepsilon_{50\%}$ (the strain corresponding to 50% of f_{cc}), the descending branch appears to be quite straight. Therefore, ε_{cc} and $\varepsilon_{50\%}$ were used to determine the slope of descending branch.

With reference to Figure 5.8, the stress-strain relationship for confined RAC is suggested as follows:

- Ascending branch (i.e., $\varepsilon \leq 0.0020$):Stress-strain relationship of unconfined normal concrete is applicable to the strains smaller than cracking strain. For the RAC columns, an average strain of 0.002 is suggested as the cracking strain;

- Transition branch (i.e., $0.0020 < \varepsilon \leq \varepsilon_{cc}$): The exact shape of the transition curve is difficult to determine. A straight line can be conservatively used. Determination of ε_{cc} is necessary to determine this portion of the stress-strain curve;

- Deterioration branch (i.e., $\varepsilon \geq \varepsilon_{cc}$): A descending straight line is suggested. A sustaining branch similar to that of unconfined concrete is assumed for the confined RAC where the stress remains constantly equal to $0.10\ f_c$.

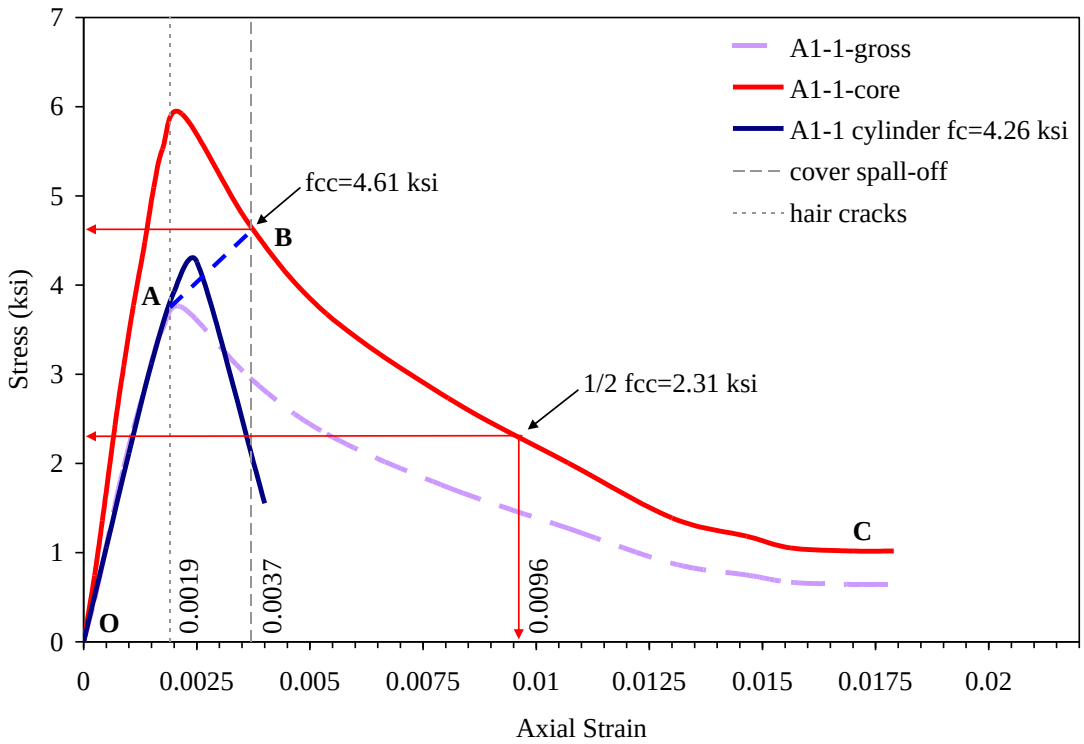

Figure 5.8 Experimental stress-strain curve for column A1-1.

5.3.3 Experimental and Predicted Values of K_s Factor

The experimental values for the *coefficient of effectiveness*, K_s, were obtained using the maximum core strength f_{cc} and insitu strength $0.85 f_c$, as presented in Table 5.1. It is clearly noted that the $(P_{conc})_{\max} / P_{cc}$ values (from Table 4.2) in general tend to overestimate the gain in the strength but it may be used for rough estimation of the real gain in the strength. Figure 5.9 shows the mathematical approach utilized in order to determine the constants β and γ in Equation 5.23. Linear regression of the experimental values of K_s with respect to β and γ, suggested that a value of 4.0 β and a values of 1/3 for γ may be employed, as shown in the figure. Based on these values, Equation 5.23 can be written as follow:

Table 5.1 Experimental Values of Strength Enhancement due to Confinement, K_s

specimen	transverse steel s (in)	transverse steel ρ_s (%)	concrete f_c (ksi)	experimental K_s	approximated K_s (Table 4.2)
A1-1	1	0.88	4.26	1.274	1.40
A1-2	1	0.88	4.41	1.251	1.26
A2-1	2	0.44	4.12	1.195	1.28
A2-2	2	0.44	4.35	1.218	1.30
A3-1	3	0.29	4.26	1.142	1.24
A3-2	3	0.29	4.05	1.135	1.21
B1-1	1	1.51	4.23	1.665	1.49
B1-2	1	1.51	4.42	1.594	1.52
B2-1	2	0.75	4.18	1.460	1.47
B2-2	2	0.75	4.32	1.470	1.49
B3-1	3	0.5	4.36	1.332	1.39
B3-2	3	0.5	4.23	1.365	1.37
C1-1	1	2.1	4.23	1.850	1.62
C1-2	1	2.1	4.06	1.921	1.60
C2-1	2	1.05	4.34	1.577	1.50
C2-2	2	1.05	4.09	1.664	1.57
C3-1	3	0.7	4.45	1.398	1.44
C3-2	3	0.7	4.13	1.386	1.42

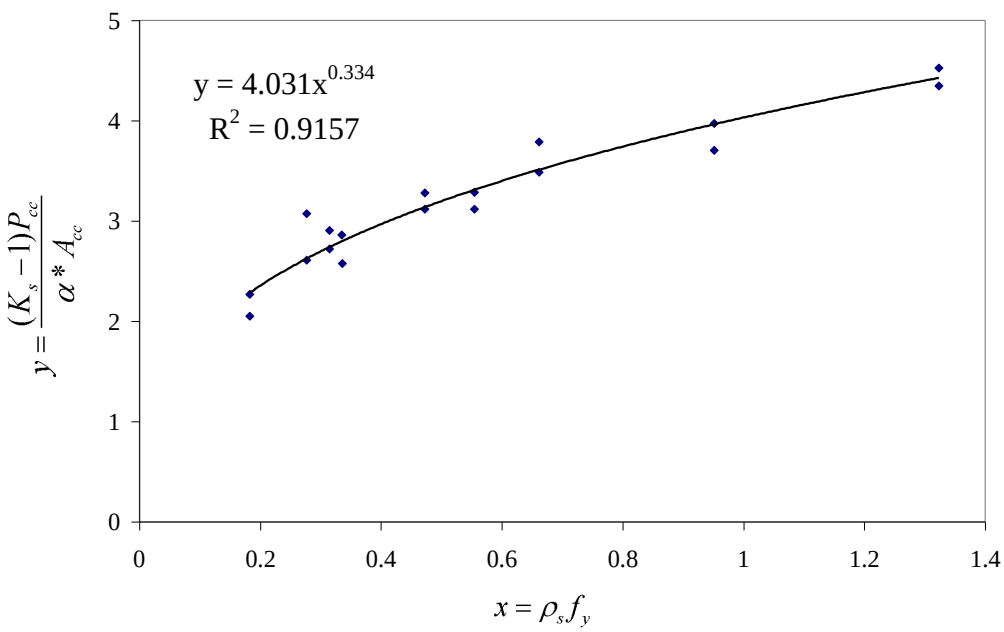

Figure 5.9 Power regression to determine β and γ.

$$K_s = 1 + \frac{1}{P_{cc}} \alpha * A_{cc} \ 4.0 \ (f_{yt} \rho_s)^{1/3} \tag{5.24}$$

It should be recalled that in calculation of K_s for normal concrete, Sheikh and Uzumeri (1982) assumed the values of 2.73 and 0.5 for β and γ, respectively.

5.3.4 Transition and Descending Branches

In order to define the complete stress-strain relationship, f_{cc}, ε_{cc} and slope of the descending branch (i.e., the deterioration rate) are required. This section is devoted to develop statistical equations to approximate these variables.

The first step in determination of the transition and descending branches is the approximation of ε_{cc} in terms of confinement variables. By examining the ε_c and ε_{cc} values, a trend comes into view as shown in Figure 5.10. From the figure, ε_{cc} can be approximated in terms of ε_c (which is assumed to be constantly 0.0025) and K_s, such that:

$$\varepsilon_{cc} = (2K_s - 1) \ \varepsilon_c \tag{5.25}$$

and the transition line can be expressed as the following equation:

$$\frac{f - f_c}{\varepsilon - 0.0020} = \frac{f_{cc} - f_c}{\varepsilon_{cc} - \varepsilon_c} \tag{5.26}$$

For the descending branch a straight line is assumed. The general expression of such a line is similar to that of the descending branch of unconfined RAC (Equation 5.4):

$$f = f_c - Z(\varepsilon - \varepsilon_c) \tag{5.27}$$

where Z is the slope. As described in sub-section 5.3.2, the slope Z can be conveniently obtained through the following equation:

$$Z = \frac{f_{cc}}{2(\varepsilon_{50\%} - \varepsilon_{cc})} \tag{5.28}$$

where $\varepsilon_{50\%}$ is the strain corresponding to 50% of f_{cc}. Examination of Figures C.1 to C.17 in Appendix C suggests that any equation used to approximate the slope of unloading branch should be a function of confinement variables such that it generates proportionally lower slopes for higher confinement values. Such an equation should also be flexible to be reduced to Equation (5.7) when there is no confinement. After extensive examination of different possible equations, the following equation is suggested:

$$Z = \frac{Z_p}{1 + \eta(\rho_s \ f_{yt})^{\lambda}} \tag{5.29}$$

where E_{fall} is the slope of descending branch in unconfined RAC (Equation 5.6) and variables η and λ are constants to be determined by regression analysis, as shown in Figure 5.11. The final form of Equation 5.29 is:

$$Z = \frac{Z_p}{1 + 16(\rho_s \ f_{yt})^2} = \frac{400 \ f_c + 100}{1 + 16(\rho_s \ f_{yt})^2} \tag{5.30}$$

and finally, the suggested set of equations for confined RAC is summarized as follows:

Ascending branch ($0 < \varepsilon \leq 0.0020$):

$$f = f_c \frac{n\ (\varepsilon / \varepsilon_c)}{(\varepsilon / \varepsilon_c)^n + n - 1} \qquad \text{Equation (5.1)}$$

$$n = \frac{E_c}{E_c - E_{\sec}} = \frac{E_c}{E_c - f_c / \varepsilon_c} \qquad \text{Equation (5.2)}$$

$$n = \frac{f_c}{2} + 3 \qquad \text{Equation (5.3)}$$

Transition branch ($0.002 < \varepsilon \leq \varepsilon_{cc}$):

$$\frac{f - f_c}{\varepsilon - 0.0020} = \frac{f_{cc} - f_c}{\varepsilon_{cc} - \varepsilon_c} \qquad \text{Equation (5.27)}$$

$$\varepsilon_{cc} = (2K_s - 1)\ \varepsilon_c \qquad \text{Equation (5.25)}$$

Descending branch ($\varepsilon \geq \varepsilon_{cc}$):

$$Z = \frac{400\ \ f_c + 100}{1 + 16(\rho_s\ \ f_{yt})^2} \qquad (5.30)$$

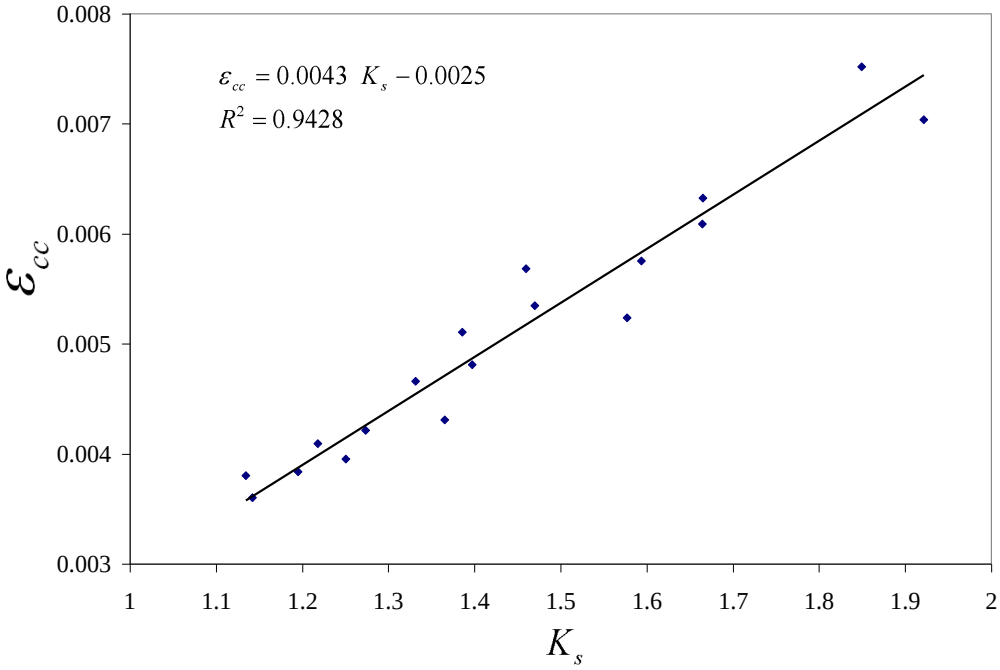

Figure 5.10 Approximation of ε_{cc}.

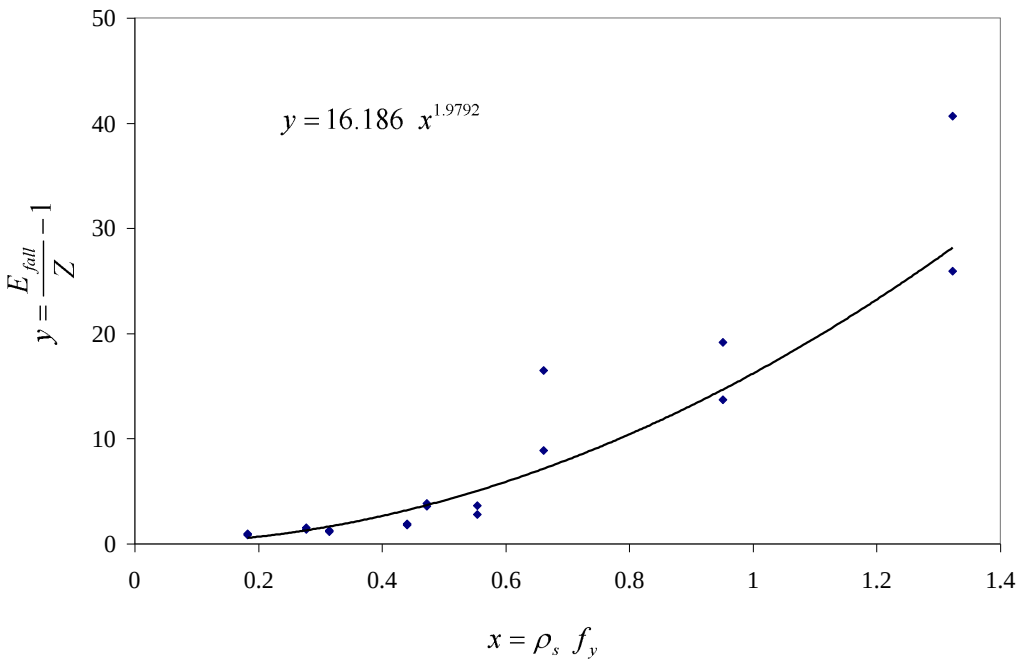

Figure 5.11 Approximation of η and λ values.

5.3.5 Sample Analysis

Given:

Column section (C2-2)	10 in. × 10 in.
Longitudinal reinforcement	4 #3 and 4 #4 (As=1.68 in^2)
Lateral reinforcement	3/8" @ 2 in. c/c
Configuration	"C" (See Figure 3.12)
Center-to-center of the outer tie	8 in.
Cylinder compressive strength	4.32 ksi
Longitudinal reinforcement yield stress	70.0 ksi
Lateral reinforcement yield stress	63.0 ksi

Calculations:

Tie length at a level $= 4\times 8 + 2\times(2\times 8 + 2\times\frac{8}{3}) = 75\ \ in.$

3/8" cross sectional area=0.0276 $in^2 \rightarrow$ Tie volume= 75 × 0.0276=2.061 in^3

Core volume=$8^2\times 2$=128 $in^3 \rightarrow \rho_s = 0.016$

(Equations 5.11) $$\alpha = 1-\frac{1}{6}\times 8\times(\frac{4}{8})^2 = 0.667 \rightarrow \alpha^* = 0.667\times(1-\frac{2}{2\times 8})^2 = 0.511$$

(Equations 4.2) $$P_{cc} = 0.85\times 4.32\times(8^2 - 1.68) = 228.8\ \ kips$$

(Equations 5.24) $$K_s = 1+\frac{1}{228.8}\times 0.511\times 8^2\times 4\times(0.016\times 63)^{1/3} = 1.564$$

(Equations 5.25) $$\varepsilon_{cc} = (2K_s - 1)\ \ \varepsilon_c = (2\times 1.564 - 1)\ \ \times 0.0025 = 0.0053$$

(Equations 5.30) $$Z = \frac{400 f_c + 100}{1+16\ \ (\rho_s f_y)^2} = 106$$

Using Equations 5.1, 5.27 and 5.30, the stress-strain curve of the confined core was calculated and plotted against the experimental results for column C2-2, as shown in Figure 5.12. From the Figure, it can be concluded that the proposed model is very accurate within the ascending and transition branches. The predicted descending branch however, slightly deviates from the experimental curve but it is within the margins of experimental results. It is worth to recall that the exact shape of the transition branch is very difficult to determine. The use of a straight line to describe the transition branch is just because of its simplicity.

Due to smaller modulus of elasticity of RAC, the mathematical models for normal concrete may not be able to accurately capture the stress-strain behavior of RAC. This is can also be seen in Figure 5.12 where the predicted stress-strain of the RAC is plotted against Sheikh and Uzumeri (1982) and Mander (1984) models which are widely used for approximating stress-strain behavior of normal concrete. As it can be seen from the figure, there is a significant difference between the slope of the ascending branch of RAC stress-strain curve and those predicted by Sheikh and Uzumeri (1982) and Mander (1984) models.

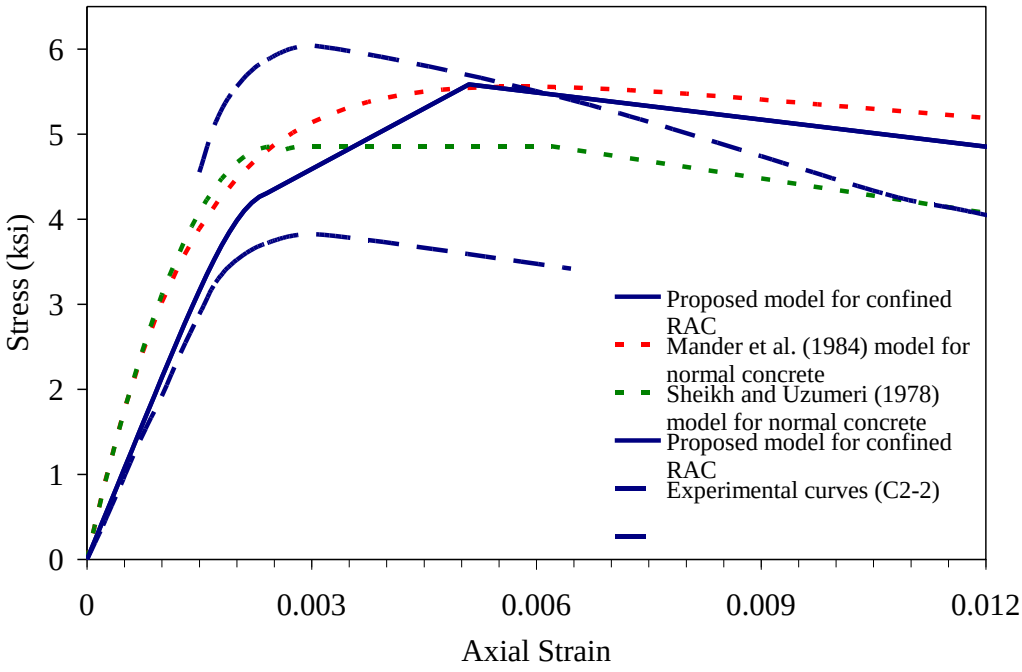

Figure 5.12 Proposed RAC model versus models for normal concrete.

CHAPTER 6

EXAMINATION OF RAC MODELS IN FLEXURE

The proposed models for unconfined and confined RAC under axial compressive stresses were examined in flexure. For this purpose, two RAC beams were constructed and tested using the MTS loading unit. Experimental load-deformation behavior of RAC beams were obtained and compared with the nonlinear behavior predicted using the proposed models.

.

6.1 Numerical Analysis

6.1.1 Material and Geometrical Properties

Geometrical properties of the beams are shown in Figure 6.1. For the purpose of analysis, the beam is longitudinally divided into multiple segments. Each cross section is divided into fibers, as shown in Figure 6.1. The reinforcing steel is assumed to be elastic-perfectly plastic, characterized by its elastic modulus and yield stress.

An average compressive strength of 4.22 ksi was obtained for two RAC cylinder samples. The mechanical properties of the reinforcing steel were the same as those of column reinforcing steel, as presented in Chapter 3, since similar ones were used. The unconfined stress-strain relationships are calculated as follows:

From Equation (5.3): $n = \frac{f_c}{2} + 3 = \frac{4.22}{2} + 3 = 5.11$

also: $E_{\sec} = \frac{f_c}{\varepsilon_c} = 1688 \text{ ksi} \rightarrow n = \frac{E_c}{E_c - E_{\sec}} = \frac{E_c}{E_c - 1688} = 5.11 \rightarrow E_c = 2099 \text{ ksi}$

$0 < \varepsilon \le 0.0025$: (Equation5.1) $$f = \frac{4.22 \times 5.11 \left(\frac{\varepsilon}{0.0025}\right)}{\left(\frac{\varepsilon}{0.0025}\right)^{5.11} + 5.11 - 1} = \frac{8626\ \varepsilon}{\left(\frac{\varepsilon}{0.0025}\right)^{5.11} + 4.11}$$

$0.0025 < \varepsilon \le \varepsilon_{cc}$: (Equations 5.6) $E_{fall} = 400 f_c + 100 = 1788$ ksi

(Equations 5.4) $f = f_c - E_{fall}(\varepsilon - \varepsilon_c) = 4.22 - 1788\ (\varepsilon - 0.0025)$

The proposed equations for RAC confined in square ties should generate reasonable results for rectilinear cross sections as long as the tie dimensions are not significantly different. The confined stress-strain relationships for the beam core RAC, are calculated as follows:

Volume of steel tie: $V_{tie} = 2 \times (2.5 + 4.0) \times 0.0276 = 0.359\ \text{in}^3$

Volume of confined core: $V_{core} = (2.5 \times 4.0) \times 1.5 = 15\ \text{in}^3$

Tie steel volumetric ratio: $\rho_s = \frac{0.359}{15} = 0.024$

(Equations 5.11) $$\alpha = 1 - \frac{\sum_{i=1}^{m} (d_i)^2}{6\ A_{cc}} = 1 - \frac{1}{6} \times \frac{2}{10}(2.5^2 + 4.0^2) = 0.258$$

Having the tie spacing s and tie dimensions b and w:

(Equations 5.14) $$\alpha^* = \alpha\ \frac{A_{cc(mid)}}{A_{cc}} = \alpha \times \frac{(b - 0.5s)(w - 0.5s)}{bw} =$$

$$0.258 \times \frac{(2.5 - 0.75)(4 - 0.75)}{2.5 \times 4.0} = 0.147$$

(Equations 4.2) $P_{cc} = 0.85 f_c \times A_{cc} =$

$$0.85 \times 4.0 \times (2.5 \times 4 - 2 \times 0.11 - 2 \times 0.05) = 32.91\ \text{kips}$$

Therefore, the *effectiveness coefficient* can be calculated:

(Equations 5.24) $$K_s = 1 + \frac{1}{P_{cc}} \alpha * A_{cc} \ 4.0 \ (f_{yt}\rho_s)^{1/3} =$$

$$1 + \frac{1}{32.91} \times 0.147 \times 10 \times 4.0 \times (63 \times 0.024)^{1/3} = 1.205$$

Also:

(Equations 5.25) $$\varepsilon_{cc} = (2K_s - 1)\varepsilon_c = (2 \times 1.205 - 1) \times 0.0025 = 0.0035$$

(Equations 5.30) $$Z = \frac{400 \ f_c + 100}{1 + 16(\rho_s \ f_{yt})^2} = \frac{400 \times 4.22 + 100}{1 + 16(0.024 \times 63)^2} \approx 47 \text{ ksi}$$

Finally, the stress-strain relation for the confined core can be presented as:

$0 < \varepsilon \le 0.0020$: $$f = (4.22) \times \frac{5.11 \left(\frac{\varepsilon}{0.0025}\right)}{\left(\frac{\varepsilon}{0.0025}\right)^{5.11} + 5.11 - 1} = \frac{8626 \ \varepsilon}{\left(\frac{\varepsilon}{0.0025}\right)^{5.11} + 4.11}$$

$0.0020 < \varepsilon \le 0.0035$: $$\frac{f - 3.89}{\varepsilon - 0.0020} = \frac{4.32 - 3.89}{0.0035 - 0.0020} = 433$$

$\varepsilon \ge 0.0035$: $$f = f_{cc} - Z \ (\varepsilon - \varepsilon_{cc}) = 4.32 - 46 \ (\varepsilon - 0.0035)$$

Ignoring the tensile resistance of concrete that is customary in the calculation of ultimate load bearing capacity, can lead to overestimation of the deflections. Currently there is no available tensile stress-strain model for RAC. It is assumed that similar to normal concrete, tensile concrete behaves in a linear-elastic manner up to the peak stress. The strain softening branch is commonly considered to be a straight line. The slope of the tensile softening branch is calculated using Bazant and Oh (1983) model:

$$E_t = \frac{70\ E_c}{57 + f_t} \tag{6.1}$$

where E_t is the slope of strain softening branch in psi, E_c is concrete modulus of elasticity (the same for tension and compression) in psi and f_t is tensile strength in psi which can be estimated using the ACI equation for estimating tensile strength:

$$f_t = 7.5\sqrt{f_c} = 7.5\sqrt{4220} = 490 \text{ psi}$$

The stress-strain model for the concrete in tension then can be calculated as follows:

$$0 < \varepsilon \le \frac{f_t}{E_c} = 0.00025: \qquad \sigma = E_c \varepsilon$$

$$\varepsilon > 0.00025: \qquad E_t = \frac{70 \times 2{,}100{,}000}{57 + 490} = 269{,}000 \text{ psi}$$

$$\sigma = f_t - E_t(\varepsilon - \varepsilon_t) = 0.490 - 269\ (\varepsilon - 0.00025) \text{ ksi}$$

The stress-strain diagrams are shown in Figure 6.2.

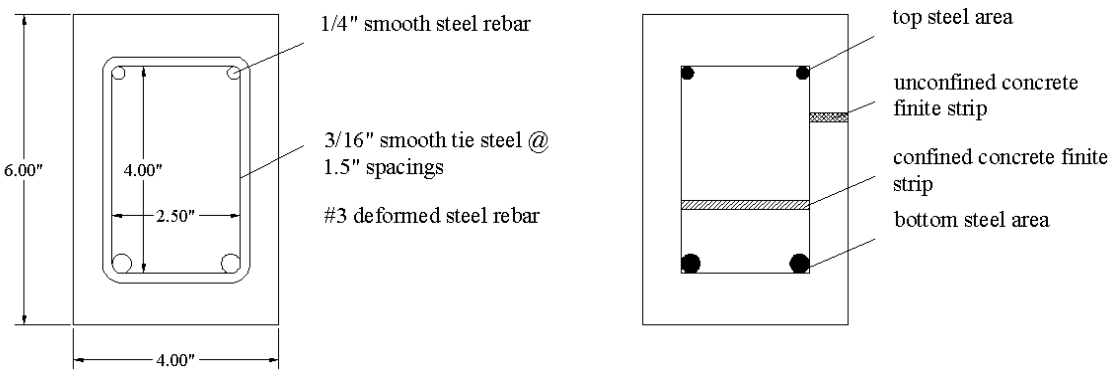

Figure 6.1 Cross-section of the RAC beams.

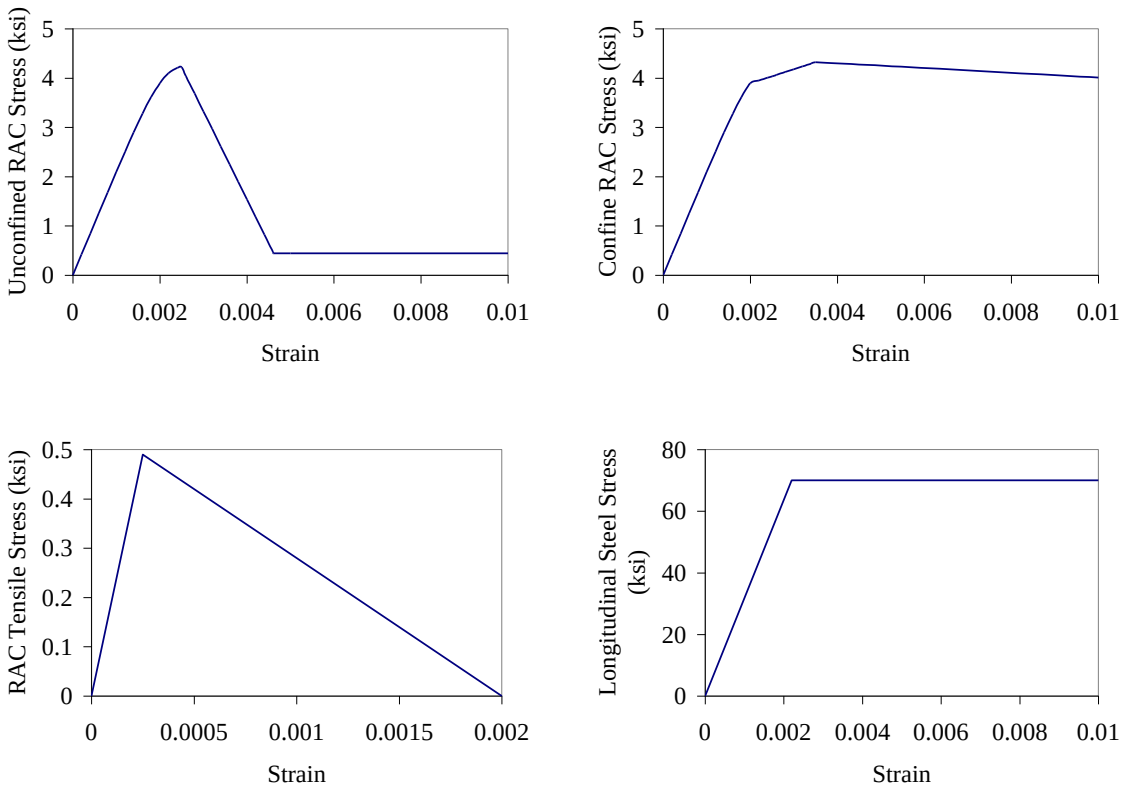

Figure 6.2 Stress-strain behavior of the materials used in the numerical analysis.

6.1.2 Calculation of Deflections

In analysis of the beams, the Bernoulli-Navier's hypothesis is employed. It states that all the beam sections remain plane and perpendicular to the longitudinal axis. This assumption is valid because a length-to-depth ratio of 7 that is relatively high and consequently the shear deformations are negligible. It is also assumed that geometrically nonlinear effects are negligible. The equations of equilibrium with respect to axial load and bending moment are:

$$N = \int_{A_{UC}} f\, dA + \int_{A_{CC}} f\, dA + \sum A_s \sigma_s \tag{6.1}$$

$$M = \int_{A_{UC}} d_c f \, dA + \int_{A_{CC}} d_c f \, dA + \sum d_s A_s \sigma_s \tag{6.2}$$

where f is the concrete stress (either tensile of compressive), σ_s is the stress in longitudinal steel, A_s is the area of longitudinal steel and d_c and d_s are the distance from concrete finite elements and steel rebars to the beam's top extreme fiber, respectively. In the above equations, the first term refers to the contribution of unconfined concrete, the second term refers to the contribution of confined concrete and the third term refers to the contribution of longitudinal steel.

According to the principle of virtual work, the midspan deflection δ can be evaluated in terms of internal moments and curvatures:

$$\delta = \int_0^L \kappa(x) \; m(x) \; dx \tag{6.3}$$

where $m(x)$ is the internal moment due to unit load in the direction of δ, $\kappa(x)$ is the curvature and L is the length of the beam. For the beams under consideration, the above integral was evaluated numerically such that the equilibrium equations were satisfied. The following steps were utilized. It should be noted that use of a computer program is necessary to run the iterations:

- Determine the relation between the internal moment and the curvature at different cross sections. For this, given a small increment of curvature, adjust the axial strain such that Equation 6.1 is satisfied. Obtain the internal moment using Equation 6.2. Repeat the same procedure to obtain the complete range of the moment-curvature;

- Using the complete moment-curvature data and the loading condition and Equation 6.3 compute the deflection.

In calculation of the moment-curvature diagram, the beam was divided to 7 equal segments, as shown in Figure 6.3. The use of smaller divisions was found to be unnecessary because it did not significantly change the results. Figure 6.4 shows the calculated moment-curvature. The data are presented in Table 6.1. M_1 through M_7 are the moments in sections 1 through 7 and κ_1 through κ_7 are the corresponding curvatures, as shown in Figure 6.4. Using the iterative approach described, the moment-curvature and load-deflection curves were computed as presented in Table 6.1.

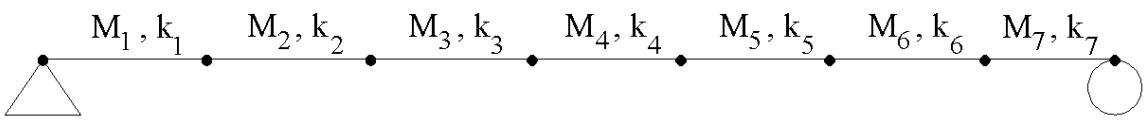

Figure 6.3 Beam divisions for numerical calculation.

6.2 Experimental Results

Figure 6.5 shows the two identical beams tested under the MTS 810 loading unit. The total beam length was 60 inches while the clear span was 42 inches. Concentrated load was applied on the middle of the beams at a constant rate of 0.0005 inch per second and the load-deformation data was recorded.

Figure 6.6 shows the development of tensile cracks and crushing in the beams prior to ultimate failure. The tensile cracks appeared at a deflection of 0.017 inch and 0.021 inch for Beam-1 and Beam-2, respectively. The cracking deflection was quite close to the calculated value of 0.022 in. The crushing of the compressive concrete started a

deflection of 0.205 inch and 0.240 inch for Beam-1 and Beam-2, respectively while the calculated cracking deflection was 0.233 inch, quite close to the experimental values. The beams exhibited considerable ductility and eventually failed in flexure, as shown in Figure 6.6. Up to a deflection of 0.40 inches, the calculated behavior is quite close to the actual behavior of the RAC beams. For higher deflection however, differences become more noticeable.

In Figure 6.7 the load-deformation curve predicted using the proposed RAC models are compared with the experimental results. As it can be noted, the prediction is very close to the experimental results. In general, the differences between the predicted and experimental curves are less than 10%. The deviation of the predicted and experimental curves may be attributed to the confining effect of the loading plats, where that are not considered in the numerical calculations.

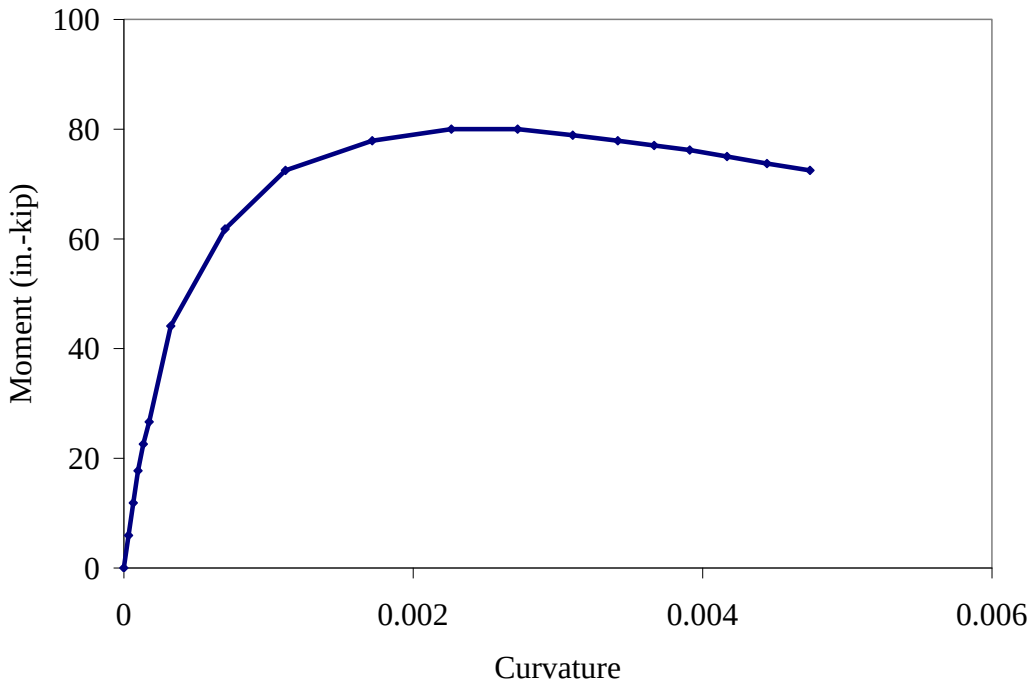

Figure 6.4 Analytical moment-curvature diagram.

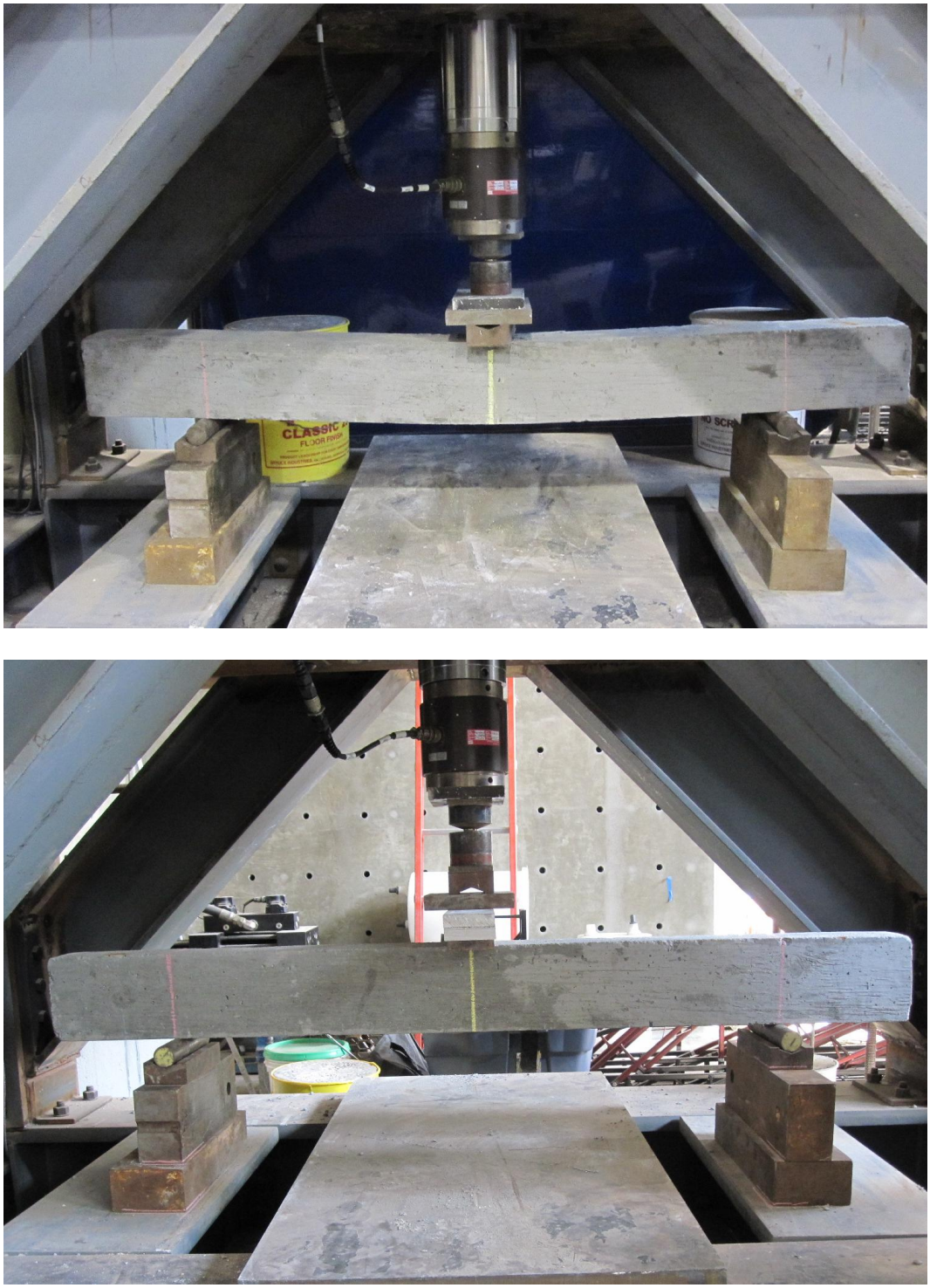

Figure 6.5 Beam test setup: (top) Beam-1, (bottom) Beam-2.

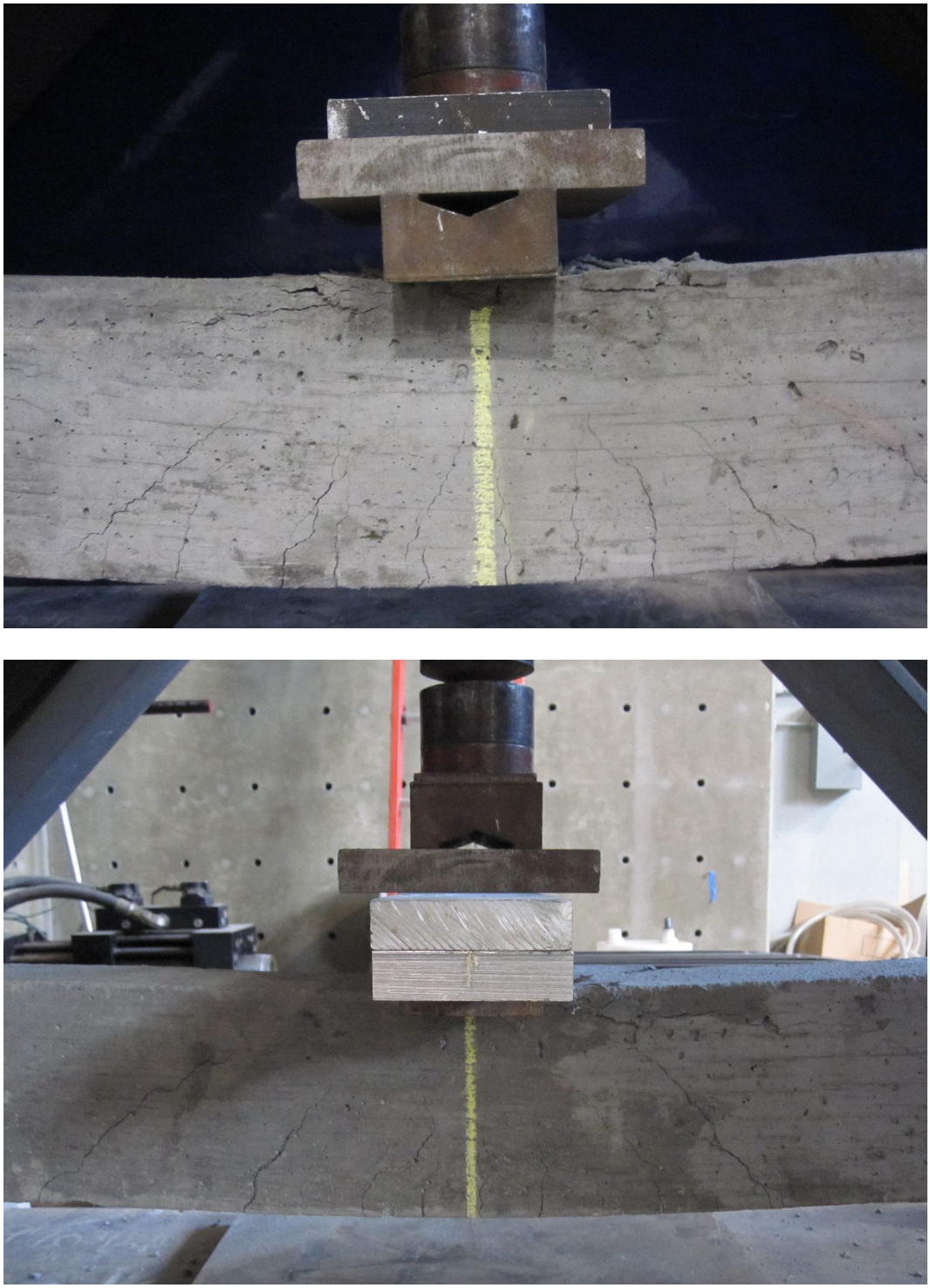

Figure 6.6 Development of cracks and crushing: (top) Beam 1, (bottom) Beam 2.

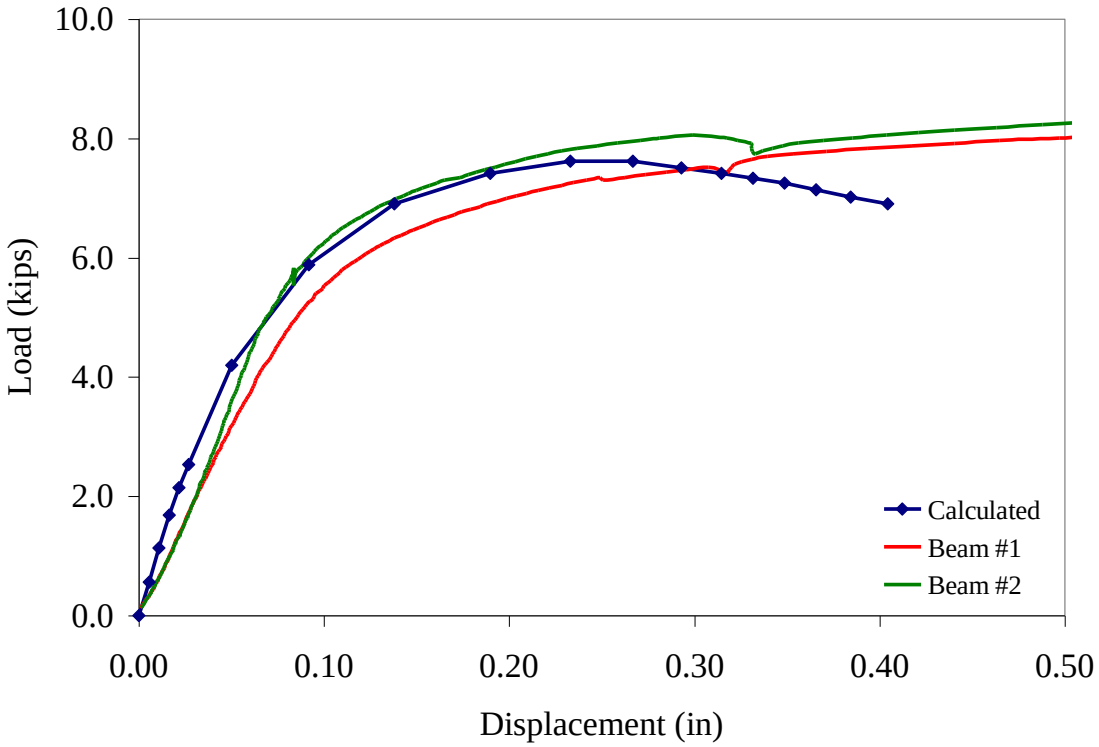

Figure 6.7 Calculated and experimental load-deformation of the RAC beams.

Table 6.1 Predicted Curvature and Deflection Values

Strain	Curvature (in^{-1})	Moment (in.-kips)	P (kips)	M_1 & M_7	M_2 & M_6	M_3 & M_5	M_4	κ_1 & κ_7	κ_2 & κ_6	κ_3 & κ_5	κ_4	δ (in)
0	0	0	0	0	0	0	0	0	0	0	0	0
0.0001	2.99E-05	5.94	0.57	0.85	2.54	4.24	5.94	8.1195E-06	1.6239E-05	2.4359E-05	3.2478E-05	0.006
0.0003	8.97E-05	11.87	1.13	1.70	5.09	8.48	11.87	1.6239E-05	3.2478E-05	4.8717E-05	6.4956E-05	0.012
0.0004	1.21E-04	17.71	1.69	2.53	7.59	12.65	17.71	2.4216E-05	4.8432E-05	7.2870E-05	9.7784E-05	0.018
0.0005	1.54E-04	22.56	2.15	3.22	9.67	16.11	22.56	3.0851E-05	6.1703E-05	9.3349E-05	1.3432E-04	0.024
0.001	3.39E-04	26.63	2.54	3.80	11.41	19.02	26.63	3.6411E-05	7.3049E-05	1.1481E-04	1.7544E-04	0.029
0.0015	5.36E-04	44.11	4.20	6.30	18.91	31.51	44.11	6.0326E-05	1.3053E-04	2.3060E-04	3.2478E-04	0.055
0.002	7.26E-04	61.79	5.88	8.83	26.48	44.13	61.79	8.5058E-05	2.1189E-04	3.7213E-04	7.0061E-04	0.101
0.0025	9.04E-04	72.48	6.90	10.35	31.06	51.77	72.48	1.0010E-04	2.5755E-04	5.4269E-04	1.1173E-03	0.148
0.003	1.06E-03	77.89	7.42	11.13	33.38	55.63	77.89	1.0771E-04	2.8063E-04	6.2890E-04	1.7170E-03	0.201
0.0035	1.24E-03	80.02	7.62	11.43	34.29	57.14	80.02	1.1068E-04	2.8965E-04	6.6260E-04	2.2642E-03	0.245
0.004	1.40E-03	80.09	7.62	11.43	34.29	57.14	80.09	1.1068E-04	2.8965E-04	6.6260E-04	2.7216E-03	0.278
0.0045	1.49E-03	78.87	7.51	11.27	33.80	56.34	78.87	1.0909E-04	2.8483E-04	6.4458E-04	3.1032E-03	0.304
0.005	1.56E-03	77.89	7.42	11.13	33.38	55.63	77.89	1.0771E-04	2.8063E-04	6.2890E-04	3.4143E-03	0.326
0.0055	1.64E-03	77.00	7.33	11.00	33.00	55.00	77.00	1.0646E-04	2.7684E-04	6.1476E-04	3.6657E-03	0.343
0.006	1.75E-03	76.17	7.25	10.88	32.64	54.41	76.17	1.0529E-04	2.7329E-04	6.0147E-04	3.9118E-03	0.360
0.0065	1.88E-03	75.05	7.14	10.71	32.14	53.57	75.05	1.0365E-04	2.6830E-04	5.8286E-04	4.1696E-03	0.377
0.007	2.03E-03	73.71	7.02	10.53	31.59	52.65	73.71	1.0183E-04	2.6279E-04	5.6229E-04	4.4460E-03	0.395
0.0075	2.17E-03	72.48	6.90	10.35	31.06	51.77	72.48	1.0010E-04	2.5755E-04	5.4269E-04	4.7425E-03	0.415

CHAPTER 7

CONCLUSIONS

7.1 General

This chapter summarizes the most important findings as well as the conclusions drawn from both the experimental and the analytical study carried out during this research. The novel models proposed for plain and confined RAC are summarized. In general, the results showed that RAC may be suitable for structural use. The chapter ends with a brief list of areas recommended for further research.

7.2 Conclusions from the Experimental Study

An extensive experimental program including testing of several plain RAC cylinders as well as 44 reinforced RAC columns, 10 inches by 10 inches in section and 32 inches in height, with different tie arrangements was conducted at the High Performance Concrete Laboratory of New Jersey Institute of Technology. The specimens were tested under quasi-static and dynamic (both monotonic and cyclic) axial compression. The following conclusions can be drawn from the results of these tests:

1. Depending on the compressive strength, the elastic modulus of plain RAC is 30% to 50% less than that of normal concrete. The higher the strength, the less the difference is;

2. The strain corresponding to maximum compressive strength of a plain RAC is 0.0025. This value is appreciably more than the average value of 0.002 for normal concrete;

3. When efficiently confined with rectilinear ties and longitudinal reinforcement, RAC can exhibit a significant gain 60% more strength compared with the design values. The gain in the strength, however, is not proportional to the increase in volumetric ratio of the ties;

4. Similar to normal confined concrete, the gain in ductility-- which is of significant interest in seismic design of structural members-- by improving confinement variables is very pronounced. This finding shows that in general, RAC may be suitable for structural and seismic use;

5. In particular, distributing the longitudinal steel around the perimeter of the column, reducing the spacing of the ties and increasing volumetric ratio of the lateral reinforcement improves the enhancing effects of the confinement;

6. The strength may be roughly approximated by finding the $(P_{conc})_{\max} / P_{cc}$ ratio. In general this ratio tend to over estimate the real gain in the strength;

7. Up to an axial strain about 0.0020 and regardless of the amount of lateral reinforcement, RAC columns behave as if they are plain. At this stage vertical hair cracks appear on the cover. Interestingly, for normal concrete columns, the strain corresponding to the onset of confinement action is similarly observed to be between 0.0015 and 0.0020;

8. The strain at which the cover spalls off is in a wide range of 0.0040 to 0.0070, depending on the amount of lateral reinforcement. For normal concrete a strain between 0.004 and 0.005 is suggested, which is a narrower range; this means that the mechanism of confinement in RAC columns has a quite slower nature;

9. The compressive failure mode of RAC columns is not different with normal concrete columns: cover spall off, core crushing and buckling of longitudinal rebars followed by breaking and possibly hook slippage of the lateral reinforcement;

10. Under high straining rates, RAC column show 7% to 26% increase in ultimate axial strength. In order to approximate the gain in strength due to high straining rates and in the absence of specific equations for RAC, the proposed equation for normal concrete may be used;

7.3 Conclusions from the Analytical Study

7.3.1 Proposed Model for Plain RAC

A set of mathematical expressions is proposed to predict the stress-strain behavior of RAC. The proposed model contains a nonlinear ascending branch and a linear falling branch followed by sustaining branch, as shown in Figure 7.1. For the sustaining branch is assumed, i.e., the falling branch continues until it meets the strain axis. The set of

equations are as follows:

Ascending branch ($0 < \varepsilon \leq 0.0025$):

$$f = f_c \frac{n\ (\varepsilon / \varepsilon_c)}{(\varepsilon / \varepsilon_c)^n + n - 1} \qquad \text{Equation (5.1)}$$

$$n = \frac{E_c}{E_c - E_{\sec}} = \frac{E_c}{E_c - f_c / \varepsilon_c} \qquad \text{Equation (5.2)}$$

$$n = \frac{f_c}{2} + 3 \qquad \text{Equation (5.3)}$$

Ascending branch ($\varepsilon \geq 0.0025$):

$$f = f_c - Z_p(\varepsilon - \varepsilon_c) \qquad \text{Equation (5.4)}$$

$$Z_p = 400 f_c + 100 \qquad \text{Equation (5.6)}$$

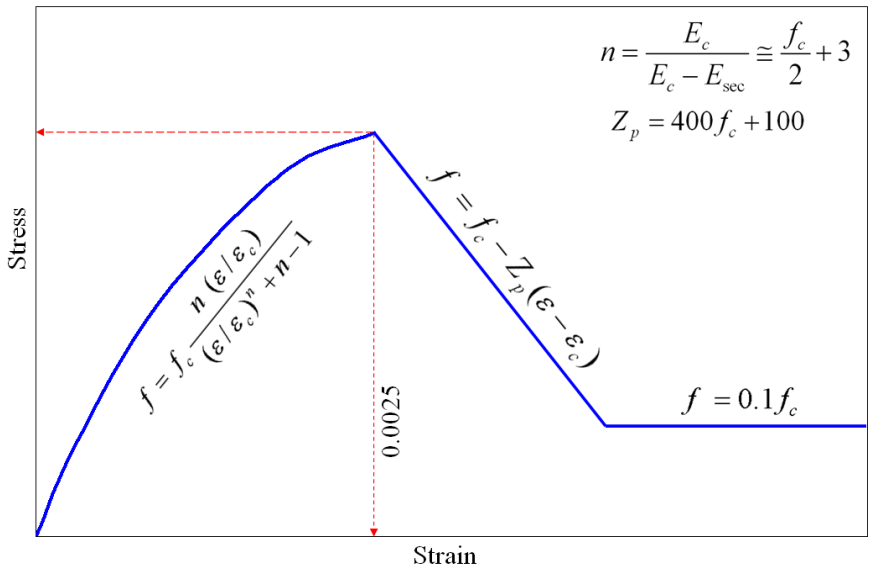

Figure 7.1 Proposed model for compressive stress-strain behavior of plain RAC.

7.3.2 Proposed Model for Confined RAC

A model for predicting stress-strain behavior of confined RAC was developed. The model is limited to normal-strength RAC with square ties. Similar to previous studies on confinement of normal concrete, the gain in the compressive strength is expressed in terms of the area of effectively confined concrete. In calculation of the effectively confined area, the effect of in-plane and vertical arching action is included. The proposed model contains a nonlinear ascending branch, a linear transition branch and a linear falling branch, as shown in Figure 7.2. A sustaining branch Similar to that of plain RAC was assumed for the confined RAC. The following set of equations is proposed to approximate the stress-strain behavior of confined RAC:

Ascending branch ($0 < \varepsilon \leq 0.0020$):

$$f = f_c \frac{n\ (\varepsilon / \varepsilon_c)}{(\varepsilon / \varepsilon_c)^n + n - 1} \qquad \text{Equation (5.1)}$$

$$n = \frac{E_c}{E_c - E_{\sec}} = \frac{E_c}{E_c - f_c / \varepsilon_c} \qquad \text{Equation (5.2)}$$

$$n = \frac{f_c}{2} + 3 \qquad \text{Equation (5.3)}$$

Transition branch ($0.002 < \varepsilon \leq \varepsilon_{cc}$):

$$\frac{f - f_c}{\varepsilon - 0.0020} = \frac{f_{cc} - f_c}{\varepsilon_{cc} - \varepsilon_c} \qquad \text{Equation (5.27)}$$

$$\varepsilon_{cc} = (2K_s - 1)\ \varepsilon_c \qquad \text{Equation (5.25)}$$

Descending branch ($\varepsilon \geq \varepsilon_{cc}$):

$$f = f_{cc} - Z_c(\varepsilon - \varepsilon_c) \qquad \text{Equation (5.27)}$$

$$Z_c = \frac{400\ f_c + 100}{1 + 16(\rho_s\ f_{yt})^2} \qquad \text{Equation (5.30)}$$

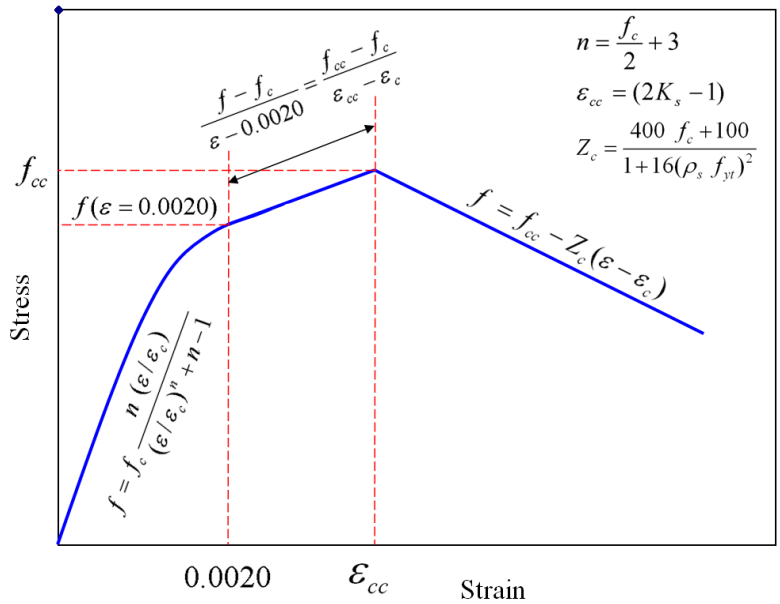

Figure 7.2 Proposed model for compressive stress-strain behavior of confined RAC.

7.4 Recommendation for Future Research

The study conducted to propose the model for confined RAC was limited to columns with square cross section and made of normal-strength RAC. Application of the proposed analytical model to other conditions such as high-strength RAC, spiral or rectangular transverse reinforcement and other design possibilities require further research. In particular, the following research areas appear to be the next steps:

1. The applicability of the proposed model to RAC made of RCA with different cleanliness and quality;
2. The applicability of the proposed model to spiral, rectangular and irregular configurations of ties. The use of full-size of near-full size specimen is recommended;
3. The applicability of the model for high-strength RAC;

APPENDIX A

FAILURE MODE OF RAC COLUMNS

In this appendix photos illustrating the failure mode of the RAC column are presented.

South and East sides North and West sides

Figure A.1 Failure of Column A1-1 under static loading.

South and East sides North and West sides

Figure A.2 Failure of Column A1-2 under static loading.

South and East sides

North and West sides

Figure A.3 Failure of Column A2-1 under static loading.

South and East sides

North and West sides

Figure A.4 Failure of Column A2-2 under static loading.

South and East sides

North and West sides

Figure A.5 Failure of Column A3-1 under static loading.

South and East sides

North and West sides

Figure A.6 Failure of Column A3-2 under static loading.

South and East sides

North and West sides

Figure A.7 Failure of Column B1-1 under static loading.

South and East sides

North and West sides

Figure A.8 Failure of Column B1-2 under static loading.

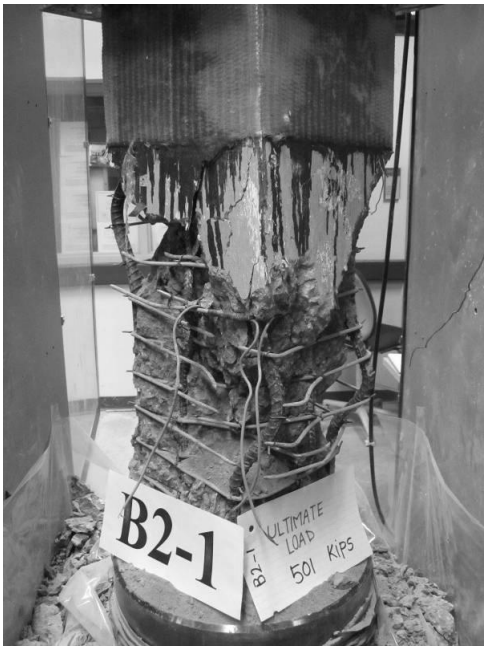

South and East sides

North and West sides

Figure A.9 Failure of Column B2-1 under static loading.

South and East sides

North and West sides

Figure A.10 Failure of Column B2-2 under static loading.

South and East sides North and West sides

Figure A.11 Failure of Column B3-1 under static loading.

South and East sides North and West sides

Figure A.12 Failure of Column B3-2 under static loading.

South and East sides

North and West sides

Figure A.13 Failure of Column C1-1 under static loading.

South and East sides

North and West sides

Figure A.14 Failure of Column C1-2 under static loading.

South and East sides

North and West sides

Figure A.15 Failure of Column C2-1 under static loading.

South and East sides

North and West sides

Figure A.16 Failure of Column C2-2 under static loading.

South and East sides North and West sides

Figure A.17 Failure of Column C3-1 under static loading.

South and East sides North and West sides

Figure A.18 Failure of Column C3-2 under static loading.

APPENDIX B

DETERMINATION OF CONCRETE CONTRIBUTION

In this appendix the contributions of concrete and longitudinal reinforcement in carrying the axial load are presented.

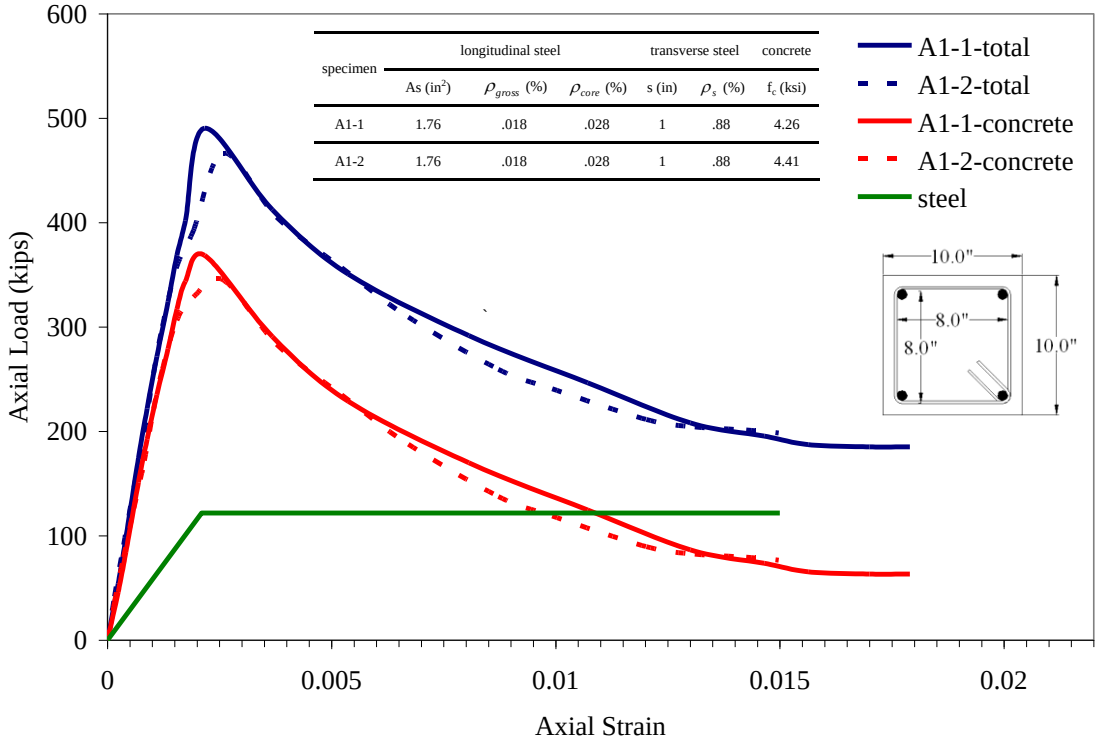

Figure B.1 Determination of concrete contributions for Columns A1-1 and A1-2.

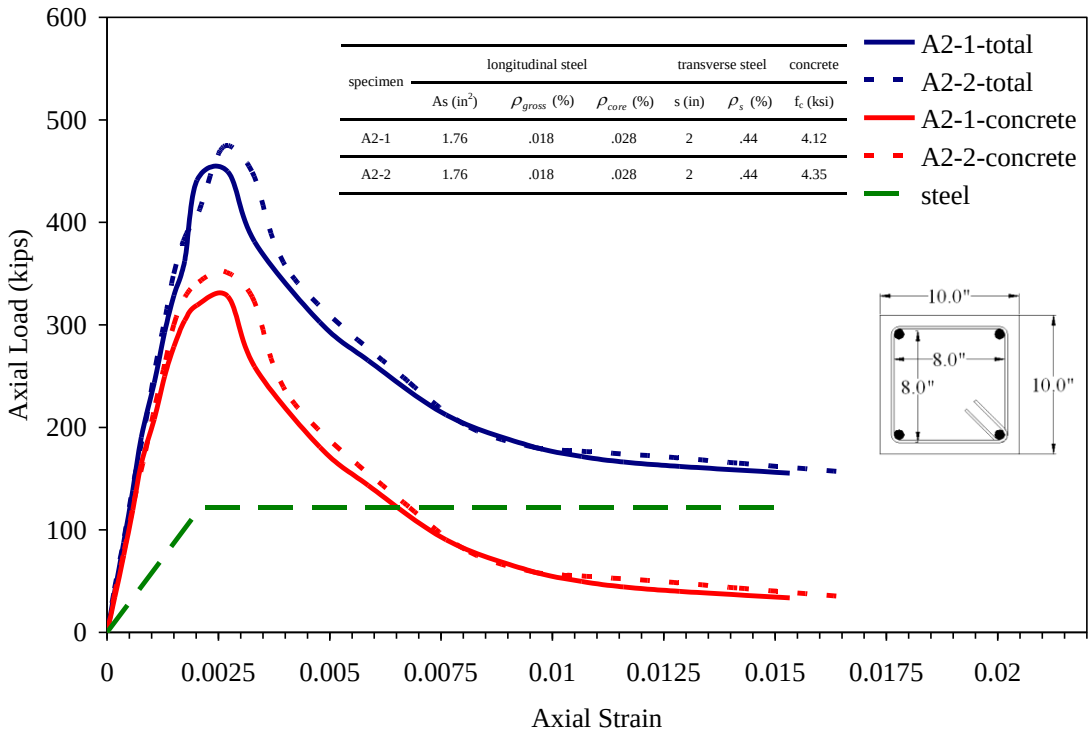

Figure B.2 Determination of concrete contributions for Columns A2-1 and A2-2.

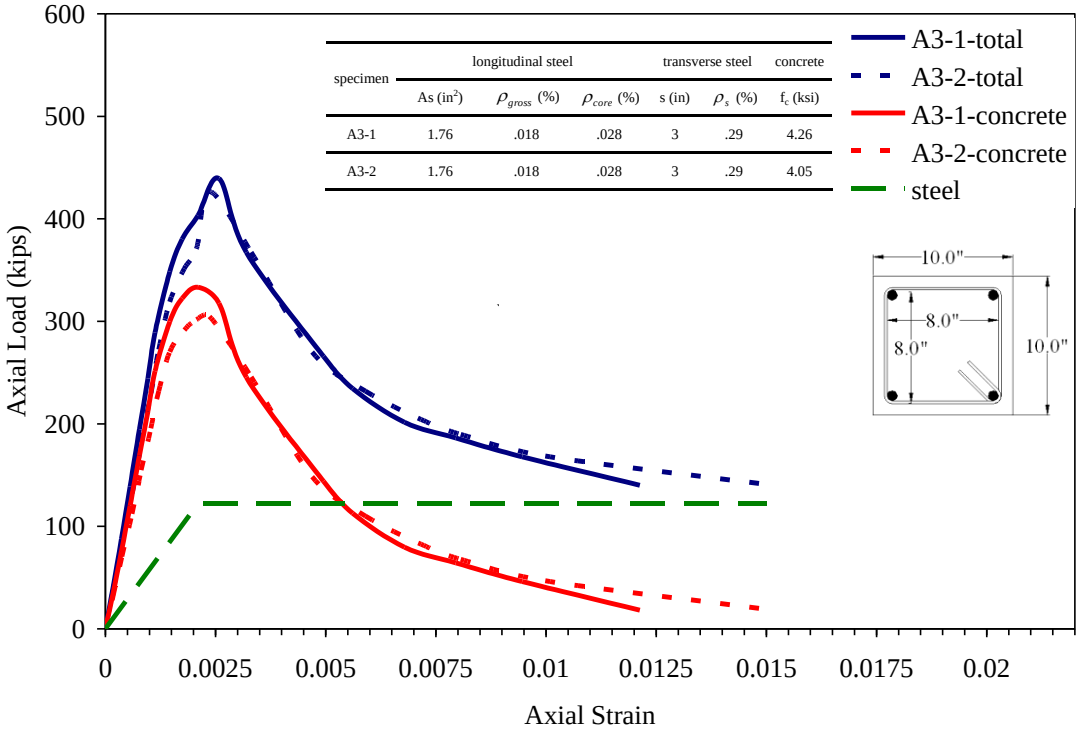

specimen	longitudinal steel			transverse steel		concrete
	As (in^2)	ρ_{gross} (%)	ρ_{core} (%)	s (in)	ρ_s (%)	f_c (ksi)
A3-1	1.76	.018	.028	3	.29	4.26
A3-2	1.76	.018	.028	3	.29	4.05

Figure B.3 Determination of concrete contributions for Columns A3-1 and A3-2.

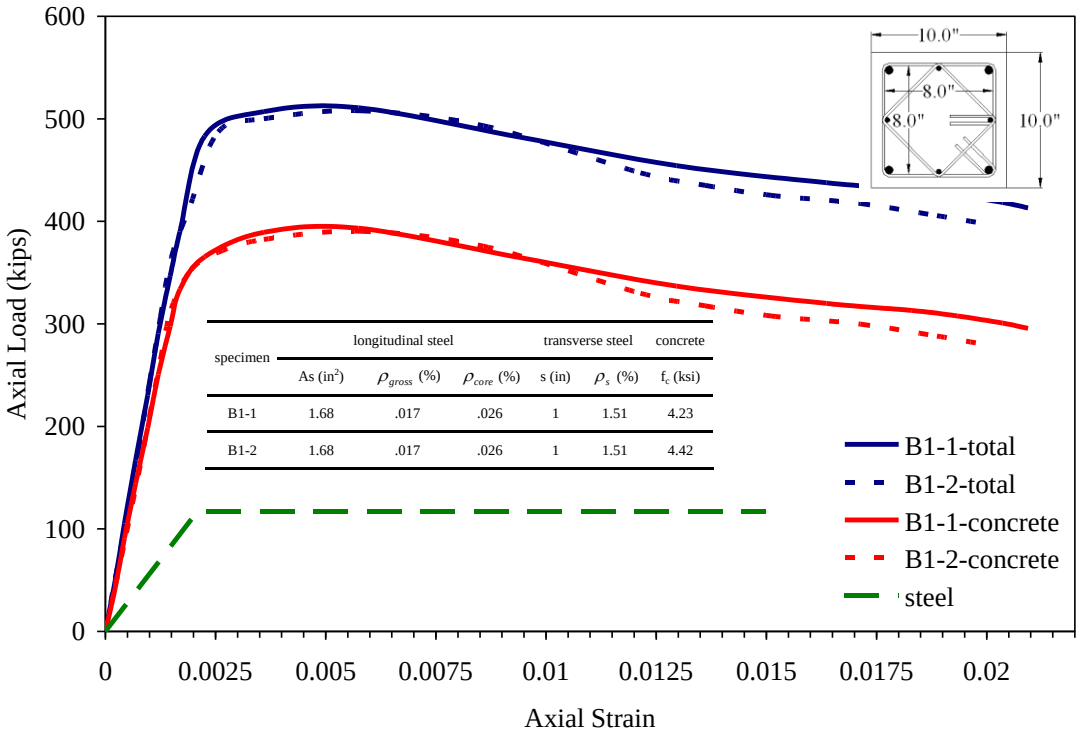

specimen	longitudinal steel			transverse steel		concrete
	As (in^2)	ρ_{gross} (%)	ρ_{core} (%)	s (in)	ρ_s (%)	f_c (ksi)
B1-1	1.68	.017	.026	1	1.51	4.23
B1-2	1.68	.017	.026	1	1.51	4.42

Figure B.4 Determination of concrete contributions for Columns B1-1 and B1-2.

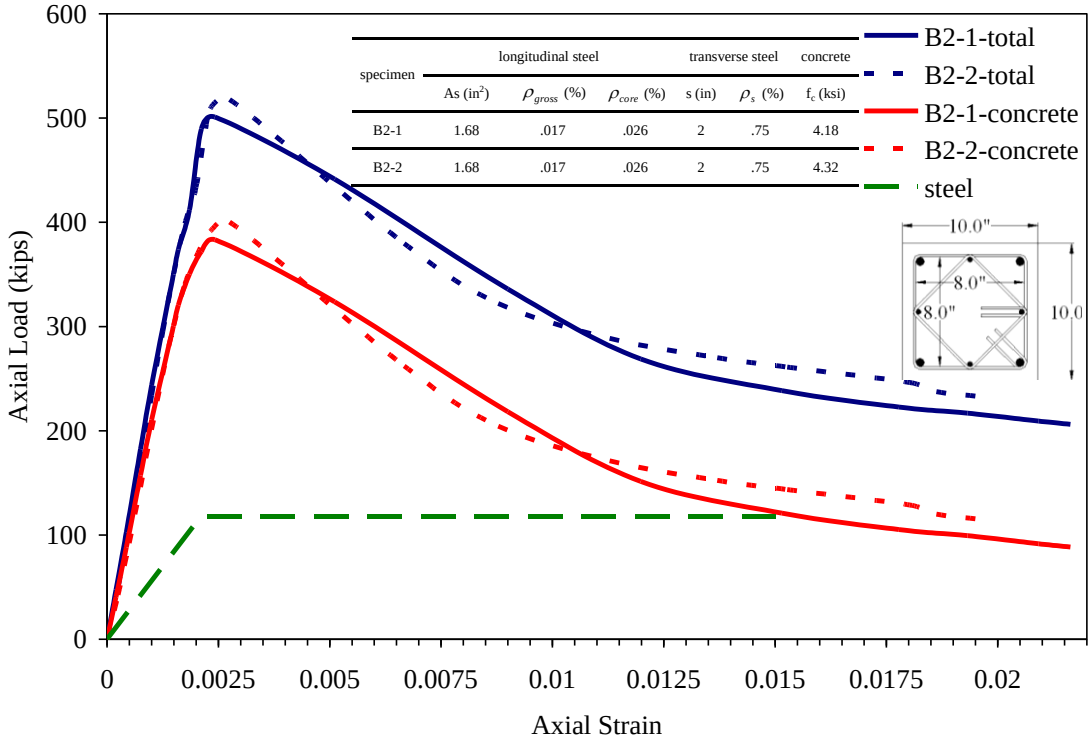

specimen	longitudinal steel			transverse steel		concrete
	As (in^2)	ρ_{gross} (%)	ρ_{core} (%)	s (in)	ρ_s (%)	f_c (ksi)
B2-1	1.68	.017	.026	2	.75	4.18
B2-2	1.68	.017	.026	2	.75	4.32

Figure B.5 Determination of concrete contributions for Columns B2-1 and B2-2.

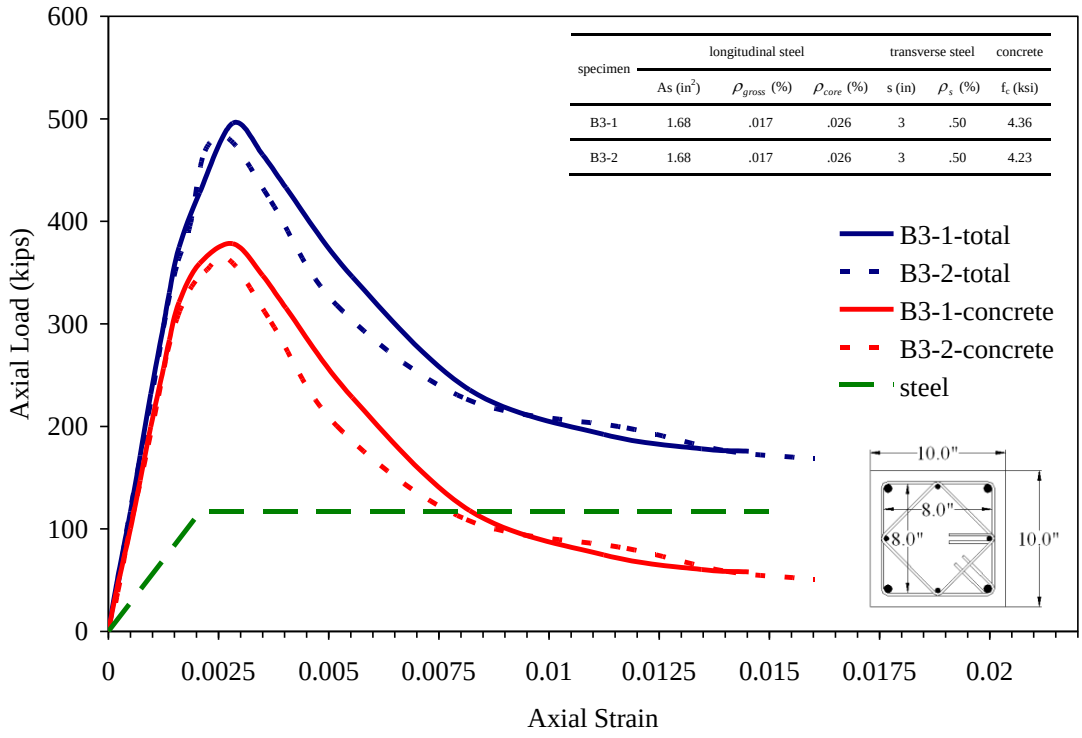

specimen	longitudinal steel			transverse steel		concrete
	As (in^2)	ρ_{gross} (%)	ρ_{core} (%)	s (in)	ρ_s (%)	f_c (ksi)
B3-1	1.68	.017	.026	3	.50	4.36
B3-2	1.68	.017	.026	3	.50	4.23

Figure B.6 Determination of concrete contributions for Columns B3-1 and B3-.2.

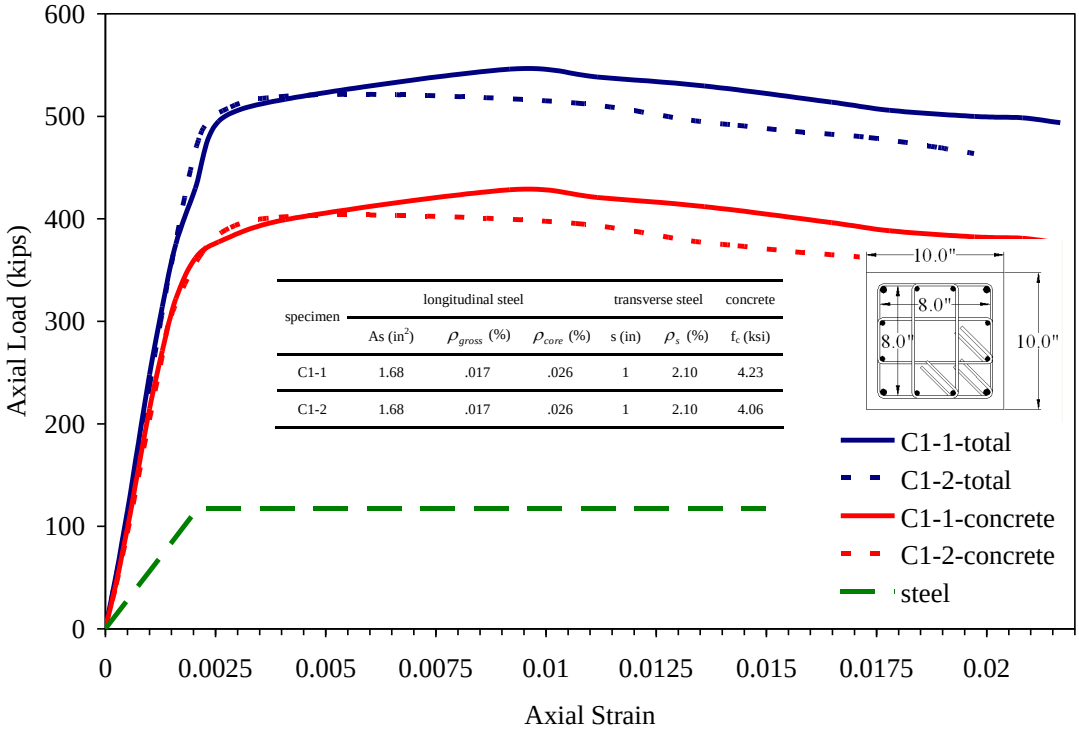

specimen	longitudinal steel			transverse steel		concrete
	As (in^2)	ρ_{gross} (%)	ρ_{core} (%)	s (in)	ρ_s (%)	f_c (ksi)
C1-1	1.68	.017	.026	1	2.10	4.23
C1-2	1.68	.017	.026	1	2.10	4.06

Figure B.7 Determination of concrete contributions for Columns C1-1 and C1-2.

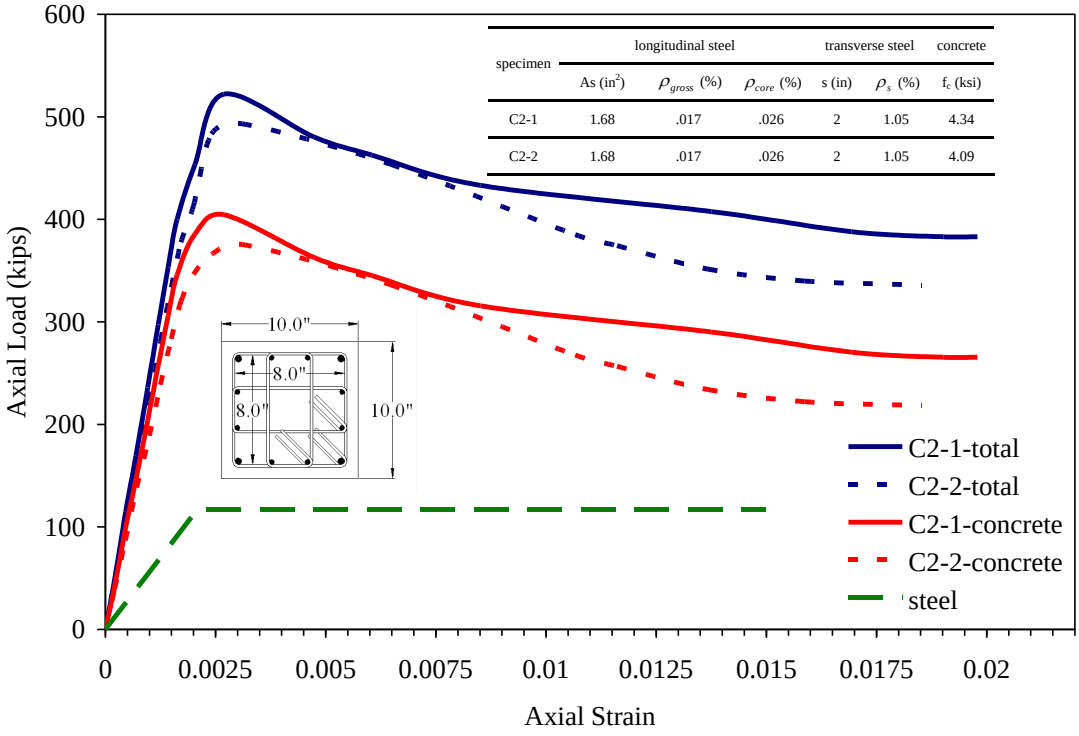

specimen	longitudinal steel			transverse steel		concrete
	As (in^2)	ρ_{gross} (%)	ρ_{core} (%)	s (in)	ρ_s (%)	f_c (ksi)
C2-1	1.68	.017	.026	2	1.05	4.34
C2-2	1.68	.017	.026	2	1.05	4.09

Figure B.8 Determination of concrete contributions for Columns C2-1 and C2-.2.

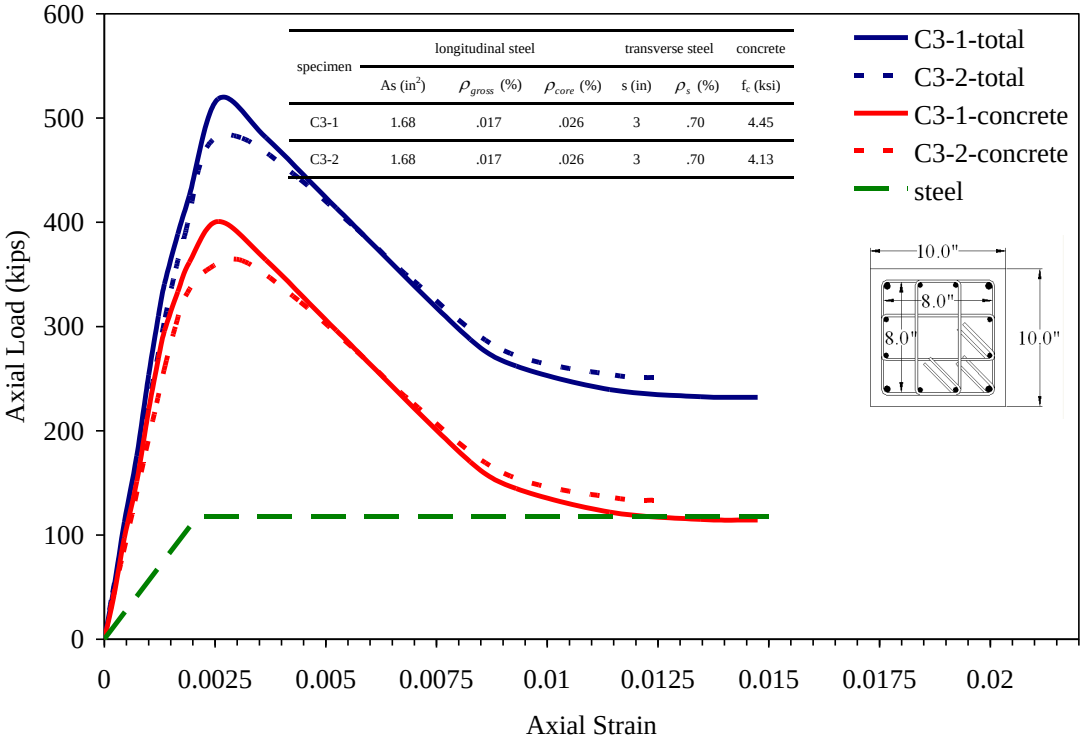

specimen	longitudinal steel			transverse steel		concrete
	As (in^2)	ρ_{gross} (%)	ρ_{core} (%)	s (in)	ρ_s (%)	f_c (ksi)
C3-1	1.68	.017	.026	3	.70	4.45
C3-2	1.68	.017	.026	3	.70	4.13

Figure B.9 Determination of concrete contributions for Columns C3-1 and C3-2.

APPENDIX C

EXPERIMENTAL STRESS-STRAIN CURVES FOR RAC COLUMNS

In this appendix the experimental stress-strain curves are presented.

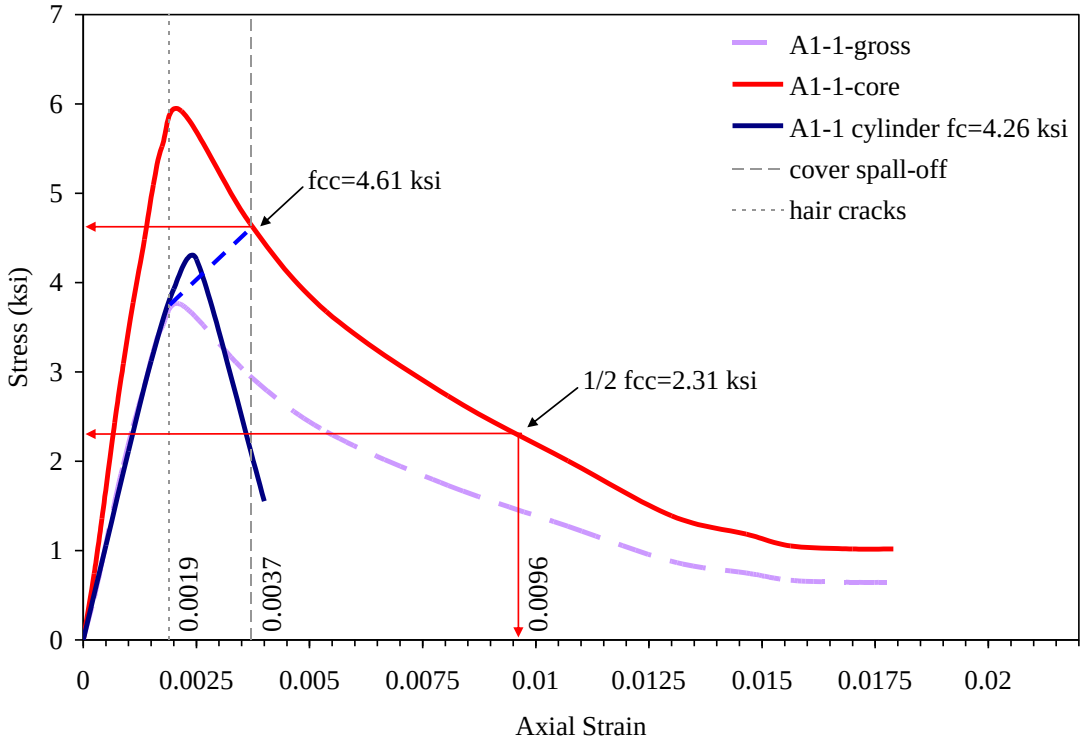

Figure C.1 Experimental stress-strain curve for column A1-1.

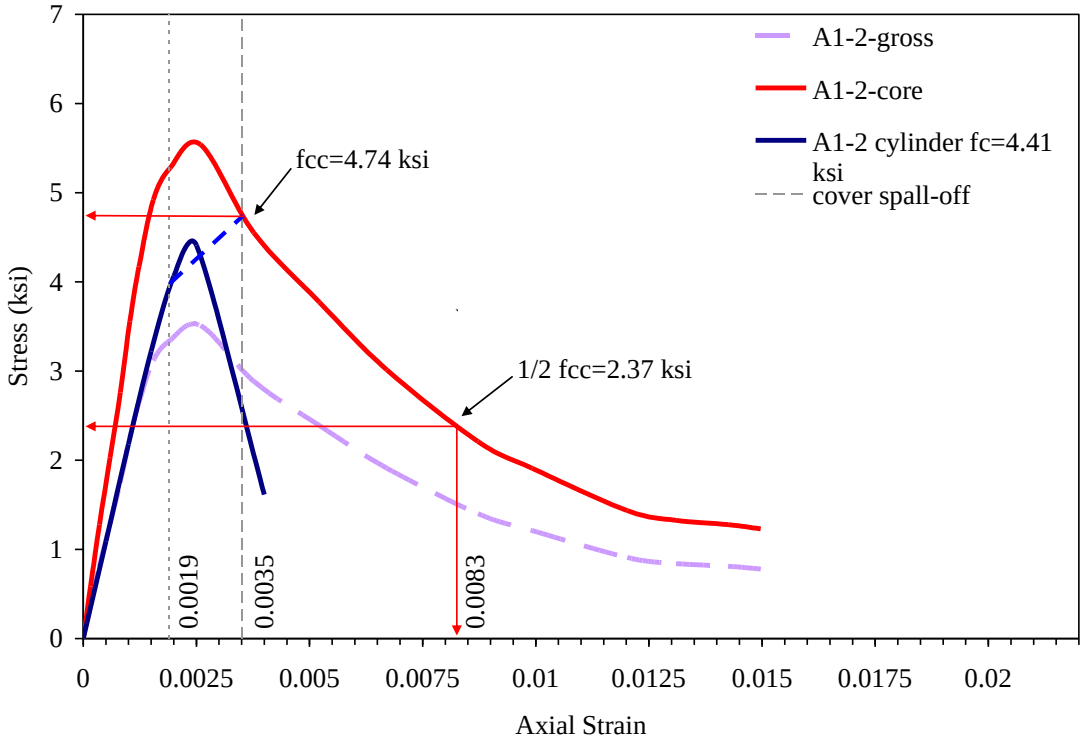

Figure C.2 Experimental stress-strain curve for column A1-2.

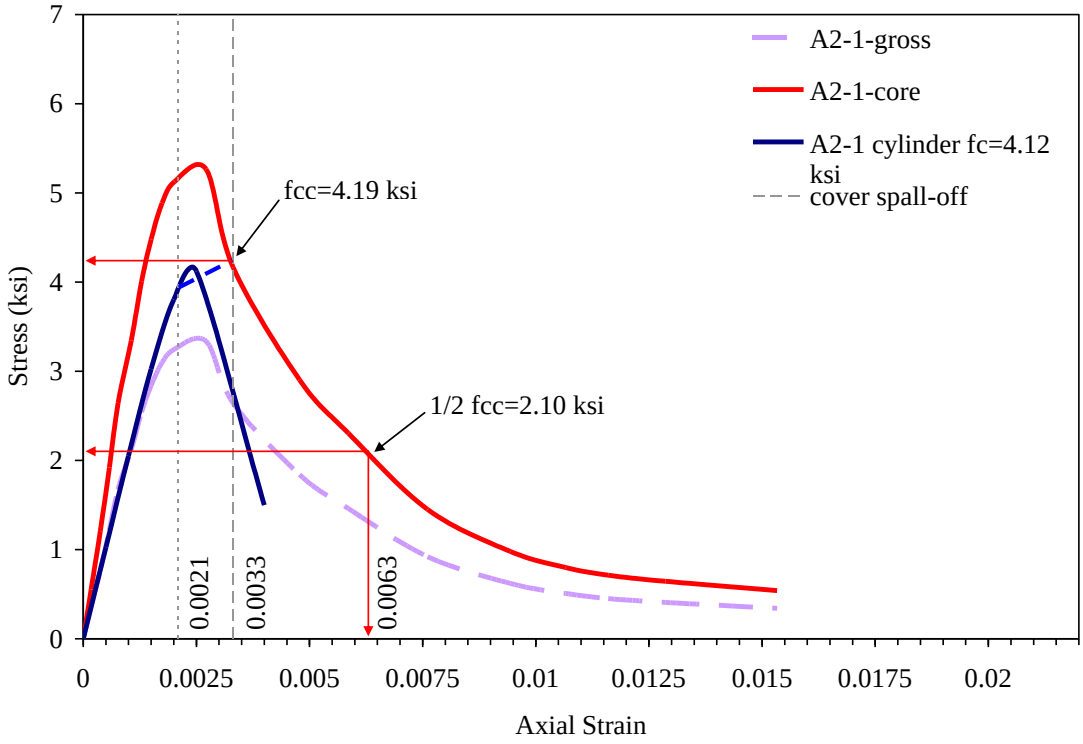

Figure C.3 Experimental stress-strain curve for column A2-1.

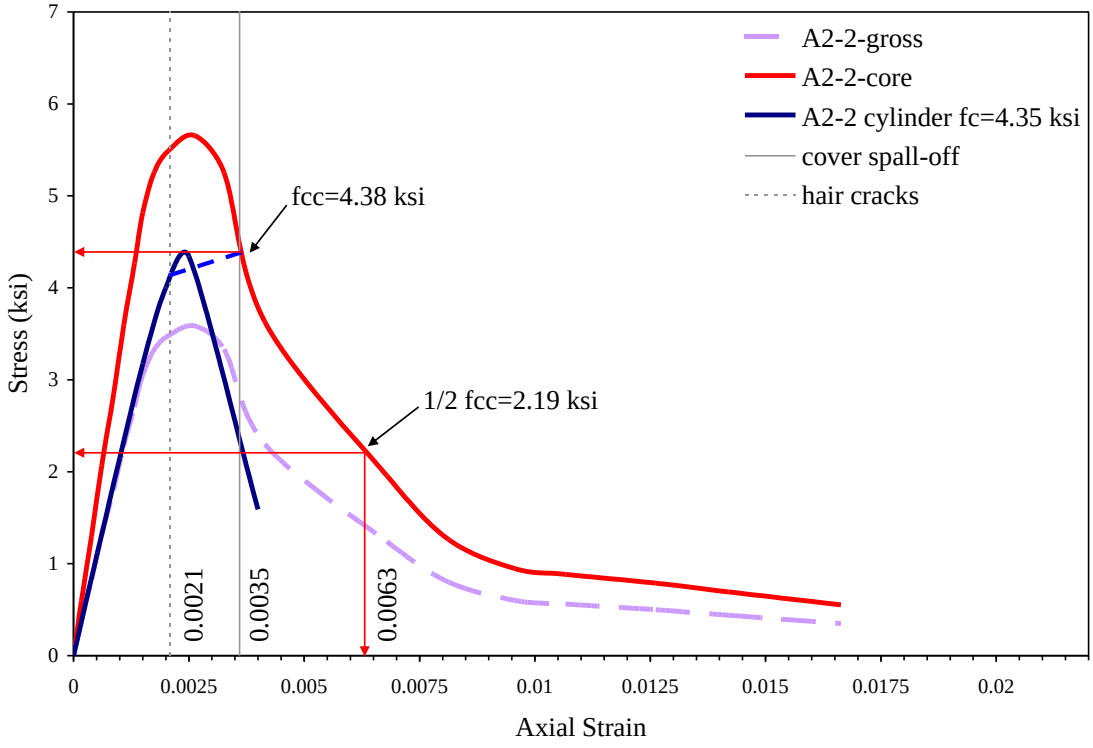

Figure C.4 Experimental stress-strain curve for column A2-2.

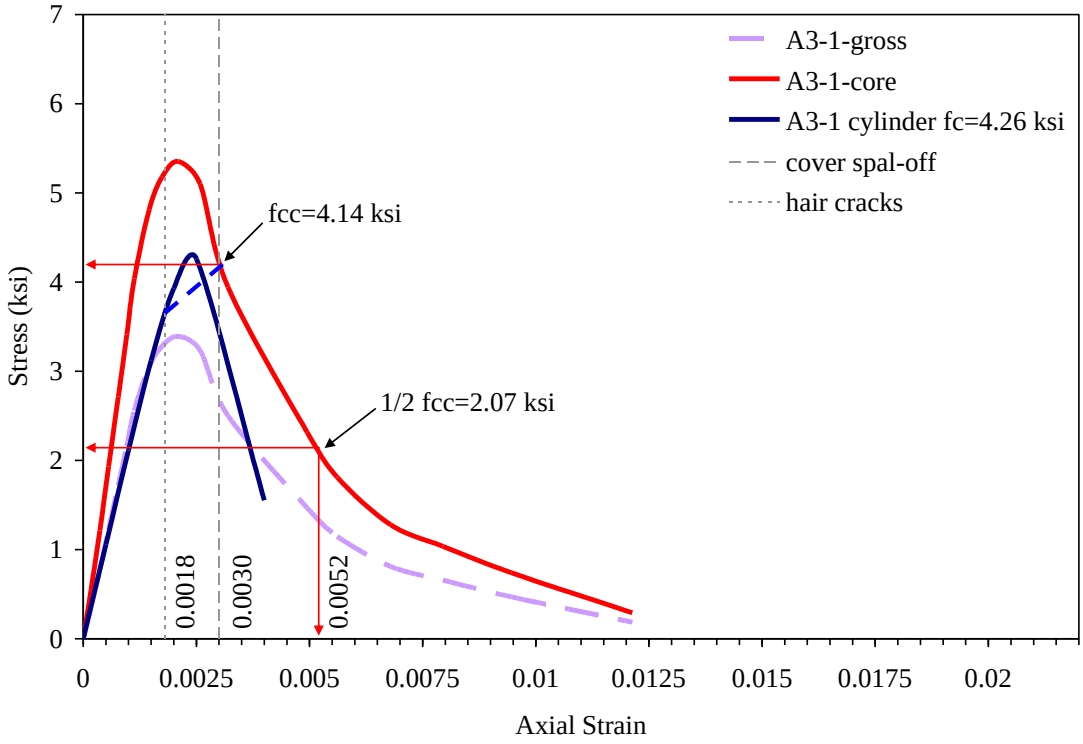

Figure C.5 Experimental stress-strain curve for column A3-1.

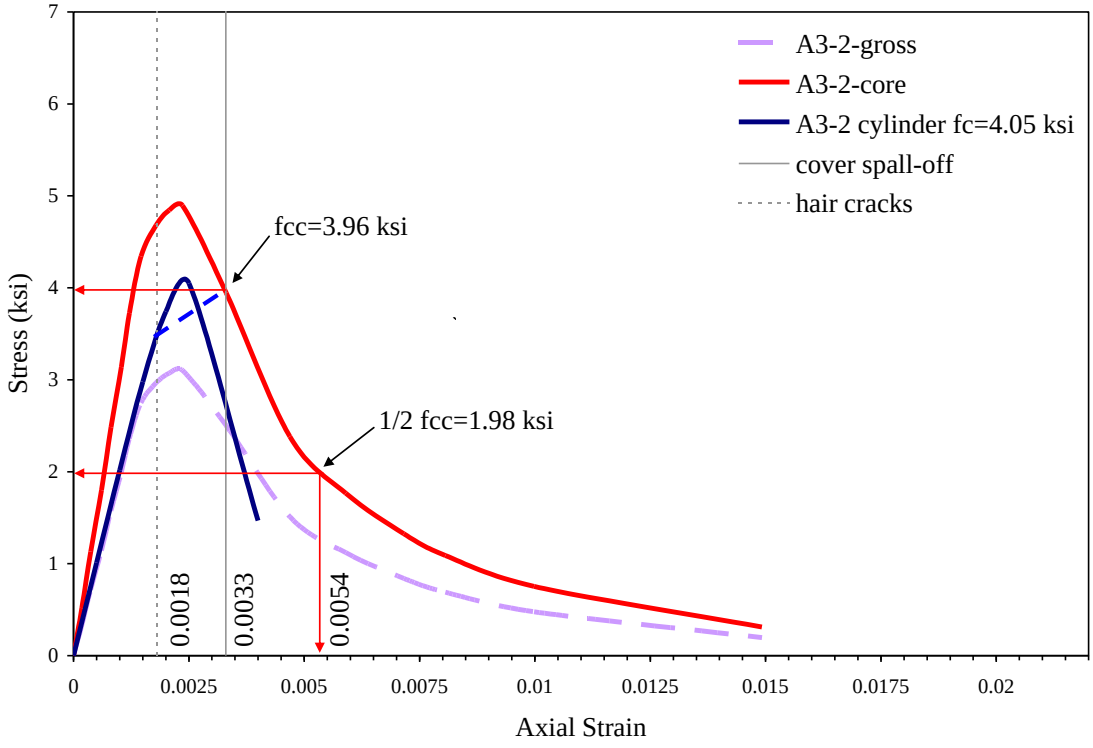

Figure C.6 Experimental stress-strain curve for column A3-2.

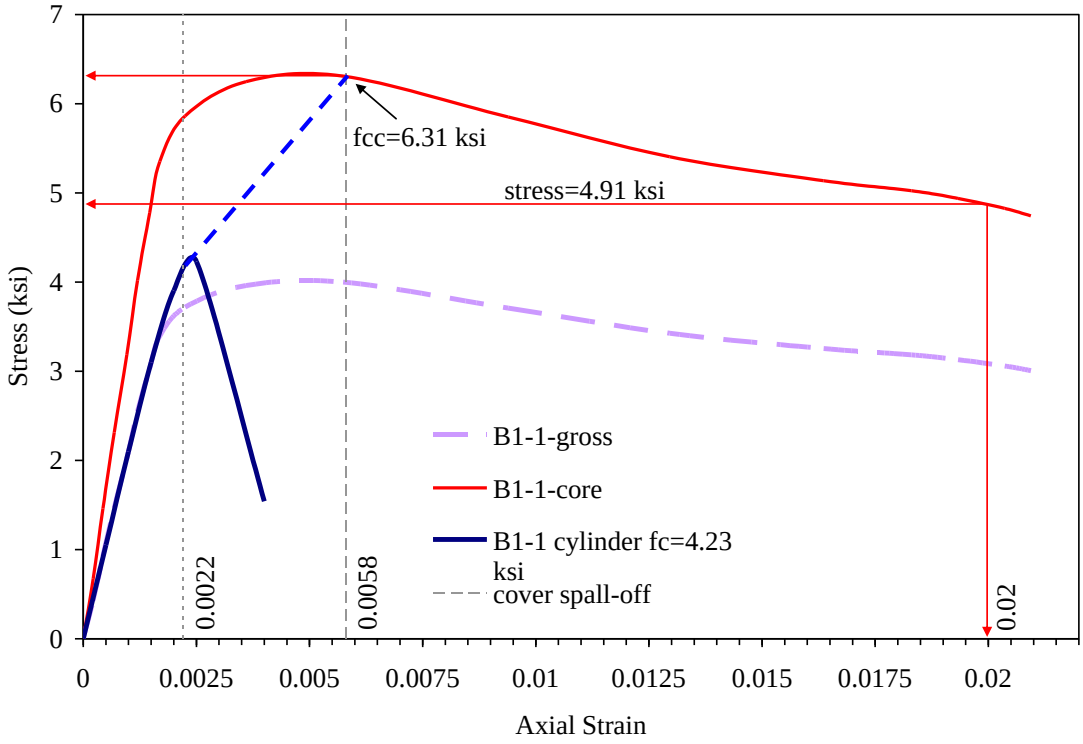

Figure C.7 Experimental stress-strain curve for column B1-1.

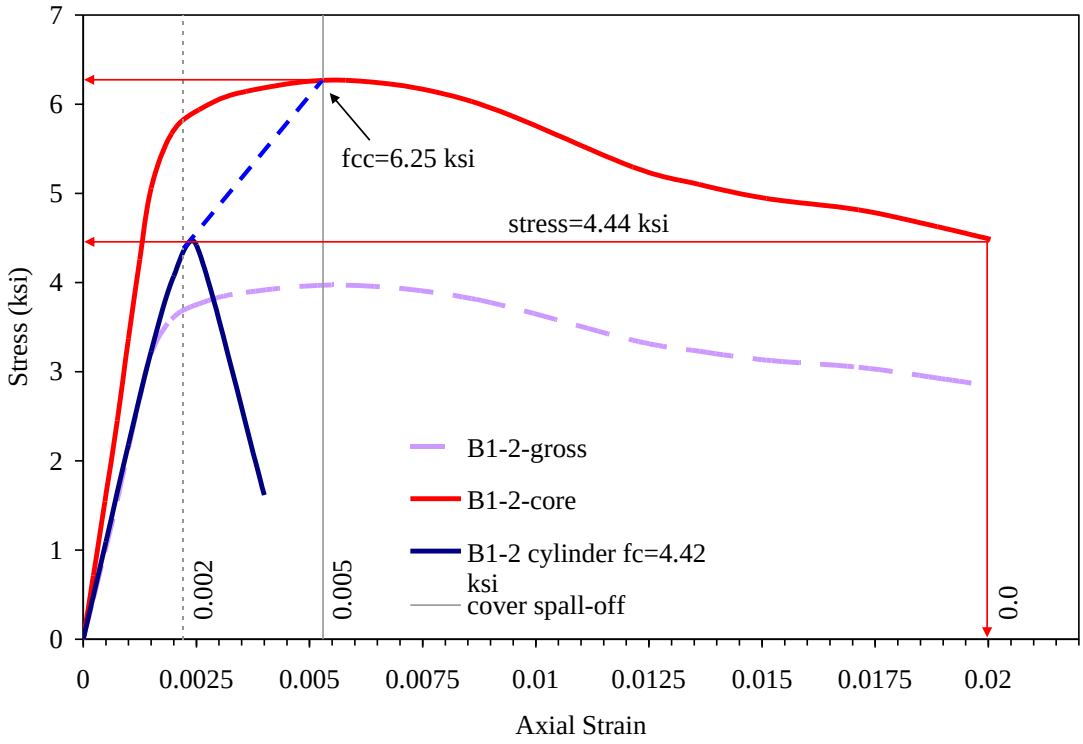

Figure C.8 Experimental stress-strain curve for column B1-2.

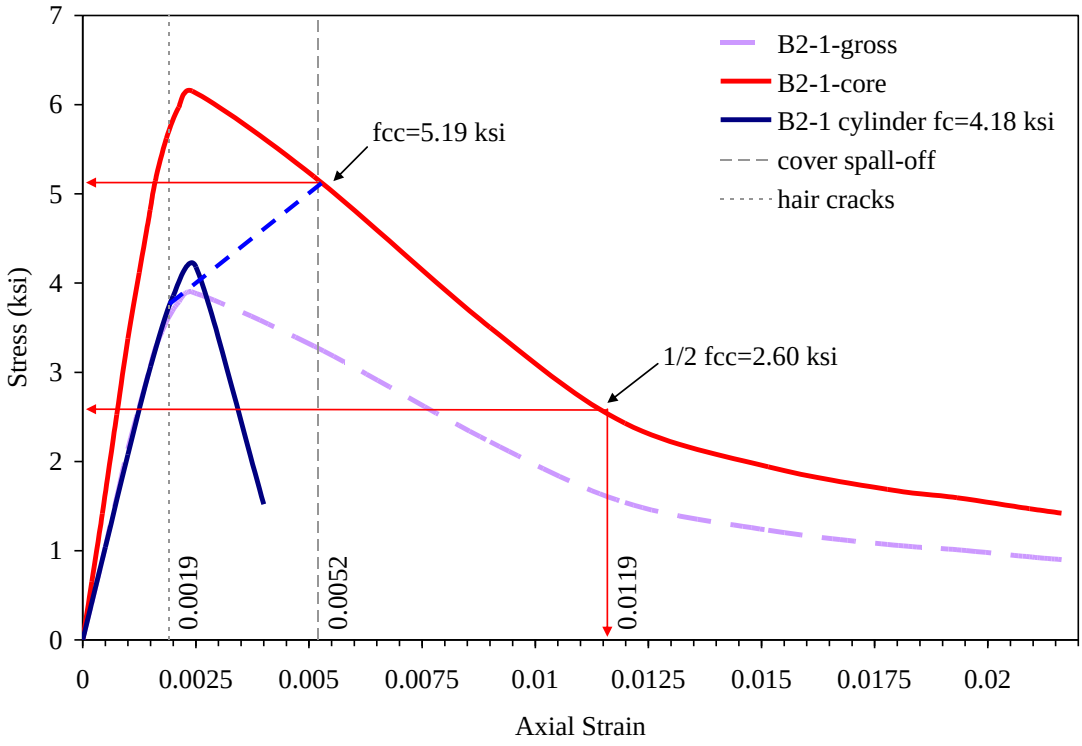

Figure C.9 Experimental stress-strain curve for column B2-1.

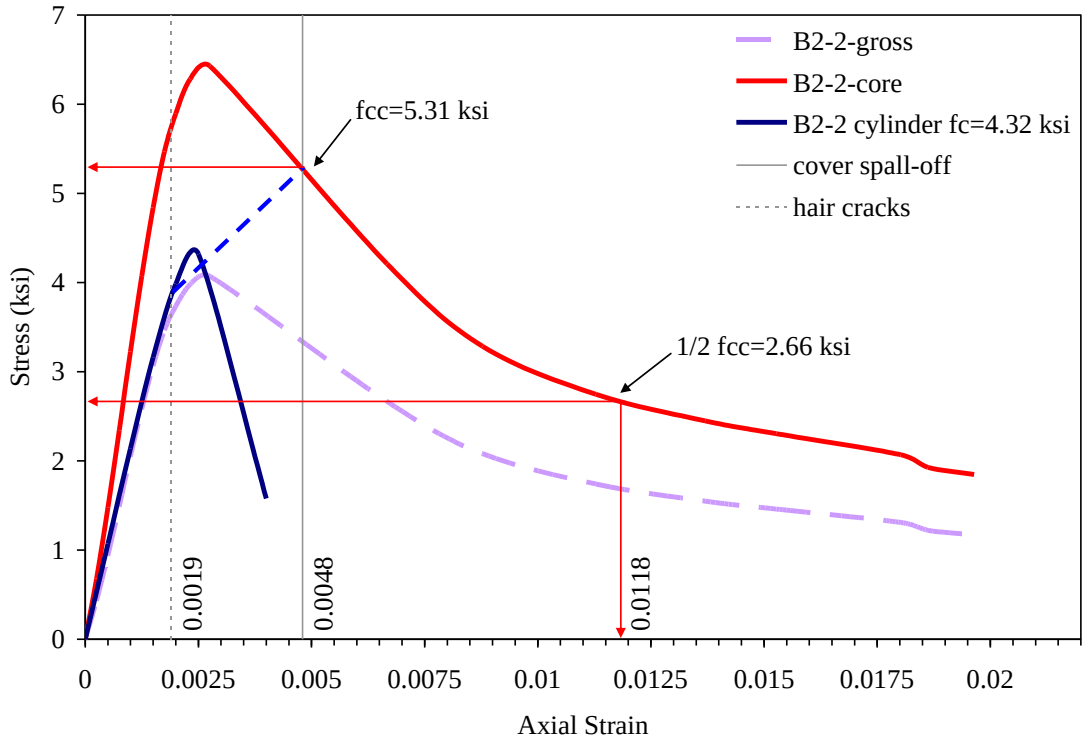

Figure C.10 Experimental stress-strain curve for column B2-2.

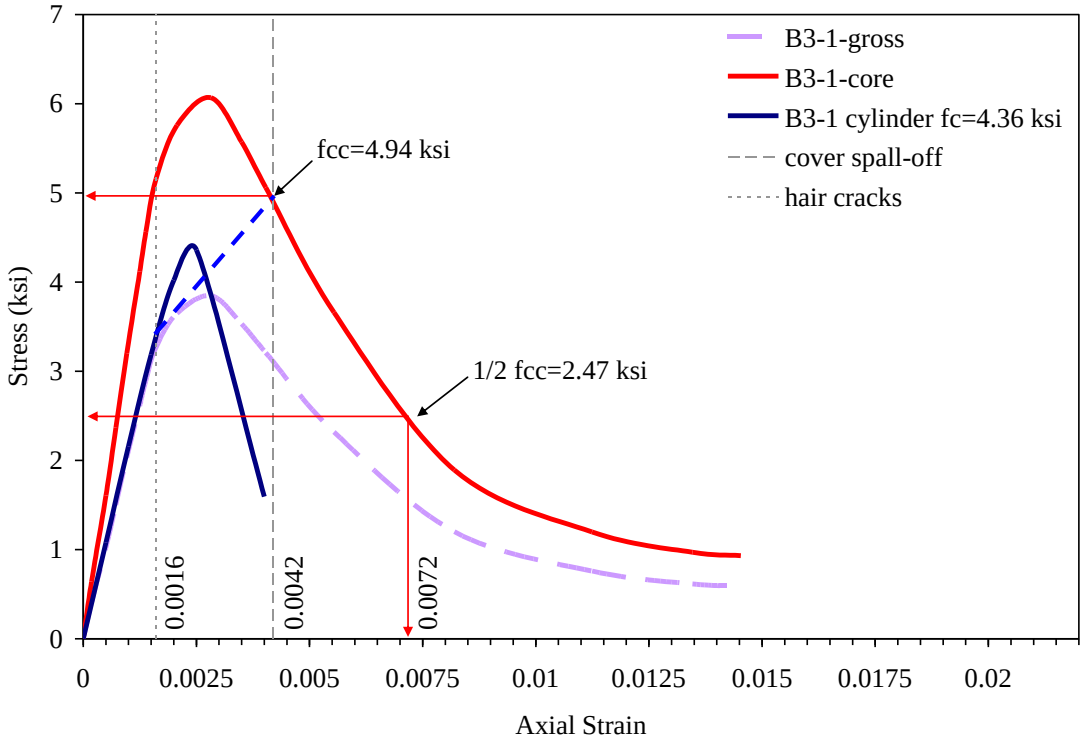

Figure C.11 Experimental stress-strain curve for column B3-1.

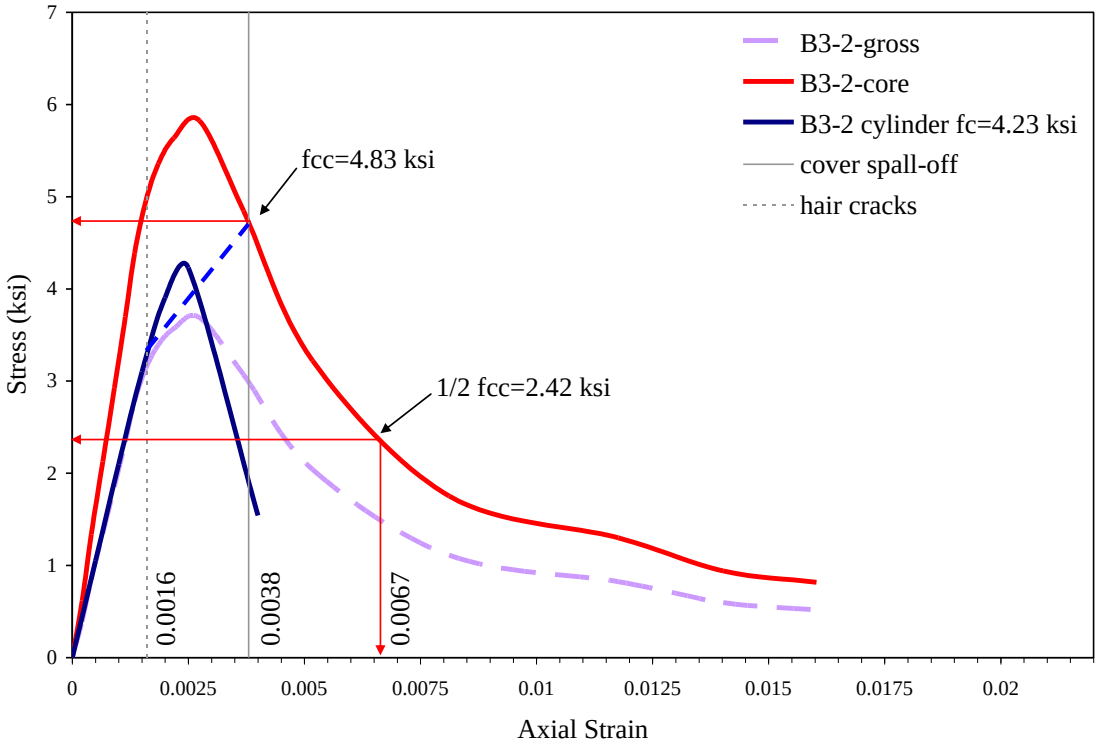

Figure C.12 Experimental stress-strain curve for column B3-2.

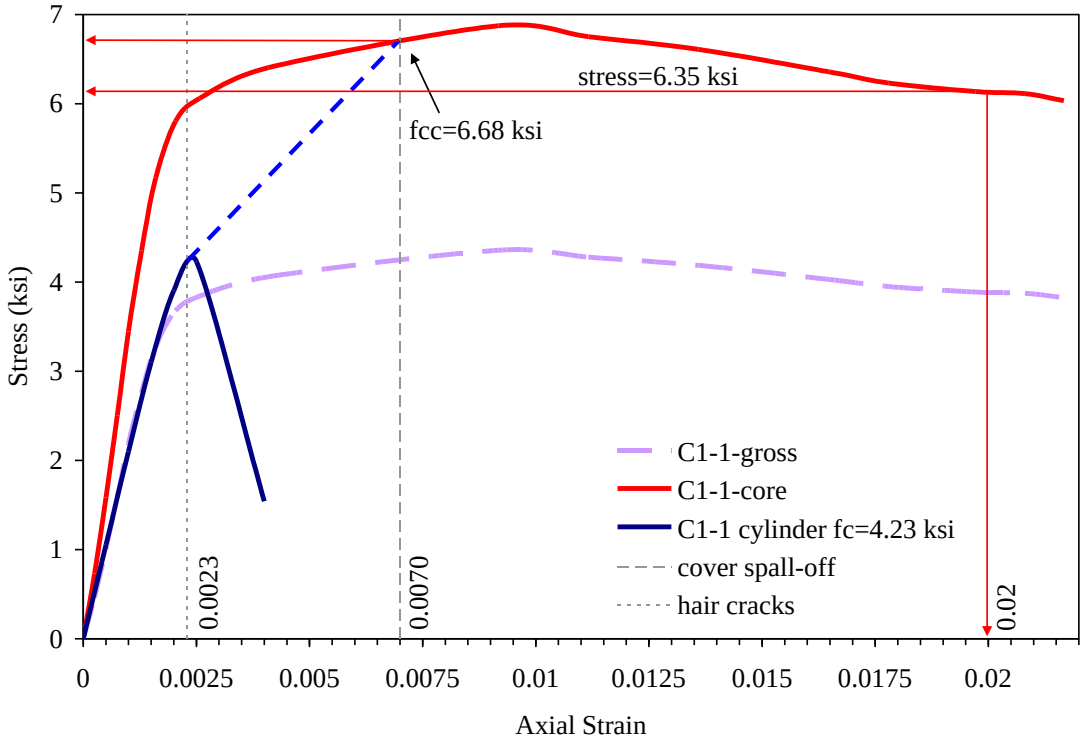

Figure C.13 Experimental stress-strain curve for column C1-1.

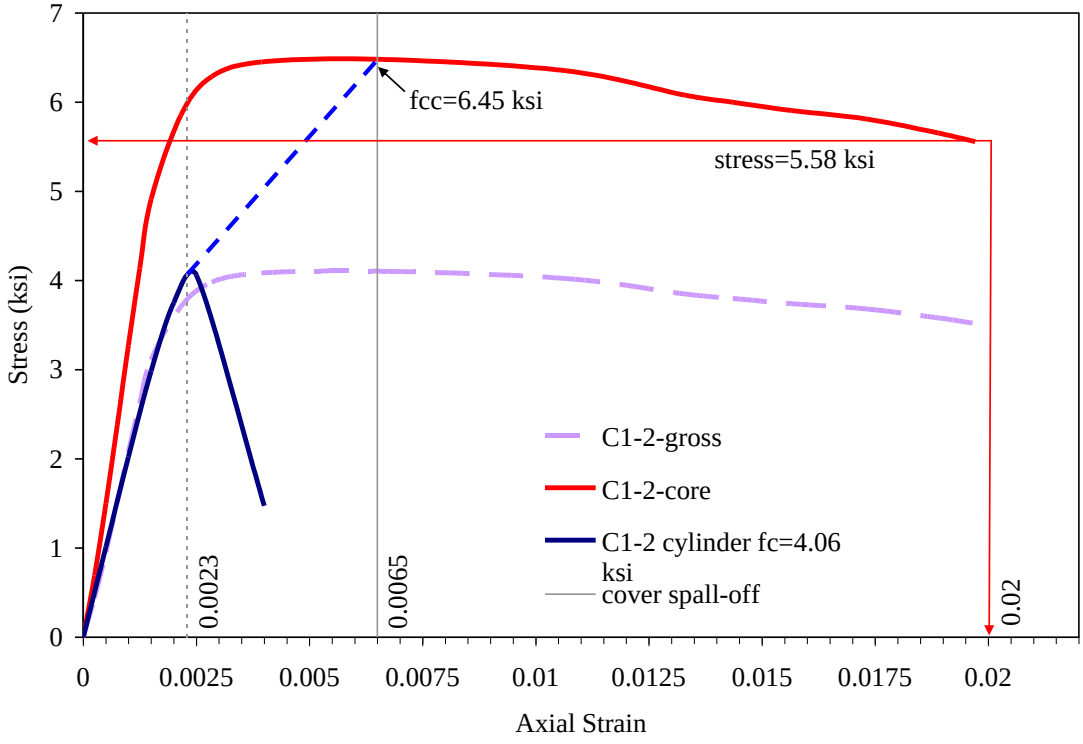

Figure C.14 Experimental stress-strain curve for column C1-2.

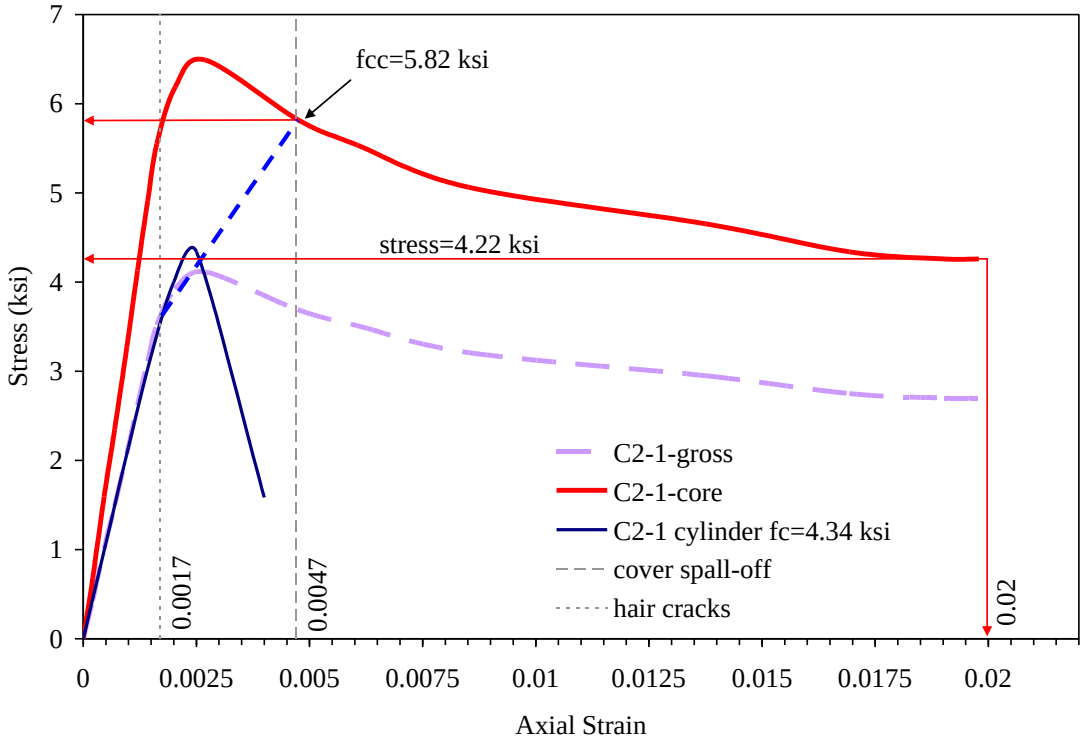

Figure C.15 Experimental stress-strain curve for column C2-1.

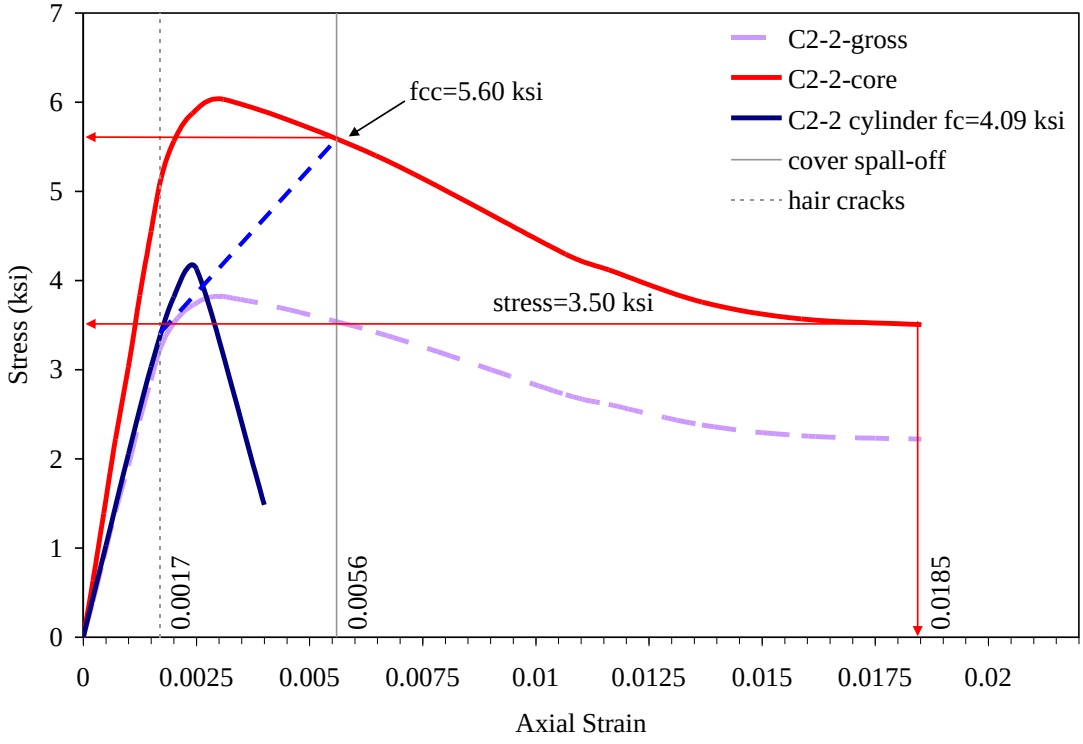

Figure C.16 Experimental stress-strain curve for column C2-2.

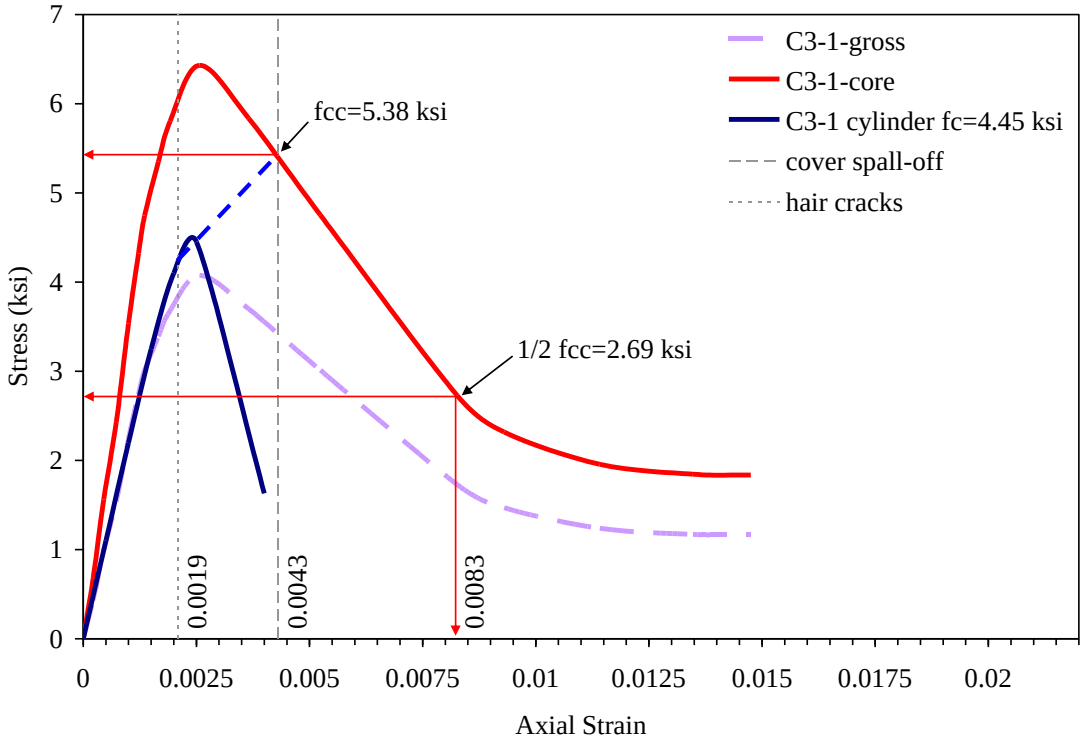

Figure C.17 Experimental stress-strain curve for column C3-1.

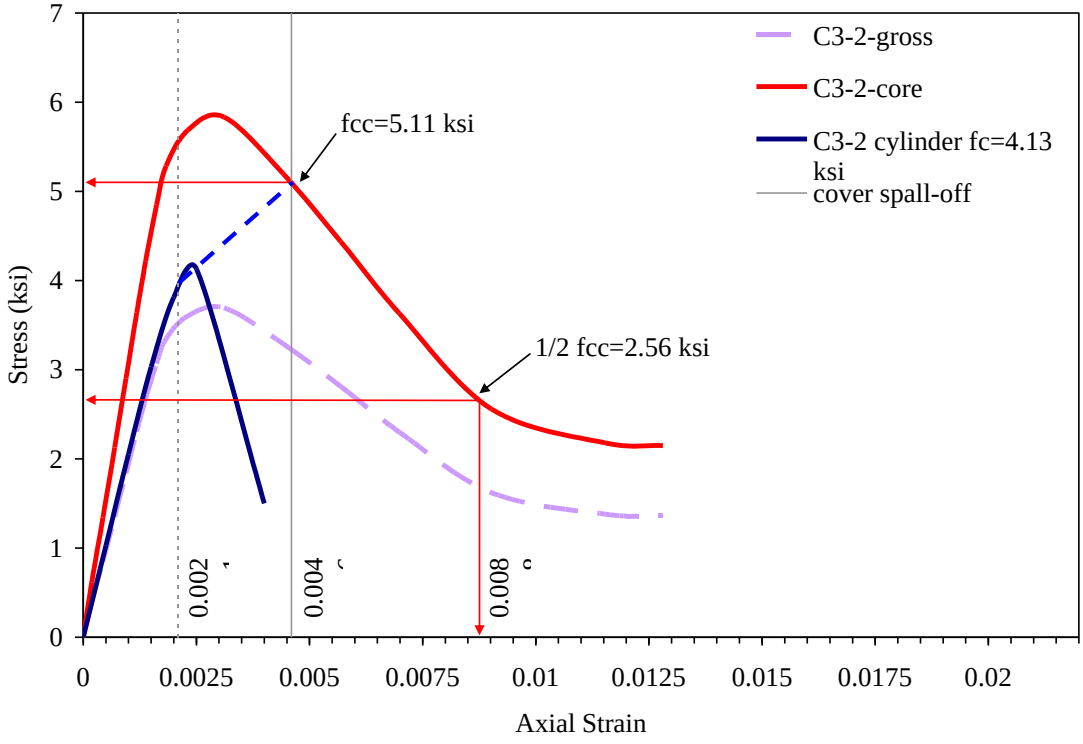

Figure C.18 Experimental stress-strain curve for column C3-2.

REFERENCES

Ahmad, S. H. and Shah, S. (1985). Behavior of hoop confined concrete under high strain rates. ACI Journal, 82(5), 634-647.

Ajdukiewicz , A. B. and Kliszczewicz, A. T. (2002). Influence of recycled aggregates on mechanical properties of HS/HPC. Cement & Concrete Composites, 24, 269-279.

Ajdukiewicz , A. B. and Kliszczewicz, A. T. (2007). Comparative tests of beams and columns made of recycled aggregate concrete and natural aggregate concrete. Journal of Advanced Concrete Technology, 5(2), 259-273.

Blakely, R. W. G. and Park, R. (1973). Prestressed concrete sections with cyclic flexure. ASCE Journal of Structural Division, 99(8), 1717-1742.

Buck, A. D. (1977). Recycled concrete as a source of aggregate. Journal of the American Concrete Institute, May, 212-219.

Building Contractors Society of Japan (1978). Study on Recycled Aggregate and Recycled Aggregate Concrete. Concrete Journal, 16(7), 18-31.

Berndt, M. L. (2009). Properties of sustainable concrete containing fly ash, slag and recycled concrete aggregate. Construction and Building Materials, 23, 2606-2613.

Corinaldesi, V. and Moriconi G. (2009). Influence of mineral additions on the Performance of 100% recycled aggregate concrete. Construction and Building Materials, 23, 2869-2876.

Dilger, W. H. et al. (1984). Ductility of plain and confined concrete under different strain rates. ACI Journal, 81(1), 73-81.

Domingo-Cabo, A. (2009). Creep and shrinkage of recycled aggregate concrete. Construction and Building Materials, 23, 2545-2553.

Etxeberria, M. et al. (2007). Recycled aggregate concrete as structural material. Materials and Structures, 40(5), 529-541.

Evangelista, L. and de Brito, J. (2010). Durability performance of concrete made with fine recycled concrete aggregates. Cement & Concrete Composites, 32, 9-14.

Evangelista, L. and de Brito, J. (2007). Mechanical behaviour of concrete made with fine recycled concrete aggregates. Cement & Concrete Composites, 29, 397-401.

Fathifazl, G. et al.(2009). Shear strength of reinforced recycled concrete beams without stirrups. Magazine of Concrete Research, 61(7), 477-490.

Franklin Associates (1998). Characterization of Building-Related Construction and Demolition Debris in the United States. Prepared for the US Environmental Protection Agency.

Gonzalez-Fonteboa, B. and Martinez-Abella, F. (2007). Shear strength of recycled concrete beams. Construction and Building Materials, 21, 887-893.

Hansen, T. C. (1992). RILEM report 6-Recycling of demolished concrete and masonry.

Hansen, T. C. and Narud, H. (1983). Strength of recycled concrete made from crushed concrete coarse aggregate. Concrete International, 5(1), 79-83.

Hognestad, E. (1951). A study of combined bending and axial load in reinforced concrete members. Bulletin No. 399, Engineering Experiment Station, University of Illinois.

Hoshikuma, J. (1997). Stress-strain Model for confined reinforced concrete in bridge piers. ASCE Journal of Structural Engineering, 123(5), 624-623.

Kent, D. C. and Park R. (1971). Flexural members with confined concrete. ASCE Journal of Structural Division, 97(7), 1969-1990.

Khatib, J. M. (2005). Properties of concrete incorporating fine recycled aggregate. Cement and Concrete Research, 35, 763-769.

Kou, S. C. et al. (2007). Influence of fly ash as cement replacement on the properties of recycled aggregate concrete on the properties of recycled aggregate concrete. ASCE Journal of Materials in Civil Engineering, 19(9), 709-717.

Levy, S. M. and Helene, P. (2004). Durability of recycled aggregates concrete: a safe way to sustainable development. Cement and Concrete Research, 34, 1975-1980.

Mahgoub, M. (1997). Reinforced Concrete Column Retrofit Using Steel Jackets. Master's Thesis. Civil Engineering Department. McMaster University, Canada.

Mander, J. B. (1988). Observed stress-strain behavior of confined concrete. ASCE Journal of Structural Engineering, 114(8), 1827-1849.

Mander, J. B. (1988). Theoretical stress-strain model for confined concrete. ASCE Journal of Structural Engineering, 114(8), 1804-1826.

Mukai T. and Kikuchi M. (1988). Properties of reinforced concrete beams containing recycled aggregate. In: Kasai Y, editor. Demolition and reuse of concrete and masonry vol. 2: reuse of demolition waste. Proceedings of the second international RILEM symposium, pp. 670–679.

Park, R. et al. (1982). Ductility of square confined concrete columns. ASCE Journal of the Structural Division, 108(4), 929-950.

Penelis, G. G. and Kappos, A. J. (1997). Earthquake-resistant concrete structures.: E & F Spon.

Priestley, M. J. N., Park, R. and Potangaroa, R. T. (1981). Ductility of spirally confined concrete columns. Proceedings of American Society of Civil. Engineers, Journal of. Structural Division. 107 (ST1), 181-202.

Rahal, K. (2007). Mechanical properties of concrete with recycled coarse aggregate. Building and Environment, 42, 407-415.

Rahman, I. A. (2009). Assessment of recycled aggregate concrete. Modern Applied Science (Canadian Center of Science and Education), 3(10), 47-54.

Rasheeduzzafar and Khan A. (1984). Recycled concrete-A source for new aggregate. Cement, Concrete, and Aggregates, 6, 17-27.

Ravindrarajah, R. Sri and Tam, C. T. (1985). Properties of concrete made with crushed concrete as coarse aggregate. Magazine of Concrete Research, 37, 29-38.

Richart, F.E., Brandtzaeg, A. and Brown R. L. (1928). A study of the failure of concrete under combined compressive stress. Bulletin No. 185, Engineering Experiment Station, University of Illinois.

Saatcioglu, M. and Razvi, S. (1992). Strength and ductility of confined concrete. ASCE Journal of Structural Engineering, 118(6),1590-1607.

Shah, S. P., Fafitis, A. and Arnold, R. (1983). Cyclic loading of spirally reinforced concrete. Proceedings of American Society of Civil. Engineers, Journal of. Structural Division, 109 (7), 1695-1710.

Sheikh, S. A. and Uzumeri, S. M. (1982). Analytical model for concrete confinement in tied columns. ASCE Journal of the Structural Division, 108(12), 2703-2722.

Sheikh, S. A. and Uzumeri, S. M. (1980). Strength and ductility of tied concrete columns. ASCE Journal of the Structural Division, 106(5), 1079-1101.

Simmons, P. N. (2006). The state of garbage in America. BioCycle, 47(4), 26-36.

Sinha, B. P., Gerstle, K. H. and Tulin, L. G. (1964). Stress-strain relations for concrete under cyclic loading. Journal of the American Concrete Institute, 61 (2), 195-210.

Tam, V. W.Y. (2009). Physio-chemical reactions in recycle aggregate concrete. Journal of Hazardous Materials, 163, 823-828.

Tam, V. W.Y. (2008). Economic comparison of concrete recycling. Conservation and Recycling, 52, 821-828.

Topcu, I. B. and Guncan, N. F. (1995). Using waste concrete as aggregate. Cement and Concrete Research, 25(7), 1385-1390.

Topcu, I. B. and Sengel, S. (2004). Properties of concretes produced with waste concrete aggregate. Cement and Concrete Research, 34(1307), 1312

United States Department of Transportation (2004). Transportation applications of recycled concrete aggregate-FHWA State of the Practice National Review.

United States Environmental Protection Agency Report EPA530-R-95-019 (2009). Estimating 2003 building-related construction and demolition materials amount.

United States Geological Survey (2009). Annual mineral commodity summaries.

United States Environmental Protection Agency (1994). List of industrial waste landfills and construction and demolition waste landfills.

Xiao, J. (2006). Seismic performance of frame structures with recycled aggregate concrete. Engineering Structures, 28, 1-8.

Yamato, T. (1998). Mechanical properties, drying shrinkage and resistance to freezing and thawing of concrete using recycled aggregate. ACI Special Publication, SP 179-7, 105-121.